NOTE TO USERS

This reproduction is the best copy available.

UMI®

Cutout Manager - A stand-alone software system to calculate output factors for arbitrarily shaped electron beams using Monte Carlo simulation

Jürgen Last, Dr. rer. nat.
Medical Physics Unit
McGill University, Montreal

December 2008

A thesis submitted to McGill University in partial fulfilment of the requirements of the degree of Master of Science in Medical Physics

©Copyright Jürgen Last 2008 All rights reserved

Library and Archives Canada

Published Heritage Branch

395 Wellington Street
Ottawa ON K1A 0N4
Canada

Bibliothèque et Archives Canada

Direction du Patrimoine de l'édition

395, rue Wellington
Ottawa ON K1A 0N4
Canada

Your file Votre référence
ISBN: 978-0-494-67064-4
Our file Notre référence
ISBN: 978-0-494-67064-4

NOTICE:

The author has granted a non-exclusive license allowing Library and Archives Canada to reproduce, publish, archive, preserve, conserve, communicate to the public by telecommunication or on the Internet, loan, distribute and sell theses worldwide, for commercial or non-commercial purposes, in microform, paper, electronic and/or any other formats.

The author retains copyright ownership and moral rights in this thesis. Neither the thesis nor substantial extracts from it may be printed or otherwise reproduced without the author's permission.

AVIS:

L'auteur a accordé une licence non exclusive permettant à la Bibliothèque et Archives Canada de reproduire, publier, archiver, sauvegarder, conserver, transmettre au public par télécommunication ou par l'Internet, prêter, distribuer et vendre des thèses partout dans le monde, à des fins commerciales ou autres, sur support microforme, papier, électronique et/ou autres formats.

L'auteur conserve la propriété du droit d'auteur et des droits moraux qui protège cette thèse. Ni la thèse ni des extraits substantiels de celle-ci ne doivent être imprimés ou autrement reproduits sans son autorisation.

In compliance with the Canadian Privacy Act some supporting forms may have been removed from this thesis.

While these forms may be included in the document page count, their removal does not represent any loss of content from the thesis.

Conformément à la loi canadienne sur la protection de la vie privée, quelques formulaires secondaires ont été enlevés de cette thèse.

Bien que ces formulaires aient inclus dans la pagination, il n'y aura aucun contenu manquant.

Canada

ACKNOWLEDGMENTS

It was Prof. Ervin Podgoršak's encouragement that first got me started to work towards a master's degree in McGill's Medical Physics graduate program and his continued support that helped me get through it. The success of the program is unthinkable without the quality, openness and enthusiasm of the academic teachers and support staff. Although I felt more than once threatened enough to quit the program I was reassured that this was totally normal and that I should hang in. I did, and today I want to express my thanks and gratitude you great people.

Thanks go out to my thesis supervisor Dr. François DeBlois who is recently became medical physics chief at the Jewish General Hospital and to MGH's physicist Michael Evans who set me straight when I was wandering on higher levels of medical physics consciousness. Prof. Jan Seuntjens as co-supervisor and Prof. Frank Verhaegen took a particular interest in my project and supported it along its way. Love of the radiochromic film method was instilled on me by Dr. Slobodan Devic. Dr. Wamied Abdel-Rahman was always available for discussion and made some critical contributions to the present work.

Without exception, the medical physics students were a delightful bunch of people. In my year Dr. Richard Benson stands out because of we share a similar background and we mutually supported each other during classes, labs and otherwise.

Last but not least I would like to thank my friend Youdan Zhang whose continued moral and nutritional support was crucial for successfully completing the master's program.

TABLE OF CONTENTS

LIST OF TABLES

LIST OF FIGURES

ABSTRACT

In external electron beam therapy arbitrarily shaped inserts (cutouts) are used to define the contours of the irradiated field. This thesis describes the implementation and verification of a software system to calculate output factors for cutouts using Monte Carlo simulations. The design goals were:

- A stand-alone software system running on a single workstation.
- Task oriented graphical user interface with shape input capability.
- Implementation on *Mac OS X*® (10.4.x Tiger).
- CPU multicore support by job splitting.
- *EGSnrc* (Patch level V4-r2-2-5) for particle transport and dose scoring.
- Validation for clinical use

The system, called *Cutout Manager*, can calculate output factors with 1% statistical error in 20 minutes on *Mac Pro* computer (Intel Xeon®, 4 cores). When the *BEAMnrc* linac model correctly reproduces percentage depth doses in the buildup region and around R_{100}, calculated and measured output factors are in good agreement with precision measurements of circular cutouts at 100 cm source-to-surface distance (SSD) and extended SSD. *Cutout Manager* simulations are consistent with measurements of clinical cutouts within a 2% error margin.

RÉSUMÉ

Lors de la radiothérapie par faisceaux d'électrons externes des masques « cutouts » sont utilisés pour définir la forme particulière de chacun des faisceaux. Ce mémoire décrit la conception et la mise en marche d'un logiciel permettant le calcul, par simulations Monte-Carlo (MC), des facteurs de débit pour ces masques.

Les objectifs de ce travail étaient les suivants:

- La création d'un logiciel complet fonctionnant sur un seul poste de travail.
- La conception d'une interface usager permettant de digitaliser les différentes formes de caches.
- L'implémentation sur *Mac OS X*® (10.4.x Tiger).
- La compatibilité du logiciel et le support sur CPU « multicores ».
- L'utilisation de *EGSnrc* (version V4-R2-2-5) pour le transport MC des particules et le calcul de la dose.
- La validation du système pour l'usage clinique.

Le système, appelé *Cutout Manager*, permet de calculer les facteurs de débit avec 1% d'erreur statistique en 20 minutes sur un ordinateur Mac Pro (Intel Xeon ®, 4-core). Lorsque le modèle BEAMnrc du linac reproduit correctement les courbes de rendement en profondeur (PDD) dans la zone d'accroissement de la dose « buildup » et près de du point R100 l'accord entre les facteurs calculés et mesurés est très bon pour les mesures cliniques précises de caches circulaires à une « distance-source-peau » (DSP) de 100 cm et pour les DSP étendues. Les calculs du logiciel « Cutout Manager » sont en accord avec les mesures cliniques de masques à l'intérieur d'une marge d'erreur de 2%.

Chapter 1 - INTRODUCTION

This chapter begins with a short introduction of linear accelerators and their use in radiotherapy. We discuss general aspects of external *direct field electron beam radiotherapy* and other electron modalities in the radiation treatment of cancer. Properties of clinical electron beams, dosimetric protocols and quality assurance (QA) requirements are discussed. We look into specific clinical aspects of electron beam radiotherapy, namely hardware setup, cutout fabrication and output factor measurement. The chapter concludes with a review of alternative electron accelerators and previous approaches to determine output factors by numerical methods.

Linacs

The linear accelerator, or short *linac*, is the workhorse in contemporary radiation oncology departments. A radiotherapy linac is essentially a miniaturized particle accelerator that produces a narrow high energy electron beam which usually impinges on a high-Z metal target to produce bremsstrahlung photons. Introduced for medical use in the 1970s, commercially available linacs have, at the time of this writing, almost completely replaced the Cobalt-60 based teletherapy units.

There are multiple reasons for this development, the most important of which is the availability of much higher effective photon energies than the 1.25 MeV of Cobalt-60. Higher energies lower the skin dose and push the maximum of dose deposition to greater depths, both useful features for radiotherapy applications. Photon beams provided by linacs typically have a bremsstrahlung spectrum whose high energy endpoint is 4, 6, 15, 18, or 20 MeV. For historical reasons a photon beam is usually characterized by the acceleration potential difference necessary to achieve the required energy: 4 MV, 6 MV, 15 MV, 18 MV or 20 MV. The effective energy of a bremsstrahlung spectrum is the energy of a monochromatic photon beam with equal absorption characteristics. As a rule of thumb the effective energy is one third of the high energy endpoint. Thus, a 4 MV linac beam has an effective energy of about 1.3 MeV, with properties comparable to Cobalt-60 teletherapy units.

Linacs are enormously versatile instruments. In *photon mode* they are often equipped with *multi leaf collimators* (MLC), a prerequisite for *intensity modulated radiation therapy* (IMRT) (Mayles, Nahum et al. 2007). Positioning precision and repeatability can reach sub-millimeter levels thus allowing for *stereotactic radiation therapy* in competition with the Cobalt-60 based *Gamma Knife®* (Elekta AB, Stockholm, Sweden). Importantly for this work, the bremsstrahlung target may be removed. In this configuration the linac is said to be in *electron mode*.

Electron mode

With the bremsstrahlung target removed, the narrow electron beam leaving the accelerator and bending magnet structures, would only irradiate a small area on the patient. Due to the strong charged-particle interaction with matter, the electron scatter off air molecules would, at a typical *source to skin distance* (SSD) of 100 cm, produce a several centimeter wide spot with a smooth radial intensity fall off. In such configuration the electron beam could be swept across the patient using an electromagnetic deflection system (dose painting).

In clinical practice this path is not followed because the required technology is complex and dose homogeneity is difficult to achieve. Instead, one or multiple stacks of thin metal foils (*scattering foils*) are inserted early in the electron beam's path, approximately at the location of the bremsstrahlung target. They are designed to fan out the electron beam in a controlled manner. Scattering foils, in combination with other internal or external components of the linac, are finely tuned to deliver an even spreading of the beam at treatment distance.

The range of nominal energies of electron beams corresponds to the range of maximum photon energies in the bremsstrahlung spectrum, i.e. typically from 4 MeV to 20 MeV. A more detailed discussion of the physical aspects of electron beams can be found in a later section.

External electron beam modalities

External beam radiotherapy (EBRT) uses electron particle beams in three distinct modalities: *Total-skin electron irradiation* (TSEI), *intraoperative electron radiotherapy* (IOERT) and *direct field irradiation* at standard or extended SSDs.

In TSEI, megavoltage electron beams are used in the treatment of cutaneous diseases that affect large parts or the entire body skin and require high doses in the first centimeter of tissue. Examples are *mycosis fungoides* (Le Bourgeois, Haddad et al. 1987) and *Kaposi's sarcoma* (Kuten, Stein et al. 1991). A scattered, uncollimated electron beam exiting the linac is directed towards a patient, who is standing with the legs spread and arms raised.

In IOERT the radiation treatment is administered directly to the tumor or affected area while they are exposed during surgery. It can be applied if the tumor is not completely resectable from critical normal tissue or if surrounding tissue may contain cancer cells. The patient usually receives a single high dose treatment without exposing nearby healthy organs to radiation. Special tubes are used to focus the beams safely on the tumor or the tumor bed. IOERT may be used with cancers of the head and neck, abdomen, pelvis and extremities and may help to preserve organ functionality (Hu, Enker et al. 2002).

This thesis is about the direct irradiation of fields on the patient's skin, a more conventional technique which is similar to external photon beam therapy. But while photons are electrically neutral, electrons are light, electrically charged particles. They interact intensely with matter and are easily deflected by scattering off air molecules. Thus, to define the irradiated area, a metal plate with an appropriately shaped hole is positioned at a distance of a few centimeters above the patient's skin. Because of their finite range and deep tissue sparing properties, direct irradiation of fields with electron beams is only useful for managing superficial lesions up to a depth of typically 5 cm. This includes but is not limited to cancers of the head and neck, electron boosts in breast cancer radiation therapy and irradiation of lymph nodes in the treatment of colon cancer.

Direct field irradiation with electrons

Many particularities of external electron beam therapy are due to the electrons being light, electrically charged particles which, compared to photons, experience a much higher interaction probability with matter:

- The scattering off air molecules changes the electron's direction, making it impossible to use the linac jaws to accurately define the field at the treatment distance.
- The range of electrons in water or tissue is finite giving rise to a depth-dose distribution that has hardly any contribution beyond a *practical range*.
- In tissue, electron scattering leads to a significant loss of dose in directly irradiated areas close to the field boundaries. Here, lost electron fluence is not replaced by contributions from surrounding sites. Consequently, a significant dose can be found in adjacent tissue which is not in the electron beam's line-of-sight. This "bulging out" effect exists for fields of all sizes and shapes but is most pronounced at low energies because electrons at the high end of the energy scale are more forward scattered.
- In the case of small field sizes whose radius is in the order of or smaller than the electron range, lateral scattering of electrons away from the central field axis leads to a significant drop of the maximum dose on this axis together with a shift of the dose maximum position towards the surface. A particular *output factor*, sometimes called *cutout factor*, is used to describe the change of dose at the dose maximum for an arbitrary cutout in relation to a standard 10x10 cm^2 field size.

To define the irradiation field on the patient's skin, a metal plate with an appropriately shaped hole is placed at a distance of several centimeters above the patient's skin (its bottom plane at about 5 cm above SSD=100 cm). Figure 1 shows a typical treatment setup for electron direct field irradiation (Rogers 2002).

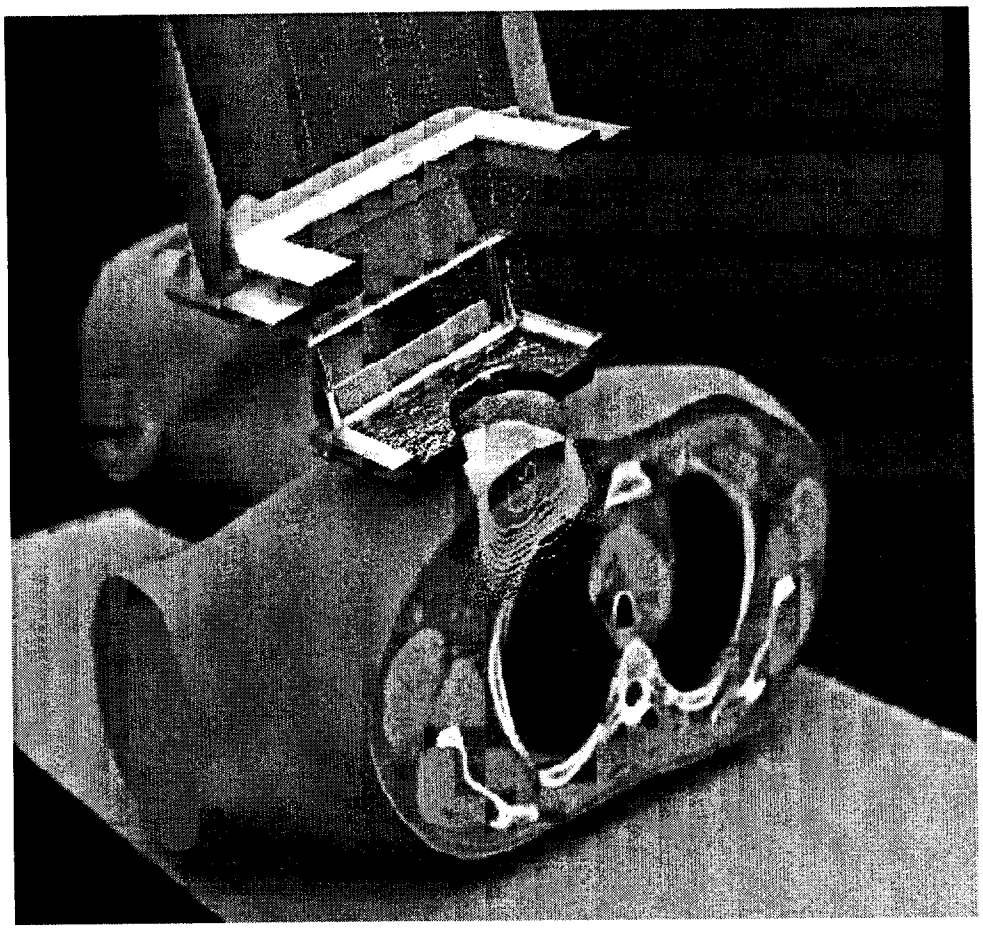

Figure 1: Linac accessories and patient setup for direct field electron radiotherapy

The plate is referred to as an *insert* or more graphically as *cutout*. The material for cutouts varies but *Cerrolow-136*® (Cerro Metal Products Co., Bellefonte, USA), a alloy of 49% bismuth, 18% lead, 12% tin, and 21% indium, is often used for its low melting range of 57-65°C and easy handling. This material has no distinct melting point. Liquid/solid solutions may exist over the range given. Use of the original *Cerrobend*® (50% bismuth, 26.7% lead, 13.3% tin, and 10% cadmium) is discouraged because of its cadmium contents. During cutout manufacturing the liquid alloy is poured into an aluminum mold frame where it remains for the duration of the treatment.

The mold frame with cutout is held in position by an accelerator accessory called *applicator* or *cone*. The applicator is a pagoda like structure of several scrapers which limit the electron beam's outer dimensions. The lowest scraper has a cradle for the mold frame. The overall dimensions of an applicator are typically 40 cm in

height and 30 cm in width. Scrapers are made from a variety of materials and connected to each other by rods. The applicator is attached to the linac by sliding it into an *accessory mount* or "*horseshoe*", as illustrated in Figure 2.

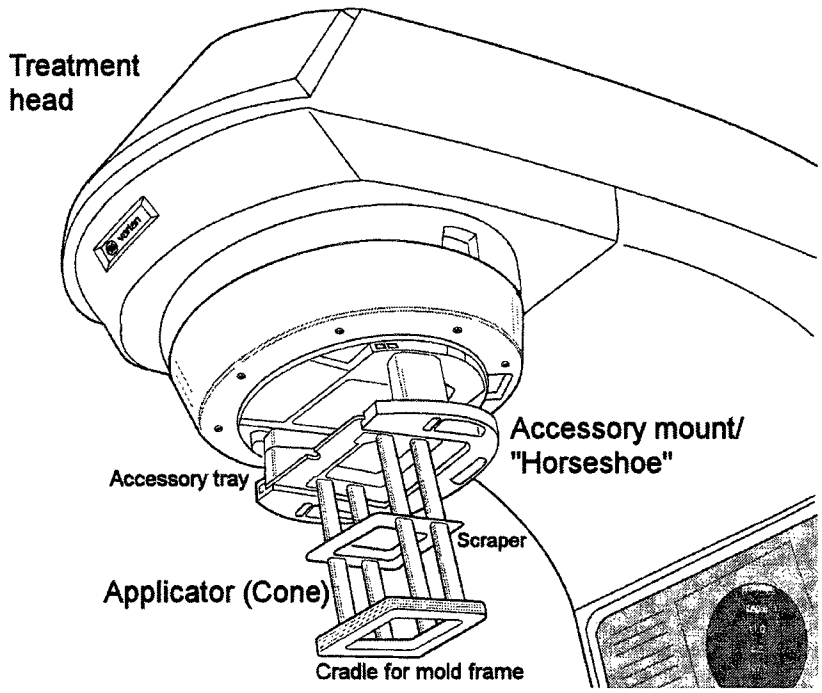

Figure 2: Electron applicator installed on a C-Series Clinac

Clinical electron beams

When operated in electron mode, the primary electron beam has a range of nominal energies that is often wider than in photon mode but with more steps. For example, the *Varian C-Series Clinac® CL21EX* (Varian Medical Systems, Palo Alto, USA) delivers 6 and 18 MV photons but is capable of 4, 6, 9, 12, 16 and 20 MeV electrons. Applicators exist for square and rectangular fields sizes between 6×6 and 25×25 cm^2.

The radiation that reaches the patient's skin is a complex mixture of both electron and photon particle fluences. The photons are created in bremsstrahlung events when electrons interact with the scattering foils, shielding material, jaws and finally with the applicator plus insert. Especially for high energies of 12 MeV and

above, the number of photons (with E>0.01 MeV) in the beam will exceed that of the electrons (with $E_{tot} > 0.7\,\mathrm{MeV}$. However, the photon contribution to the absorbed dose in the phantom will be at most 15%.

The beam properties of most interest for dosimetric purposes are:

- The percentage depth-dose along the beam axis in a water phantom.
- Output factors.
- The absolute output for the absorbed dose to water at a reference point or the dose maximum. Established with electron beam reference dosimetry.

Lateral dose profiles

To ensure reproducible dosimetric conditions at any treatment depth in the tissue, lateral dose profiles should be flat and symmetric around the central axis. Flatness is usually defined as the standard deviation of dose values within the central 80% of the field width, normalized to the on-axis value (given in %). A simpler way to measure the flatness F is to find the maximum $D_{\max}$ and minimum $D_{\min}$ within the central 80% of the field and use the relationship:

$$F = 100 \cdot \frac{D_{\max} - D_{\min}}{D_{\max} + D_{\min}} \%$$

Symmetry S can be assessed by determining the areas under a dose profile (for electrons taken at depth R_{100}) left and right of the central axis extending to the 50 % dose level of the central axis point:

$$S = 100 \cdot \frac{area_{left} - area_{right}}{area_{left} + area_{right}} \%$$

The AAPM-proposed tolerances for both beam flatness and symmetry are 3% (Kutcher, Coia et al. 1994).

Commissioning and QA procedures require profile measurements with "open" beams at all energies and applicator sizes. In case of the CL21EX, manufacturer-supplied steel cutouts are used, that define 6×6 cm^2, 10×10 cm^2, 15×15 cm^2, 20×20 cm^2 or 25×25 cm^2 fields at SSD=100 cm.

To ensure flat and symmetric lateral dose profiles, linac components are designed to deliver a homogenous particle fluence over the widest permissible beam cross-

section. To accomplish this, manufacturers ingeniously combine different sets of scattering foils with different jaw settings. Figure 3 is an example for a 10×10 cm^2 profile at 6 MeV measured with radiochromic film.

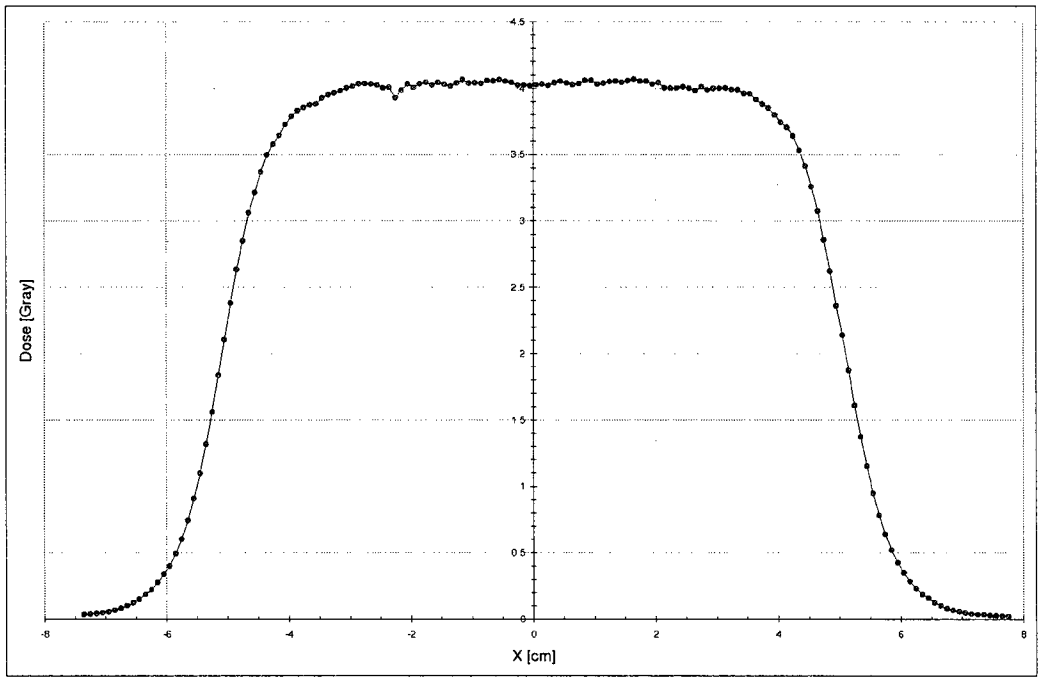

Figure 3: Profile for a 10×10 cm^2 cutout at the depth-dose maximum

Jaw settings

The collimator jaws open to a specific field size whenever an electron energy is selected at the console and an electron applicator is installed in the accessory mount. The following table lists the jaw settings for the Varian C-Series Clinacs:

Applicator size	4, 6, 9 MeV	12 MeV	15, 16 MeV	18, 20, 22 MeV
[cm^2]	[cm^2]	[cm^2]	[cm^2]	[cm^2]
6×6	20×20	11×11	11×11	11×11
6×10	16×13	16×11	16×10	16×10
10×10	20×20	14×14	14×14	14×14
15×15	20×20	17×17	17×17	17×17
20×20	25×25	25×25	23×23	22×22
25×25	30×30	30×30	28×28	27×27

Table 1: Collimator field sizes for different electron applicators and energies

Central axis percentage depth-dose (PDD)

Measured on the central beam axis, perpendicular to the surface, the central axis percentage depth-dose is the dose at a given depth expressed in percent of the maximum dose on this axis. PDD curves are used to characterize clinical electron beams and this work follows the guidelines and quantities laid out in the AAPM Report no. 32 of Task Group No. 25 (TG-25) (Khan, Doppke et al. 1991).

TG-25 proposes that the following parameters be used to characterize the electron central-axis depth-dose curves (See Figure 4):

- R_{100} – The depth of the dose maximum in water. R_{100}
- R_{90} and R_t – The depth of the deepest 90% dose level. This is a measure of the clinically useful portion of the electron PDD curve. The task group recommends R_{90} as the therapeutic range R_t which is a measure of the clinically useful portion of the electron PDD curve.
- R_{50} – The depth of the 50% dose level.
- R_P – The practical range. Determined from depth-dose or depth-ionization measurements as the depth of the point "where the tangent at the inflection point of the falloff portion of the [PDD] curve intersects the bremsstrahlung background".
- $\%D_S$ – The relative surface dose. Defined at 0.5 mm depth.
- $\%D_X$ – The relative dose from the x-ray (bremsstrahlung) component. Extrapolated from dose measurements beyond the maximum range of the electrons.

Note: This work also uses the term R_{80} for the depth of the 80% dose level.

When a water phantom is irradiated using a manufacturer-supplied reference cutout that defines a 10×10 cm^2 field at SSD=100 cm, the depth-dose exhibits several typical features:

- Very little dose is delivered beyond the practical range R_p, roughly equivalent to E[MeV]/2 (in centimeters).

- The dose beyond R_p is due to bremsstrahlung created mainly in the flattening filter. At higher energies the bremsstrahlung tail can reach nearly 10% of the dose maximum.
- For low to medium energies, the depth of the dose maximum increases with energy and scales with E[MeV]/5 (in centimeters). At high nominal energies around 20 MeV the maximum moves back towards the surface.
- The entrance skin dose increases monotonically with increasing energy from about 80% at 6 MeV to 95% at 20 MeV.

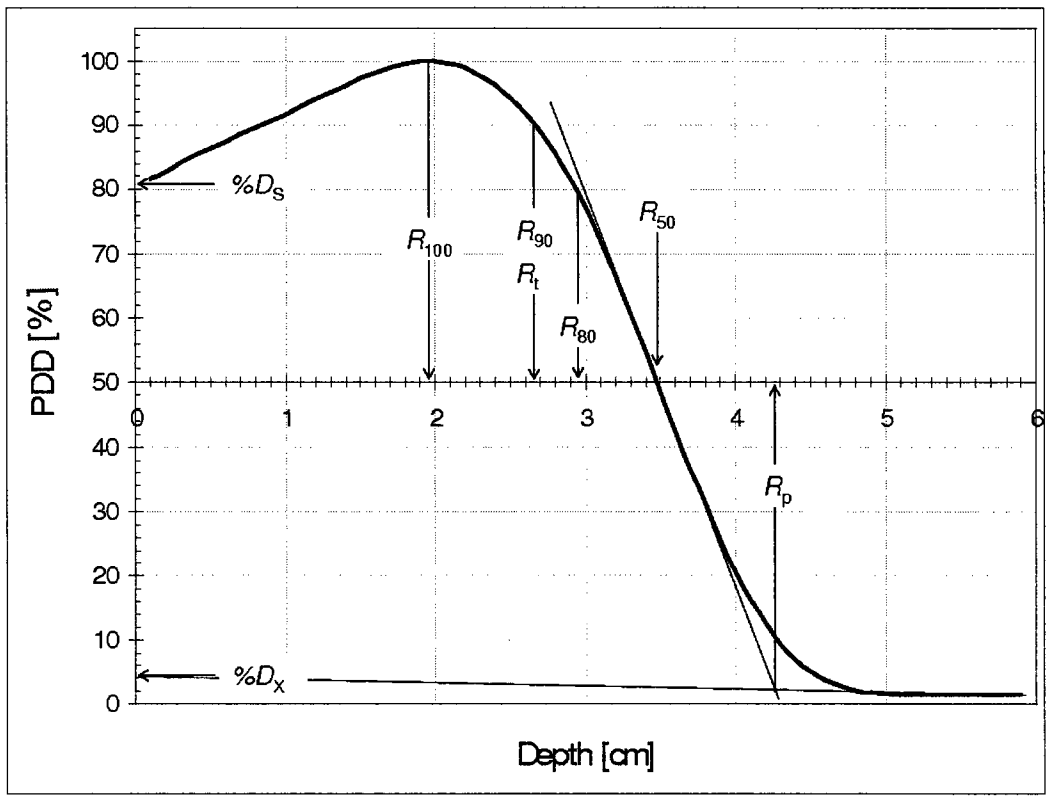

Figure 4: Parameters of an electron PDD curve (example for a 9 MeV beam)

Output factors

At all nominal energies, linacs are calibrated to deliver 100 cGy absorbed dose to water per 100 monitor units in the depth-dose maximum, for a 10x10 cm^2 fields and SSD=100 cm. When, under otherwise equal conditions, the reference cutout is changed to a different size or an arbitrary shape, the PDD curve and the

absolute dose at its maximum will most likely change too. An example is illustrated in Figure 5. PDDs were measured at 6 MeV with *GAFCHROMIC®* *EBT* film, a product of International Specialty Products, New Jersey, USA.

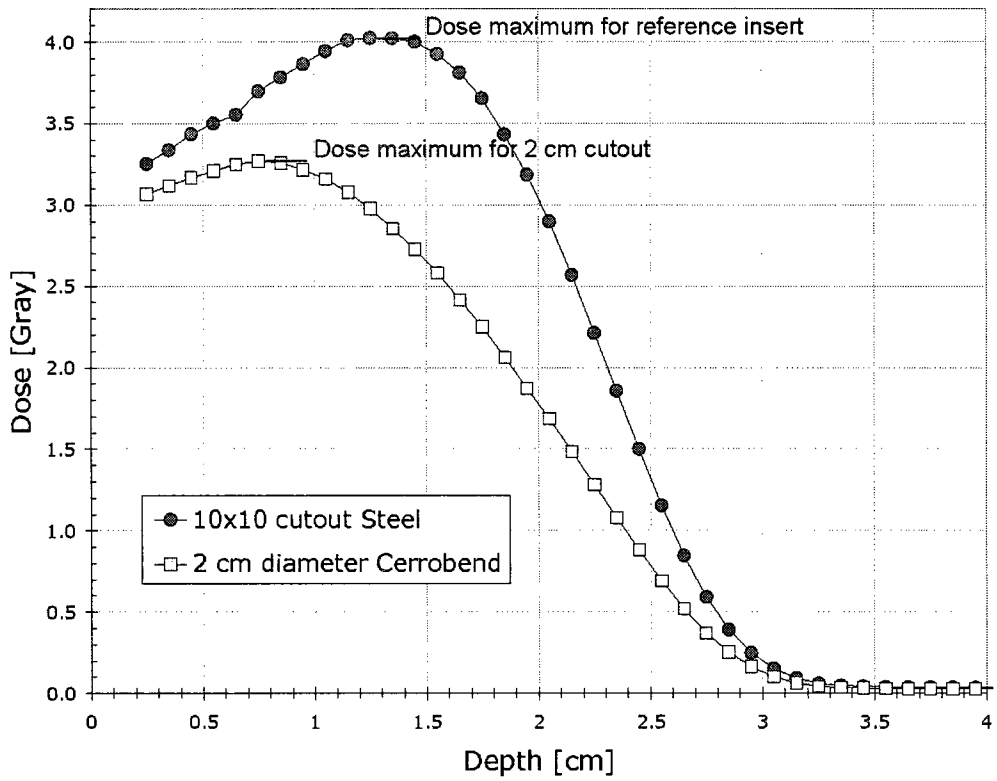

Figure 5: Depth-dose distributions for a 10×10 cm^2 applicator and a 2 cm diameter cutout

Report TG-25 provides a comprehensive analysis of the mechanisms that lead to output changes in the depth-dose profiles. These are some of the processes that contribute to this effect:

- Different jaw positions for different combinations of nominal energies and applicator sizes lead to changes in the scattering patterns for both electrons and photons.
- Different sets of scattering foils for different energies produce changes in the scattering pattern for electrons and the (energy) fluence of bremsstrahlung photons.

- As the size of the cutout becomes smaller, the dose contributions from electrons scattered into the phantom from the inside faces of the cutout increase.
- As the size of the cutout becomes smaller, the effect of dose bleeding becomes more noticeable. Due to the multiple scattering of electrons in the phantom, dose "moves" away from the central axis and does not get replaced with off-axis contributions. This effect is also referred to as loss of *lateral equilibrium.*

TG-25 goes on to define the quantity *output factor* $OF(F)$ as "the ratio of dose D_F per monitor unit U at d_{max}, for a given field size F to that for the reference field size F_0 at its own $d_{max,0}$":

$$OF(F) = \frac{D_F / U(F, d_{max})}{D_{F_0} / U(F_0, d_{max})}$$

Clinically, D_F and D_{F_0} are measured using the same number of monitor units and the output factor simply becomes the ratio D_F / D_{F_0}. The output factor is often multiplied by 100 and reported as the dose output in cGy per 100 monitor units, e.g. 94.3 cGy/100 MU.

This definition essentially prescribes a measurement of two ionization readings at the depth-dose maxima. One for the clinical cutout and one for a 10×10 cm^2 reference field. The output factor is the ratio of these two, ideally stopping power ratio corrected, values.

Electron beam reference dosimetry

The goal of reference dosimetry is to establish the absolute absorbed dose to water output of a linac at a reference point in a water phantom. The dose at the dose maximum can then be determined from the known PPD curve. Customarily, linacs are adjusted to deliver 100 cGy per 100 monitor units (MU) at the point of depth-dose maximum on the central axis for a 10×10 cm^2 field at 100 cm SSD.

In North America, "*AAPM's TG-51 protocol for clinical reference dosimetry of high-energy photon and electron beams*" (Almond, Biggs et al. 1999) has been

adopted as the standard procedure for electron beams between 4 and 50 MeV (and for photon beams with nominal energies between ^{60}Co and 50 MV). The following outlines the *electron protocol*:

- The protocol uses cylindrical or plane-parallel ion chambers with absorbed-dose-to-water calibration factors, $N_{D,w}^{60Co}$, which are traceable to national primary standards.
- The absorbed dose to water for a clinical beam of quality Q is $D_w^Q = M\, k_Q N_{D,w}^{60Co}$. M is the fully corrected ion chamber reading and k_Q is the quality conversion factor. Ionization is proportional to the chamber reading which measures a charge.
- Values of k_Q are presented as a function of Q for many ion chambers.
- Beam quality Q is specified for electron beams by R_{50}, measured in a beam with field size 10×10 cm^2 on the surface of a water phantom at an SSD of 100 cm ($\geq 20\times20$ cm^2 for R_{50}>8.5 cm).
- The beam quality specifier, R_{50}, is determined from the measured value of the 50% ionization depth I_{50}:

  $R_{50} = 1.029\, I_{50} - 0.06\, cm$ (for $2 \leq I_{50} \leq 10$ cm) or

  $R_{50} = 1.059\, I_{50} - 0.37\, cm$ (for $I_{50} > 10$ cm)

- The reference depth d_{ref} for calibration purposes is $0.6\, R_{50} - 0.1\, cm$. It is the depth at which the *point of measurement* of the ion chamber is placed to measure the absorbed dose. "The point of measurement for a cylindrical chamber is on the central axis of the chamber and this is always placed at the reference depth when measuring dose at an individual point (as opposed to a depth-dose curve)."

One can see that the percentage depth-ionization (PDI) curve is central to the TG-51 protocol. From it I_{50} is determined, whose value is then used to calculate R_{50} and ultimately d_{ref}.

When the PDI curve is multiplied with the depth-dependent water-to-air stopping-power ratio, the result is a percentage depth-dose curve, which in turn can be used to determine the absorbed dose to water at the dose maximum from the dose at d_{ref}. Details of the stopping-power ratio correction are discussed in the next paragraph.

After the initial measurement of the PDI curve, a correction for the effective point of measurement may have to be applied: For cylindrical chambers the PDI is shifted to shallower depths by $0.5 r_{cav}$. No correction is necessary for plane-parallel chambers, where the point of measurement and effective point of measurement coincide with front (upstream) face of the chamber air cavity.

It is noteworthy that:

- For measurements of the absolute dose at the reference depth d_{ref}, a cylindrical ion chamber's point of measurement (center of chamber) is placed at the reference depth. No correction for the effective point of measurement is necessary since the gradient effects are implicitly included in the correction term P_{gr}^{Q} for electrons. However, relative dose measurements, as in the case of output factors, require a correction for the effective point of measurement, i.e. the center of a cylindrical chamber must be at $R_{\max} + 0.5 r_{cav}$.
- In TG-51, R_{50} can also be determined from a depth-ionization curve for an ion chamber converted into a depth-dose curve [with the stopping power ratio correction].
- The TG-51 protocol allows the use of a "good-quality" diode detector to determine R_{50} in an electron beam. No stopping power ratio correction is necessary.

The water-to-air stopping power ratio correction

In PDD measurements, the quantity of clinical interest for our application is the absorbed dose-to-water. The electrometer reading of an air-filled ion chamber measures the ionization in air, which is proportional to dose-to-air. The transition

from dose-to-air to dose-to-water is dealt with in Bragg-Gray and Spencer-Attix cavity ionization theories.

According to these theories, dose-to-water can be determined from dose-to-air measurements, by multiplying the latter quantity with the ratio of effective mass collision stopping powers in water and air. *Effective* mass collision stopping power, because it is averaged over the differential charged particle fluence spectrum Φ_P at the point-of-interest.

Spencer-Attix theory introduces the concept of restricted stopping powers $\overline{L}$ and is considered more accurate. The applicable correction factor is called restricted mass collision stopping-power ratio:

$$\left(\frac{\overline{L}}{\rho}\right)_{air}^{water} = \frac{\int_0^{E_{max}} \Phi_P \left[\overline{L}/\rho\right]_{water} dE}{\int_0^{E_{max}} \Phi_P \left[\overline{L}/\rho\right]_{air} dE}$$

When a megavolt photon beam transverses a water phantom, photons are removed from the beam in Compton scattering, pair production and photo effect events. These interactions create a fluence of electrons (including knock-on electrons or δ-rays) and positrons. As the photon beam transverses the phantom, some beam hardening occurs due to the photo effect, leading to a slight decrease of low-energy photon fluence. Similarly, preferentially high energy photons are removed because of pair production. At therapeutic energies between 1 and 20 MeV the dominant interaction is Compton scattering which affects photons in this energy range equally. The photon beam becomes weaker but does not change its quality. Thus the differential fluence spectrum of primary and secondary charged particles remains essentially constant at all depths at which charged particle equilibrium (CPE) has been reached. The practical consequence is that there is little change in the mass collision stopping-power ratio with depth.

For clinical electron beams with nominal energies between 4 and 20 MeV the situation is quite different. In this energy range, the energy loss in water amounts to approximately 2 MeV per cm path length. As the primary electrons move

deeper into the water phantom the smaller becomes their kinetic energy. The differential fluence spectrum of primary and secondary electrons is thus shifted towards lower energies with increasing depth and the water-to-air restricted mass collision stopping-power ratio becomes depth dependent.

In practice, the mass collision stopping-power ratio can not be determined with the above formula because the differential charged particle fluence spectrum Φ_p is generally not known. Burns et al. used Monte Carlo simulations to calculate mass collision stopping-power ratios at various depths for clinical electron beams, characterized by R_{50} values between 0.98 and 18.6 cm (Burns, Ding et al. 1996). They fit a empirical function of the form

$$\left(\frac{\bar{L}}{\rho}\right)_{air}^{water}(R_{50},z)=\frac{a+b(\ln R_{50})+c(\ln R_{50})^2+d(z/R_{50})}{1+e(\ln R_{50})+f(\ln R_{50})^2+g(\ln R_{50})^3+h(z/R_{50})}$$

to the simulation results and obtain the following eight coefficients:

$a=1.0752$	$b=-0.50867$	$c=0.088670$
$d=-0.08402$	$e=-0.42806$	$f=0.064627$
$g=0.003085$	$h=-0.12460$	

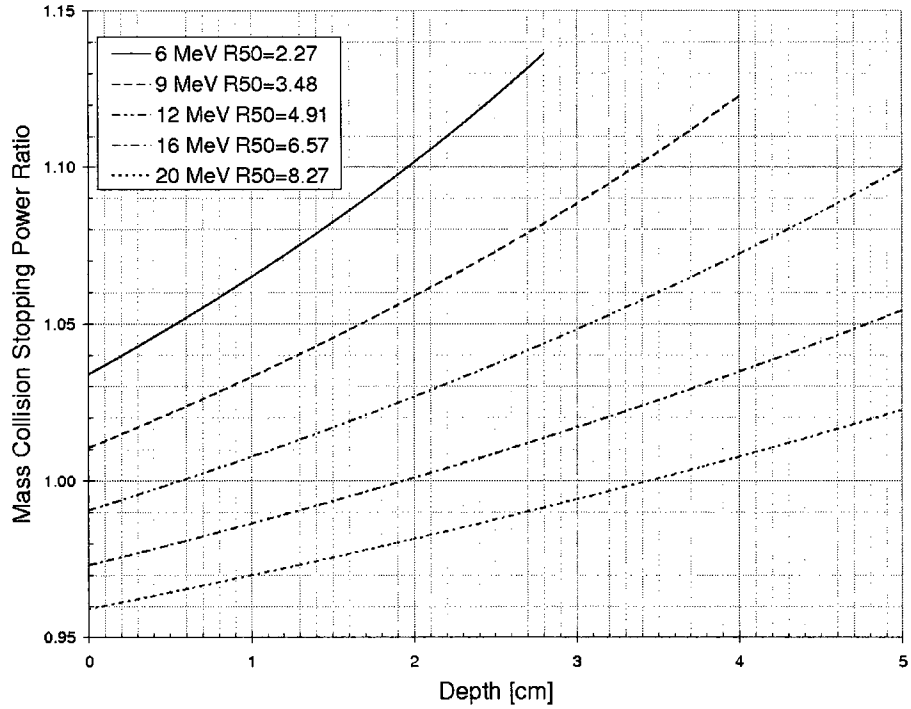

Figure 6: Mass collision stopping power ratio vs. depth (Burns, Ding et al. 1996)

For z/R_{50} ranging between 0.2 and 1.1 the fit function has an rms deviation of 0.4% and a maximum deviation of 1% from the Monte Carlo simulation value. At greater depths up to $z/R_{50} = 1.2$ the maximum deviation increases to 1.7%. Figure 6 plots Burns' empirical function vs. depth for R_{50} values from measurements at the Clinac 21EX(B).

Quality assurance procedures

In North America, the quality assurance procedures outlined in the AAPM's TG-40 report "*Comprehensive QA for Radiation Oncology*" are widely adopted (Kutcher, Coia et al. 1994). Many hospitals and oncology centers have implemented stricter procedures, frequencies or tolerances than those given in the report.

Of the many guidelines only a few are specifically concerned with electron beams:

- Daily electron output constancy checks have a tolerance of 3% of the nominal value. This tolerance is higher than the monthly and annual

checks because the measurement does not require temperature/pressure corrections.

- Monthly output constancy checks have a tolerance of 2% and require temperature/corrections.
- Annual electron output calibration constancy checks (reference dosimetry) have a tolerance of 2% .
- Annual electron output constancy vs. gantry angle checks have a tolerance of 2%.
- Electron beam flatness constancy (monthly) has a tolerance of 3%.
- Electron beam symmetry (monthly) has a tolerance of 3%.
- Output factor constancy (annually) has a tolerance of 2%.

It is stated in the report that the above tolerances together with many other limits placed on the electrical and mechanical performance of the linac, are intended to achieve an overall dosimetric uncertainty of ±5%.

A short history of electron accelerators

Attempts to accelerate electrons to megavolt energies date back to the year 1929 when Robert van de Graaff build the first model of a direct current electrostatic generator. This early machine only developed 80 kV but in 1933 a huge double generator was constructed in an airship hangar at Round Hill, Massachusetts, which delivered a voltage greater than 5 MV.

The first clinically used Van de Graaff was installed 1937 at the Huntington Memorial Hospital in Boston. It operated at over 1 MV. The second machine was at the Massachusetts General Hospital delivering electrons up to 1.25 MeV kinetic energy. Van de Graaffs were used until the early 1980s when they had been large replaced by betatrons and linear accelerators.

Betatrons accelerate electrons in a torus-shaped vacuum tube that serves as the secondary coil of a powerful HF transformer. The concept was developed in 1940 by Donald Kerst at the University of Illinois. The reachable energies are much higher than with a Van de Graff, up to about 300 MeV. From early on, Betatrons were used for radiotherapy at treatment energies up to 45 MeV. Treatment at laboratory Betatrons were at first experimental due to the large size and high cost.

Later, in the 1980s, smaller, clinical Betatrons became available but cost and low dose rate prevented a wide adoption of this technology. Around the same time microtrons, a combination of linear accelerator and cyclotron, became available for electron acceleration. Ultimately the simpler design of a linear accelerator won out with the additional advantage of being able to deliver photon AND electron beams.

Clinical practice at the Montreal General Hospital

At the time of writing, direct field irradiation with electron beams at the MGH is almost exclusively performed using two *Varian Clinac® 21EX* accelerators, A and B. Linac *CL21EX(A)* is capable of delivering electrons at nominal energies 4, 6 9, 12 and 16 MeV, although 4 MeV is not used clinically. *CL21EX(B)* covers the energies 6, 9 ,12, 16 and 20 MeV. Calibration and tuning of both machines is such that they virtually perform identically. Cases that require higher energies or setups not available at the CL21EXs are occasionally treated on a *Varian Clinac® 2300* whose nominal energies are 6, 9, 12, 15, 18, 22 MeV.

Applicators for the *Clinac® 21EX* come in sizes that can accommodate 6x6 cm^2, 6×10 cm^2, 10×10 cm^2, 15×15 cm^2, 20×20 cm^2 and 25×25 cm^2 mold trays.

Making the mold: Steps involved in making a cutout

In its user's guide for the *Clinac® 21EX*, Varian suggests a procedure that is remarkably hands-on:

- With a pen, the radiation oncologist first outlines the contours of the irradiation field on the patient's skin.
- The smallest mold tray capable of accommodating a cutout for the desired shape size is chosen. A thin, transparent plastic cover plate is placed and secured inside the mold tray where it sits just above the top plane of the cutout. Mold tray plus cover plate are inserted into the bottom shield of the mounted applicator.
- With the field light turned on, an outline of the treatment field is traced on the cover plate with a felt tip or grease pen.

- For cutout fabrication the mold frame is removed from the applicator and the outlines drawn on the cover plate are transferred to a piece of *Styrofoam*® (Dow Chemical Company, Midland, USA) which is subsequently cut with a band saw.
- To avoid leakage, gaps between mold frame and cover plate are sealed with tape. The Styrofoam shape, which is a negative of the cutout hole, is aligned with the outline on the cover plate and secured with something heavy to prevent shifting.
- Molten *Cerrobend*® is poured into the volume around the *Styrofoam*® shape. When the *Cerrobend*® has solidified, cover plate and *Styrofoam*® plug are removed and some finishing machining is done on the cutout. The cutout thickness varies between 15-20 mm.

Prescriptions

Therapeutic prescriptions should follow ICRU Report 71 "Prescribing, Recording, and Reporting Electron Beam Therapy" (International Commission on Radiation Units and Measurements. 2004). According to the report, the radiation oncologist should select beam energy and beam delivery system (cutout shape and applicator size) so that the maximum of the depth-dose curve is reached in the center or (or central part) of the planning tumor/target volume PTV. The ICRU reference point for reporting should always be selected at the centre (or in the central part) of the PTV and should be clearly indicated. If these conditions are met, the dose maximum occurs in the center (or central part) of the PVT. The following dose values should be reported:

- The peak absorbed dose to water.
- Location of and dose value at the ICRU reference point if not located at the level of the peak-absorbed dose.
- The maximum and minimum dose in the PTV, and dose(s) to organ(s) at risk (OAR) derived from dose distributions and/or dose volume histograms.

In hospital practice, treatment doses are often prescribed to the R_{80} depth. At the same time maximum and minimum dose in the PTV and doses to OARs are usually NOT available because treatment planning systems (TPS) are rarely used in electron therapy planning. For the selection of beam energy the radiation oncologist relies on the PPDs measured for 10×10 cm^2 cutouts or open fields and on experience since PDD data for small or irregularly shaped cutouts is usually not available.

Clinical output factor measurements

At the Montreal General Hospital there are two setups for measuring output factors. If, in relation to a 10×10 field, no significant shift of R_{max} is expected, an NE 2571 thimble type ionization chamber (NE Technology Ltd., Reading, UK) is used in combination with a $30\times30\times10$ cm^3 *Solid Water*® (Gammex Inc., USA) phantom. The phantom has three channels whose centers correspond to the R_{max} in solid water at the nominal energies. Each linac has its custom made phantom. This is an example for the CL21EX(B):

- 4, 6 MeV: Center at 1.56 cm. At 4 MeV this position corresponds to R_{50}.
- 9 MeV: Center at 2.3 cm.
- 12, 16 MeV: Center at 3.1 cm. This position is also used for 20 MeV.

The NE 2571 ion chamber is tightly embedded in a cylindrical solid water block which also serves as a buildup cap around the sensitive volume. When this cylinder is completely inserted into one of the channels, the center of the ion chamber coincides with center markings on the phantom's surface. It is thus easy to position the ion chamber either on the beam axis or at the point of interest for an arbitrarily shaped cutout.

Some specifications of the NE 2571 chamber may be of interest. The radius of the sensitive volume is 3.15 mm, height is 2.4 cm, surrounded by a 0.375 mm graphite wall of 1.7 g/cm^3. The central electrode is made of aluminum and has a diameter of 1 mm. It becomes clear that, due its lengthy geometry, NE 2571 should only be used when the ionization is sufficiently constant along its axis and tip and bottom of the sensitive volume are not getting too close ($< R_{max}$) to the

field boundaries. It takes about 15 minutes to set up and execute this kind of measurement.

As the cutout becomes smaller, irregular or exhibits narrow structures a shift of R_{max} towards shallower depths is expected and a determination of R_{max} is called for. An additional complication arises for curved or narrow fields when it is difficult to define the point of interest for the output factor measurement.

The setup used for this kind of measurement consists of a Markus plane-parallel ion chamber (PTW, Freiburg, Germany), a $20\times20\times3$ cm^3 solid water plate and several 20×20 cm^2 solid water slabs whose thicknesses vary between 1 and 5 millimeters. The solid water plate possesses a 3 cm diameter circular recess that receives the *Markus*® chamber and a narrow slit for the wiring. When installed, the surface of the plate is flush with the top of the chamber.

Specifications of the Markus chamber are as follows: Effective diameter of the collection volume is 4.5 mm, plate separation is 2 mm and the entrance window is ~2.5 mg/cm^2 polyethylene (~0.03 mm). With such a thin membrane the effective point of measurement can be assumed to coincide with the upper window surface. The narrow and shallow effective volume makes this chamber a preferred choice for PID/PDD measurements, with the disadvantage of small charge collection efficiency.

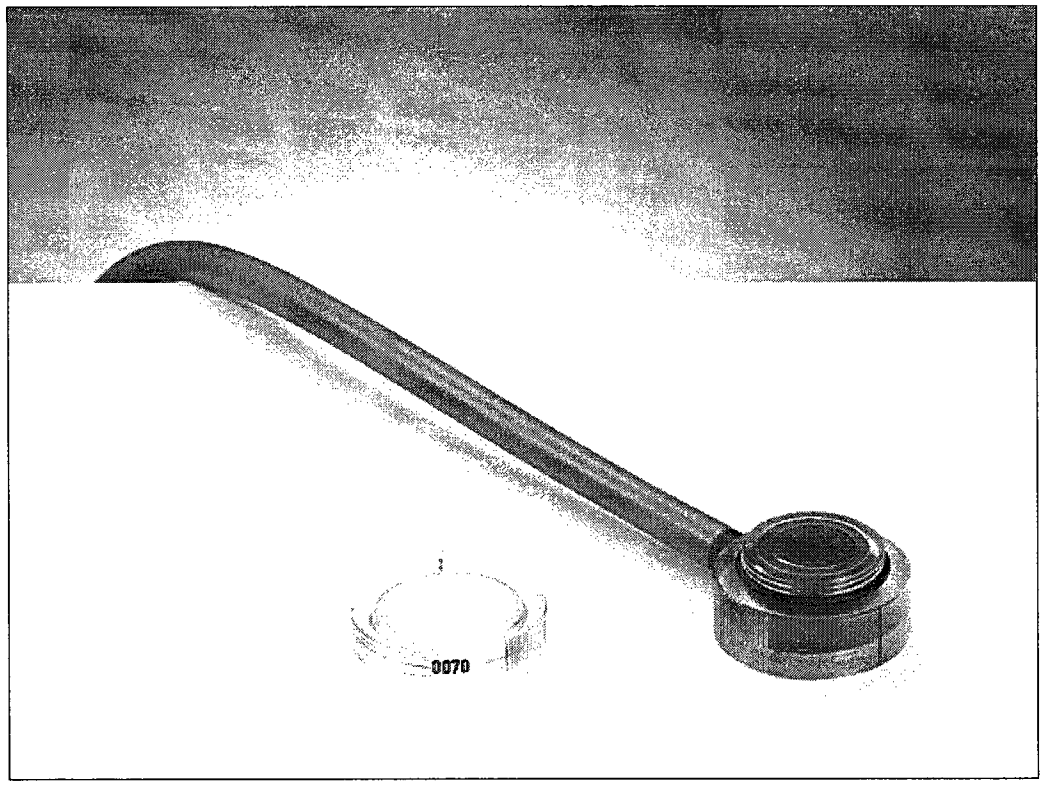

Figure 7: A PTW *Advanced Markus® Electron Chamber*

To measure R_{max} , ionization measurements are performed at varying (*Solid Water®*) depths by placing appropriate combinations of the thin *Solid Water®* slabs on the detector plate. The upper surface of the top slab must always be kept at SSD=100 cm. The resulting PID curve is usually not corrected for stopping power ratios and taken as PDD. Once R_{max} has been found, 2-3 ionization reading are recorded. The same procedure is followed to establish the reference dose for the 10x10 field and the output factor is calculated. It takes about 25 minutes to set up and execute this kind of measurement.

It is difficult to say at which point the measurement setup should switch from the *Solid Water®* phantom to the more time consuming, but potentially more accurate slab technique. At low nominal energies, the lateral scattering of the electrons in the phantom is more pronounced – at higher energies the electrons are more forward peaked. Measurements of circular cutouts show that R_{max} shifts occur when the radius of the cutout hole approaches or falls below R_{max} of a 10×10 cm^2 field.

Accuracy considerations

Particularly the solid water phantom technique is prone to systematic errors. The depths at which the channels are drilled, were determined at the time of linac commissioning. With time, the beam quality changes and shifts of R_{max} occur. A recent PDD measurement with an IC-10 ion chamber (IBA Dosimetry AB, Uppsala, Sweden) and a water phantom reveals large deviations of the phantom depth from the actual (water) values: +30% at 6 MeV (phantom 1.56 cm, measured 1.20 cm), +20% at 9 MeV (phantom 2.3 cm, measured 1.97 cm), +12% at 12 MeV (phantom 3.1 cm, measured 2.76 cm) and –4% at 16 MeV (phantom 3.1 cm, measured 3.34 cm).

While the PID/PDD curve is relatively flat around R_{max} at higher energies, the situation is disturbing for the more "peaked" PDD distributions at 6, 9 and 12 MeV. Here the measurement actually takes place on the high gradient slope above R_{max}, and small variations of the PID shape can lead to large deviations in the ionization readings. This, together with the NE 2571's less than ideal geometry, leads to a rather poor conservative accuracy estimate of 3-5% for small cutouts. Output factor measurements are relative measurements, and one could argue that a positioning offset would still result in the correct dose ratio. This is only true for cutouts that do not alter the depth-dose shape. But these cutouts usually have unity output factors anyway and do not require dose corrections.

Numerical determination of output factors

Output factors for arbitrarily shaped electron beams are usually determined by direct dose measurement in a phantom under near-treatment conditions. There was always an interest to substitute output factor measurements with calculation methods but due to difficulty in establishing suitable algorithms and parameterization methods few centers rely on calculations. A notable development are modern treatment planning systems like *Eclipse*® (Varian Medical Systems, Palo Alto, USA) which offers a parameterized calculation model (Generalized Gaussian Pencil Beam, GPB) as well as a Monte Carlo simulation based algorithm (Electron Monte Carlo, eMC).

Historically, the use of cutouts to arbitrarily define field contours was preceded by sets of lead blocks, arranged on a tray. These blocks approximated the tumor contours with a superposition of rectangles. Thus, much work from the late 70s and early 80s focused on OF calculations for square or rectangular fields.

In an attempt to calculate electron beam dose distributions in inhomogeneous tissue, Hogstrom et al. calculated isodose lines using an algorithm that sums contributions from individual pencil beams (Hogstrom, Mills et al. 1981). They used measured square-field depth-dose data as input for the calculations and modeled the side scatter with the Fermi-Eyges theory of thick-target multiple Coulomb scattering. They derive a mathematical expression for output factors from their depth-dose formulas.

In the same year, the same authors published a paper that aimed to predict electron beam output factors for square and rectangular electron beams (Mills, Hogstrom et al. 1982). Using the same pencil beam approach and side scatter model as before, they come up with a function whose 2 parameters are fit to measured data from an AECL Therac-20 medical linear accelerator (Atomic Energy of Canada Limited, Mississauga, ON Canada). The authors claim that their data, calculated for a wide range of square and rectangular fields, agrees within approximately 1.7% with the measured values.

Output factors for arbitrarily shaped fields were calculated by Bruinvis et al. (Bruinvis, Van Amstel et al. 1983; Bruinvis, van Amstel et al. 1983). Their method is based on a Gaussian pencil beam model that has one pencil beam for the primary beam and one pencil beam for the electrons coming from the field-defining block. In combination with a Clarkson type integration method the authors claim to be able to reduce the difference between calculation and measurement to 2% or lower.

Driven by the desire to devise a method suitable for a "programmable calculator", Mills et al. published a paper that finds that the output of a rectangular field X,Y is given as $OF(X,Y)=OF(X,10)\times OF(10,Y)$ (Mills, Hogstrom et al. 1985). To determine the output factors OF(X,10) and OF(10,Y), they would take sets of

measured output factors for rectangular fields with one 10 cm side and fit a 4^{th} order polynomial function to the data.

Until the mid 90s more papers were published that tried to determine output factors using similar semi empirical analytical dose calculation algorithms, fits of parameterized equations to measured data, Clarkson type integration or combinations thereof (Chen 1988), (McParland 1989; McParland 1989), (Jones, Andre et al. 1990), (McParland 1992), (Muller-Runkel 1992), (Tenhunen and Lahtinen 1994), (Kurup, Glasgow et al. 1995) and (Jursinic and Mueller 1997). In essence, the reported deviation from measured values is in the order of 2% or smaller for simple shapes.

The mechanisms that underlie dose deposition of electron beams are very complex. The accelerated electron beam, a primary collimator, scattering foils, shielding, jaws, windows, the applicator and finally the cutout, determine the particle fluence that impinges on the patient. In the mid 1970s powerful computer mainframes became available and with their emergence many complex science problems that resist analytical description were successfully solved using the Monte Carlo simulation method. This method repeatedly follows the development of a physical system based on interaction probabilities instead of closed equations. Starting from a well defined initial state, thousands if not millions of histories are repeated, each slightly different from the other because random numbers decide on the outcome of a particular interaction or transition. Physical quantities can be extracted and scored as the system develops. Their systematic errors (accuracy) are usually due to model limitations, whereas the statistical error (precision) is a function of the number of histories.

Since the 1980s the high energy physics community massively applies Monte Carlo simulations to efficiency calculations of high energy particle detectors. In medical physics it took until 1998 for a calculation of electron beam output factors based on Monte Carlo simulations to appear (Kapur, Ma et al. 1998), although other MC based work related to dosimetric problems had been done years before. The breakthrough was probably caused by the emergence of *BEAM*,

a Monte Carlo simulation environment for radiotherapy treatment units based on the *EGS4* code system (Rogers, Faddegon et al. 1995).

In their work, Kapur et al. model the electron mode of the popular Varian Clinac 2100C linear accelerator. They analyze the photon and electron contributions to the depth-dose curve and lateral profiles coming from various parts of the linac. Calculated output factors for square fields at SSD 100 cm between 1×1 cm^2 and 20×20 cm^2 and applicable cone sizes agree within their statistical uncertainty (1-2%) with the measured data.

Similarly, Zhang et al. model a Siemens MD2 linear accelerator . They report that their calculated output factors for square fields at standard and extended SSD (115 cm) agree with careful diode measurements within 1% except for the smallest cutouts at extended SSD where the deviation is about 1.5%.

While the latter papers rather explore the feasibility of the method and analyze radiation components to explain the patterns of dose deposition, Verhaegen et al. have a more applied and clinically relevant focus (Verhaegen, Mubata et al. 2001). They model a Varian Clinac 2100C and a Varian Clinac 2100CD with the same nominal energies but different primary electron energies and show that their *EGS4/BEAM* model delivers accurate output factors for both linacs. In an attempt to study arbitrarily shaped contours, their selection of fields includes circular cutouts with diameters between 2 and 8 cm. Taking into account the lateral dimensions of the plane parallel ion chambers (NACP, PTW/Markus), the output factors obtained from measurements agree with the Monte Carlo simulations within 2%. The authors conclude that MC simulations of linear accelerators can be used to calculate output factors reliably. The models reproduce dose profiles correctly and render them feasible for treatment planning systems. To speed up calculations, it is suggested that particle transport in the cutout shall be limited to a thin "skin" region of 1-5 mm, depending on the electron energy.

Finally, Turian et al. combine Monte Carlo simulations with semi empirical analytical methods (Turian, Smith et al. 2004). For square, circular, semi-circular, rectangular and elliptical standard shapes of varying size, they calculate output factors and fit the result to polynomial functions. The variables of these functions

are the cutout dimensions. The authors claim that their method could be used with about 99% of the clinically used cutouts and that they have resulted in tremendous labor savings!

It is interesting to note that up to the year 2004 no work was published that addressed output factor calculations for cutouts with truly irregular contours. Around that time, in the Medical Physics Unit of McGill University, J. Seuntjens, with the help of F. Verhaegen, developed a first version of *cutout*, an *EGSnrc* user code to transport particles emerging from a phase space file through a arbitrarily shaped block and score the depth-dose in a water phantom. The *EGSnrc* code was complemented with a graphical user interface, written by François DeBlois, that implemented essential functions to define cutout shapes and treatment parameters and controlled job execution. The system was called *Cutout Manager* and ran on a Linux platform. In her M.Sc. thesis C. Albaret describes and evaluates this "Automated System for Monte Carlo determination of cutout factors of arbitrarily shaped electron beams" (Albaret 2004).

Motivation for this work

Compared with clinical measurements, computational determination of output factors based on Monte Carlo simulations has the potential of delivering accurate results with superior precision within minutes. At the same time accurate PDD curves become available for review by the radiation oncologist. In the case of irregularly shaped cutouts, where the location of the dose maximum is in doubt, the analysis can be done for several points of interest or even on a pre-defined grid.

Another practical reason for a computer-based system is that the calculations can be performed at any time and do not have to wait for the linac to become available after the scheduled patient treatments.

The present master thesis is an extension of the earlier work done by Jan Seuntjens, Frank Verhaegen, François DeBlois and Claude Albaret. Its goal is to upgrade the Linux *Cutout Manager* to a stand-alone software application for a multi-core workstation which uses the latest *EGSnrc* version, *EGSnrcMP* (Release V4-2-2-5) and to validate its operation.

Chapter 2 – USER'S GUIDE

This chapter is a guide to the new *Cutout Manager* application that was developed as part of the present master thesis. We give an overview of its key capabilities and a detailed description of the user interface and program parameters.

Key capabilities

The *Cutout Manager* is a complex software system that integrates a task oriented user interface for managing *cutout jobs* and the *EGSnrc* particle transport code on the basis of the *Mac OS X*® operating system. All three aspects of the system are represented in following list of key capabilities:

- Cutout job management in *user mode – Cutout Browser*.
  - Scrollable list of existing cutout jobs.
  - Listbox columns for linac name, energy, applicator size, patient ID, field name and job status.
  - Cutout jobs can be sorted by any column header in any order.
  - Display the completion progress for running jobs in near real time.
  - Apply filters for linac, energy and the applicator size on the cutout job list. Advanced display filtering is realized using *regular expressions*.
  - Automatic preview of the cutout shape for a selected job.
  - Display output factor, R_{max}, R_{90} and R_{80} for a selected job.
  - Job log can be displayed for the selected job after completion.
  - Depth dose information is accessible for the selected job during execution and after completion.
  - PDD curve can be displayed for the selected job during execution and after completion..
- Job Control in *user mode – Cutout Browser*.
  - Load an existing cutout job into the *Cutout Workbench* for editing.
  - Start the execution of the selected cutout job.
  - Clear the results of an earlier run for the selected cutout job.
  - Delete a cutout job.

- Cutout job parameter management in *user mode – Cutout Workbench.*
    - Enter/modify **patient first** and **last name**.
    - Enter a **7 digit numerical ID number**.
    - Enter a **field name** descriptor to record additional information.
    - Enter/change the **physicist's initials**.
    - Select the **accelerator model**.
    - Select the **nominal energy**.
    - Select the **applicator (cone) size**.
    - Enter/ modify the **cutout shape**.
    - Move the **point of interest** for dose calculations.
    - Select the **cutout material** and the **gap material**.
    - Enter/ modify the **cutout thickness**.
    - Enter/ modify the **source to skin (SSD) distance**.
    - Save the cutout job to the *Cutout Browser* job list.
    - Clear all user definable field in the *Cutout Workbench.*
- *EGSnrc* parameters in *expert mode.*
    - Enter/change the **number of particle histories** to control the precision of output factor calculations.
    - Select whether the program calculates a **dose distribution**, generates an **output phase space file** or both (Output type).
    - Display the EGS parameters of the selected cutout job on the *Cutout Browser* tab.

User Interface

The *Cutout Manager* application opens a single window at startup. Activities that belong to functionally related areas are implemented as tabs. Once a tab is activated, the window switches to one of the following layouts: *Cutout Browser*, *Cutout Workbench* and *Preferences*. A fourth *Help* tab is left empty at the time of this writing. In addition to the main window, additional windows open on demand to display graphical and textual information pertaining to cutout job processing and results.

Initially, the *Cutout Manager* starts up in a *user mode*, that offers the basic functionalities and default settings for output factor calculations. In *expert mode*, additional information is displayed and many run-time parameters affecting *EGSnrc* and the *Mac OS X*® environment, can be adjusted. To enable *expert mode*, press the *Switch to expert mode* button and enter the pre-defined password.

The *Cutout Browser*

This tab provides a list of cutout jobs and associated functions. It is depicted in Figure 8. The list area at the top of the window is stretched horizontally over the full tab width. In it, a maximum of 15 cutout jobs are displayed. If more than 15 entries exist, the list of cutout jobs becomes scrollable in vertical direction. Information about cutout jobs is organized in 6 columns: Linac (accelerator name), MeV (nominal energy), Applicator (applicator size), ID (patient identification), Field name (arbitrary descriptor) and Status (information on job execution status).

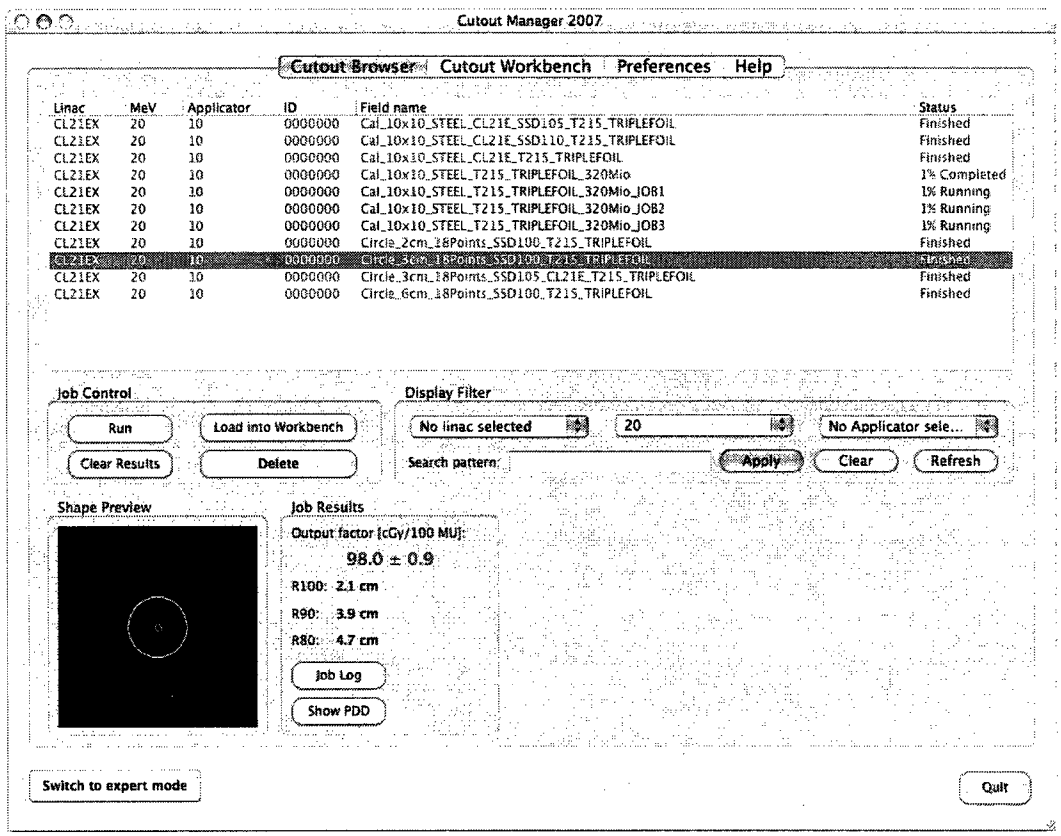

Figure 8: Screenshot of the *Cutout Browser* tab in user mode

The status column provides color coded, near real time information about the completion status of a cutout job:

- *Not started* (black): New cutout job, not scheduled for execution.
- *Started* (blue): Currently executing job that has completed less than 1% of its calculations. No preliminary results.
- *n% Completed* (red): Currently executing job that has completed 1-100% of its calculations. Preliminary results are available.
- *Finished* (green): Completed cutout jobs. Final results are available.

Applying a *Display Filter*

When many cutout jobs exist, it may become difficult to find the right one. The tools provided in the *Display Filter* box allow the user to restrict the range of displayed jobs. This can be done by either pre-selecting the linac, nominal energy and applicator size from pull-down menus and by entering a *regular expression* to define a search pattern. For example, in Figure 8 the preselected nominal energy is 20 [MeV].

Regular expressions define search patterns for character strings. They are powerful tools and potentially describe very complex matching conditions in a single text string. While a comprehensive discussion of regular expressions is outside the scope of this work we will describe some basic elements of their syntax (the double quotes are not part of the regular expression):

- "<string>" Matches the occurrence of character string <string>.
- "[a-zA-Z]" Matches an alphabetic character.
- "[0-9]" or "\d". Matches a digit.
- "\s" Matches a whitespace character (space, tab, newline, etc.).
- "." Any single character except a line break, including a space.
- "*" Repetition character. Zero or more characters.
- "+" Repetition character. One or more characters
- "?" Repetition character. Zero or one character.

Shape Preview* and *Job Results

When a job is selected by clicking on a line in the list, the contours of the cutout are shown in the *Shape Preview* box. This allows for an easy visual inspection of the entered shape. The *Job Results* box shows preliminary or final calculation results, if available. The values provided are the output factor, R_{100}, R_{90}, and R_{80}. The quoted error of the output factor is purely statistical and is based on dose fluctuations encountered during the Monte Carlo simulations.

Pressing the *Job Log* button opens a window that displays the accumulated job logs for a cutout job at the top and a listing of depth-dose data at the bottom. The depth-dose data is presented in units of Gy/particle, a choice of units common in *EGSnrc* calculations. While the depth-dose data is available at any time during and after execution, the accumulated job logs can only be seen after successful completion of a job.

Similarly to the *Job Log* button, the *PDD button* opens a window that displays the depth-dose data as a PDD curve, indicating all available dosimetric parameters. Since the dose scoring is limited to first 5 cm in depth, values for R_{90} and R_{80} may not be available at higher energies. This also applies to the numbers available in the *Job Results* box. While the PDD window is open, its contents is automatically updated when new values become available or if a different line selected in the cutout job list.

Cutout *Job Control*

The functions grouped together in the Job Control box are central to job execution. They act on the current selection in the list of cutout jobs. The actions of the buttons here are self-explanatory, but a few comments are useful.

The *Run* button starts the execution of a cutout job. A small *Shell Output* window will open, displaying information about the scheduled batch jobs (See Figure 9). It can be closed at any time without affecting job execution.

Starting a job also causes a change in the list of cutout jobs: the status (and color) of the selected job will initially appear as "started" and change according to its progress in the completion cycle. Depending on the preferences chosen for

distributed computation, more lines with the same field name, appended by "_JOBn", may appear in the job list box. This indicates that the original job was split into a number of sub-jobs.

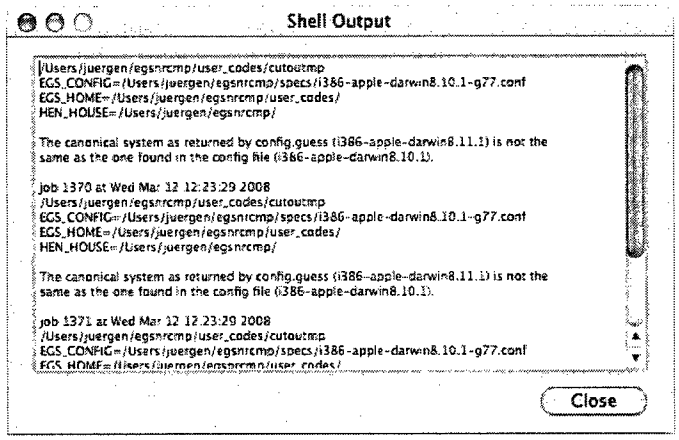

Figure 9: The *Shell Output* window lists the submitted cutout jobs

In the current unreleased version of the software care should be taken to not re-run a completed or currently executing job since this could lead to problems with file access and stall the calculations. Prior to re-running a cutout job, all existing results need to be erased using the *Clear Results* button. Even in the case that these precautions are not met, there is no risk of calculation errors because each cutout job is handled independently and the final result is always defined by the last cutout job run.

Some parameters of a cutout job can be modified without creating a new cutout job. Most prominently this includes the cutout shape, but it is also possible to alter the patient names and the physicist initial. In expert mode it is possible to change the target precision, distributed computation settings and *EGSnrc* parameters. The *Load into Workbench* button will bring up the selected job on the *Cutout Workbench* tab. Changes to the patient ID, linac name, nominal energy, applicator size and field name will, upon saving, create a new entry in the list of cutout jobs or cause an already existing job's parameters to be overridden.

The *Cutout Workbench*

The *Cutout Workbench* tab is used to create new cutout jobs or modify existing ones. The *Patient Data and Descriptors* box provides input fields for the patient's first and last name, patient ID, field name and the physicists initials (Figure 10). Some restrictions apply to the field's formats:

- First and last name – Upper and lowercase alphanumerical characters.
- Patient ID – Follows the standard at the Montreal General Hospital and must contain exactly 7 numerical digits [0-9].
- Field name – Must contain only alphanumerical characters [0-9], [a-z, A-Z] and the underscore character "_". Special characters and blank spaces are not allowed.

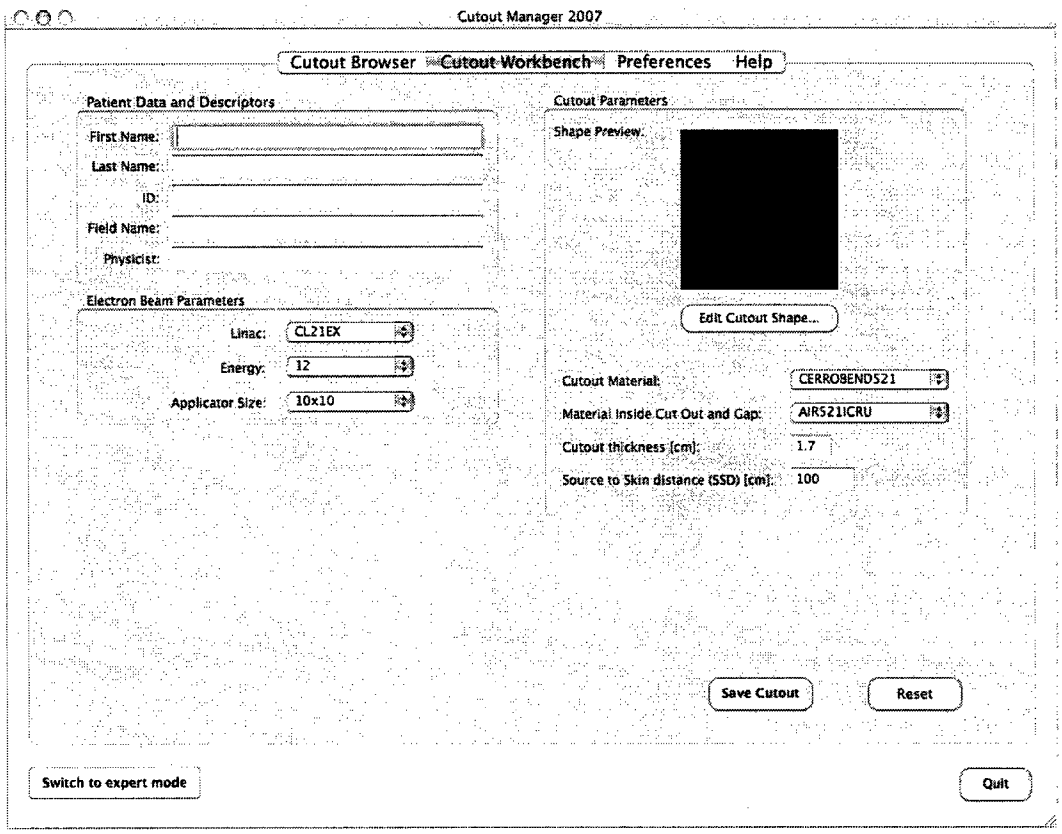

Figure 10: Screenshot of the *Cutout Workbench* tab in user mode

Electron beam parameters

Treatment options are defined in the *Electron Beam Parameters* box. Three drop-down menus are available for selecting the linac, nominal energy and treatment cone (applicator) size. The range of available choices for energies and cone sizes depends on the selected linac.

Similarly, the *Cutout Parameters* box features drop-down menus for the cutout material (default *Cerrobend®*, *EGSnrc* identifier *CERROBEND521*) and the material inside the cutout (default air, *EGSnrc* identifier *AIR521ICRU*). The latter material is also assumed for the space between the cutout and the phantom. These standard settings usually do not require any change. There are input fields for the cutout thickness (default 1.7 cm) and the SSD (default 100 cm) both of which must be entered in centimeters.

Cutout Digitizer

A central function of the *Cutout Manager* is the shape input. Pressing the *Edit Cutout Shape* button opens a digitizer window. The initial layout of *Cutout Digitizer* for a 10×10 cm^2 mold tray is shown in Figure 11.

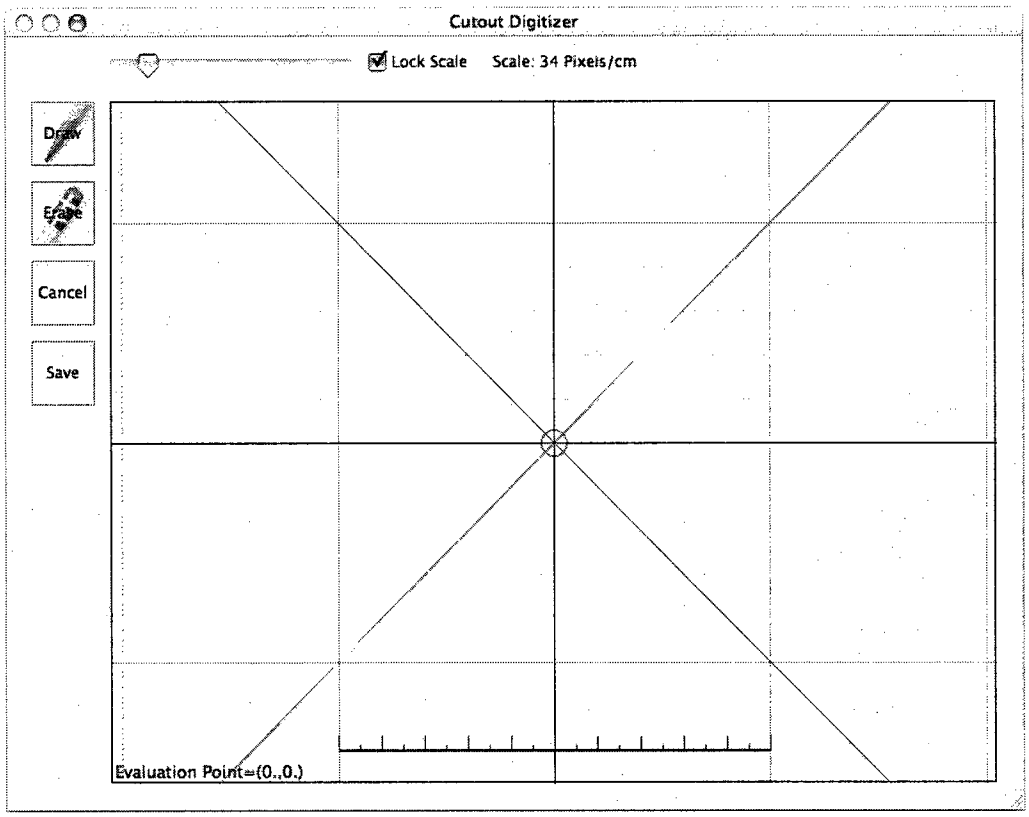

Figure 11: The *Cutout Digitizer* window for a 10×10 cm^2 mold tray

The window consists of a large graphics area, four buttons and one slider. A white section within the otherwise green graphics area has the dimensions of the plastic cover plate used to outline the contours of the cutout. A 2D grid with a 1 cm spacing and a number of orthogonal and diagonal crosshair lines complete the picture.

The slider can be used to adjust the size of the graphics area grid to the monitor resolution. Although the monitor scale is a preset parameter in the *Cutout Manager's* preferences file, the monitor scale may have to be adjusted if one switches to a different monitor. To do the adjustment, first uncheck the *Lock Scale* check button. Using the slider, the grid can be stretched or contracted until the red scale bar at the bottom of the graphics area has a width of exactly 10 cm.

To define the cutout contours, the *Draw* button must be selected (the button text will switch to "drawing"). Input is done either free hand or with the plastic cover plate (with the contours draw on it) centered around the midpoint. With the mouse

pointer one follows the contours either clockwise or counter-clockwise. A mouse click stores the current coordinates under the pointer.

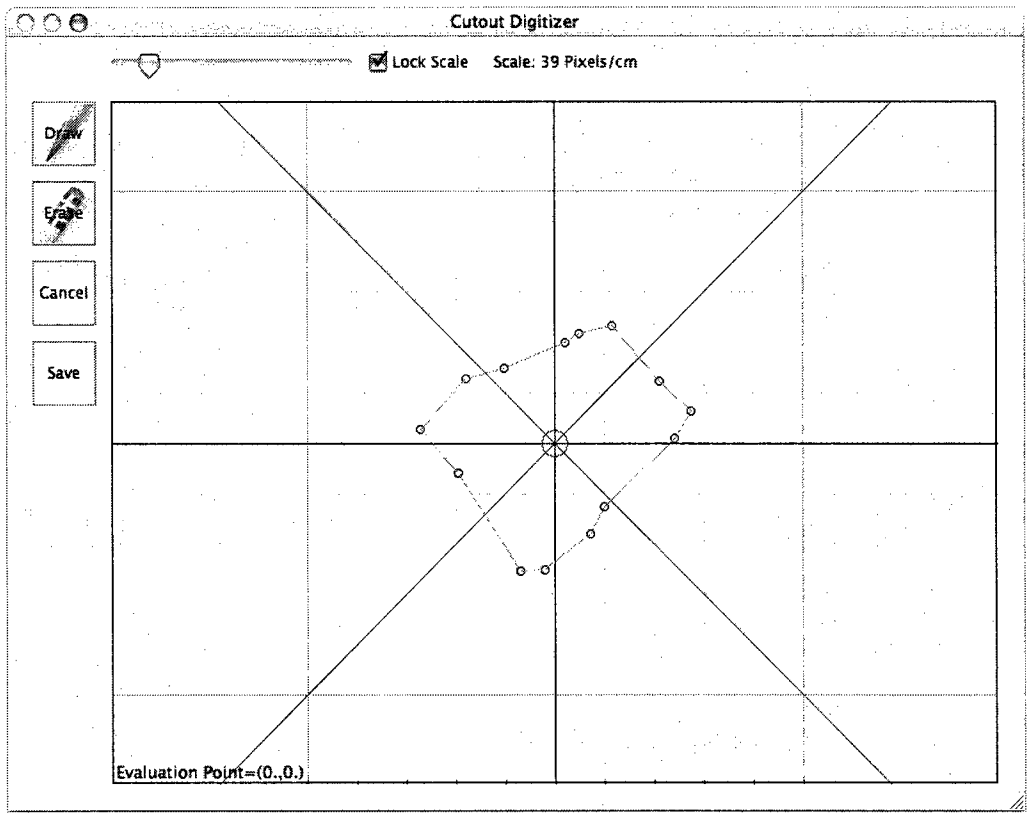

Figure 12: Example of contours for a 6×6 cm^2 cutout

While in drawing mode, pressing of the *Erase* button will subsequently remove the last recorded point. Although there is no upper limit for the number of stored points, it is recommend that as few points as necessary shall be defined.

Selecting the *Draw* button again will leave drawing mode and the button text switches back to "Draw".

A red circle in the graphics area indicates the point of interest (POI) at which the output factor is to be determined. The diameter of the circle reflects the diameter of the scoring region. To move the POI drawing mode must be off. The POI's absolute position is displayed in the lower left corner.

Selecting the *Erase* button outside of drawing mode will erase the entire contour.

To save the contour, close the digitizer window and return to the *Cutout Workbench*, press the *Save* button. *Cancel* closes the digitizer window and leaves the shape unchanged.

Expert mode extensions

In default mode, the *Cutout Manager* runs 10 million particle histories to achieve typical output factor errors between 0.7% at 6 MeV and 1.5% at 20 MeV. At lower energies the input phase space files contain relatively more electrons than photons. Electrons deposit more energy in the phantom which leads to a smaller statistical error of the dose per particle. For a given applicator size, the statistical error is independent of the size of the cutout shape, because the initial particles in the phase space files are sampled from a square area that is larger than the insert tray. No output phase space files are created. The settings for distributed computing are presets in the preferences file.

In expert mode, the number of histories can be freely set or selected from 3 preset values. Dose scoring and phase space file creation can be enabled or disabled. Finally it is possible to fine tune the environment for batch job execution.

The name of the phase space file is automatically generated and updated from inputs in the *Patient Data and Descriptors* box. It is displayed in a text field and can be edited to redirect the output to a different location. Note that any changes to the patient data and descriptors will reset the phase space path and file name.

On multi-processor/multi-core hardware a cutout job should be split in as many sub-jobs as there are processing cores. Sub-jobs usually receive their random generator seeds randomly. The switches in the preferences file should be set accordingly. However, for diagnostic purposes it may become necessary to enforce that a cutout job is run as a single job. This feature can be enabled by selecting the *Run as a single job* radio button.

If a (sub-)job should start with a pre-defined random generator seed, the *Use fixed seeds* check box must be selected. In this case, at least as many seeds must be specified in the seeds text box as there are multiple jobs.

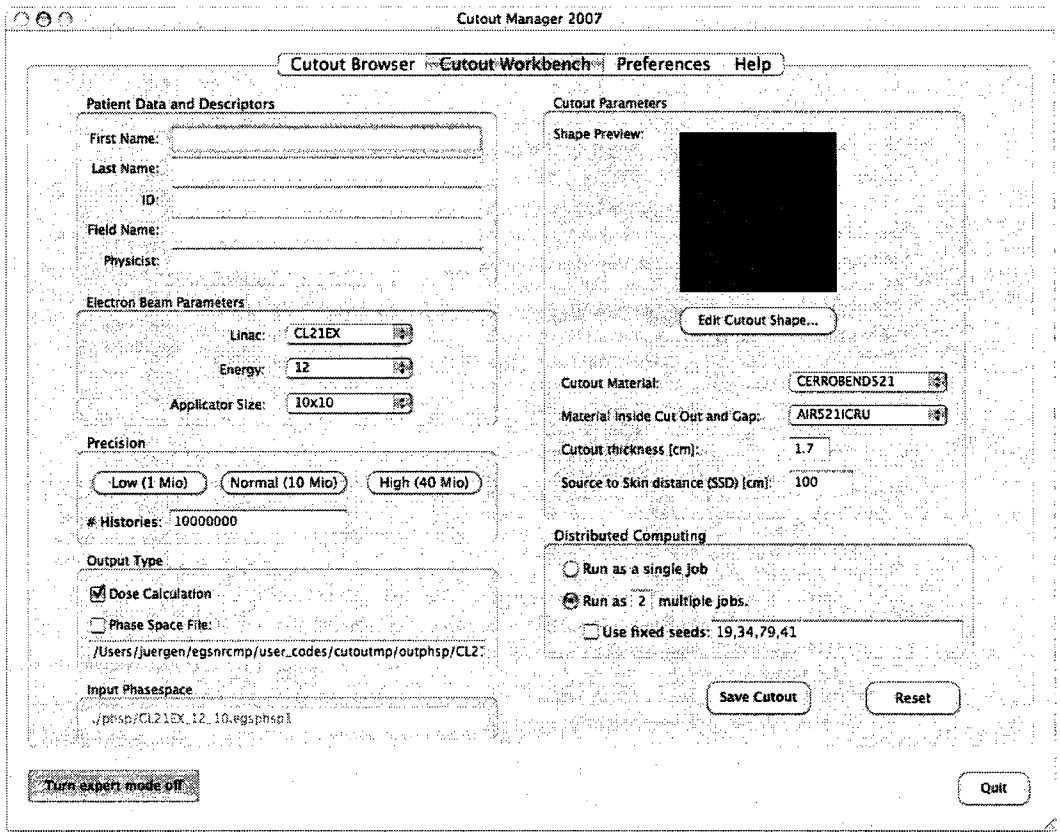

Figure 13: Screenshot of the *Cutout Workbench* tab in expert mode

The *Preferences* tab

The contents of this tab is only visible in expert mode. Initially, it shows the values and settings of program parameter as they are defined in the *Cutout Manager* preferences file. If parameter values are changed, they will be taken as default values and are applied to all subsequently created cutout jobs. The changed values are not preserved. The *Cutout Manager* will revert to its stored settings upon restart.

The *Monte Carlo Settings* box has editable fields for the values of ECUT, PCUT, read and write buffer sizes, the PEGS (cross-section) file name and the backscatter switch. The backscatter switch controls whether particles that are scattered back from the cutout block are discarded from further analysis. The default setting is NO (backscattered particles are not removed).

For a detailed explanation of ECUT and PCUT the reader is referred to the *EGSnrc* documentation (Kawrakow and Rogers 2006). To speed up execution the

electron transport threshold energy ECUT was set to 0.7 MeV. For photons PCUT has the usual value of 0.01 MeV. The buffer values impact the phase space reading routine and should not be changed.

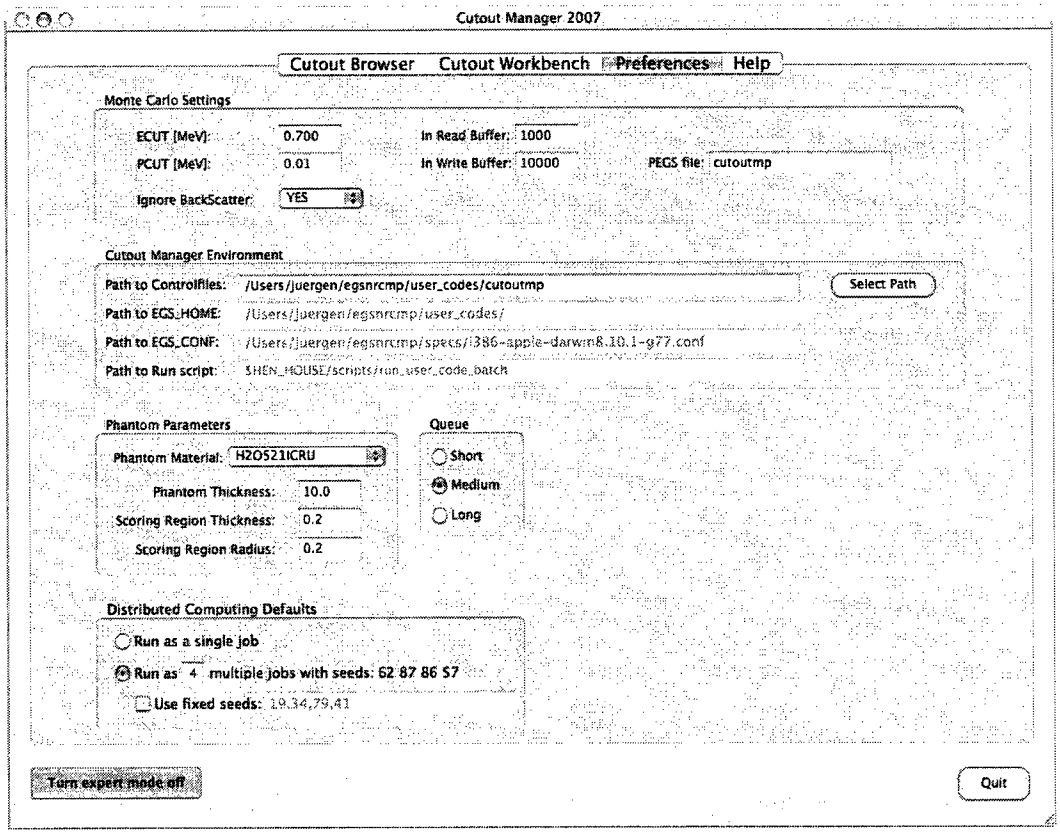

Figure 14: Screenshot of the *Preferences* tab in expert mode

Cutout job data is called *control files* and is stored in the computers file system. Occasionally it is useful to point the control file path to a different directory, for example a cutout job repository. To do this, click the *Select path* button in the *Cutout Manger Environment* box. The other parameters in the *Cutout Manger Environment* box are paths to EGS_HOME, EGS_CONF and the script used to submit the batch jobs. They are read-only.

Chapter 3 – VALIDATION AND RESULTS

This chapter describes the clinical setup and validation of the *Cutout Manager*. During the setup phase, PDD curves are measured, a *BEAMnrc* model of the linac is established and the model's parameters are varied to match calculated and measured PDDs. Based on these parameters, phase space files are subsequently created for the desired nominal electron energies and applicator sizes. Validation consists of output factor measurements for a variety of cutout shapes and subsequent comparison with the computer generated results.

PDD Measurements with ionization chamber and water tank

Measuring PPD curves serves two purposes. Firstly they provide the reference PDDs against which the accelerator model and parameterization are tested, secondly they are used to determine the depth of the dose maxima for output factor measurements.

PDD curves were established for the Varian Clinac 21EX in electron mode at 6, 9, 12 16 and 20 MeV, applicator size 10x10 cm^2 and four different cutout shapes:

- Square 10x10 cm^2 "open" field, steel, SSD=100, 105 and 110 cm.
- Circular 2, 3 and 6 cm diameter, *Cerrobend*®, SSD=100 cm.

The 3 cm diameter cutout was also measured at SSD=105 cm.

Materials and method

We used a Wellhöfer WP700 water scanner system with a Wellhöfer IC-10 ionization chamber and water tank (IBA Dosimetry AB, Uppsala, Sweden). The WP700's computer and electrometer are on a moveable cart. During the measurement the cart was in the linac control room, connected by cables to the water tank step motors and the ionization chamber. The charge was measured with a Keithley 6517A electrometer (Keithley Instruments Inc., Cleveland, USA). A total of 35 ionization curves were measured for 5 energies and 7 cutout configurations. The curves were shifted upstream by one half of the IC-10 radius ($r_{IC\text{-}10}$ = 0.3 cm), 0.15 cm, and subsequently multiplied with depth dependent water-to-air stopping power ratios. The stopping power ratio correction follows

the function by Burns et al. which is parameterized in terms of R_{50} (Burns, Ding et al. 1996). The R_{50} values were taken from previous CL21EX(B) measurements. Burns' numbers were compared with *EGSnrc* calculations. The *sprrznrc* user code takes a phase space file as input and transports the particles therein through a phantom. It scores the dose deposition of a fluence of primary and secondary charged particles (in water) to small test volumes of either water or air. The result is a more realistic (restricted) mass collision stopping power ratio curve versus depth. Figure 15 shows Burns' and *sprrznrz* data for a 9 MeV electron beam an 10×10 cm^2 field size (Simulated for the Varian CL21EX(B) linac, $R_{50}=3.48\,cm$).

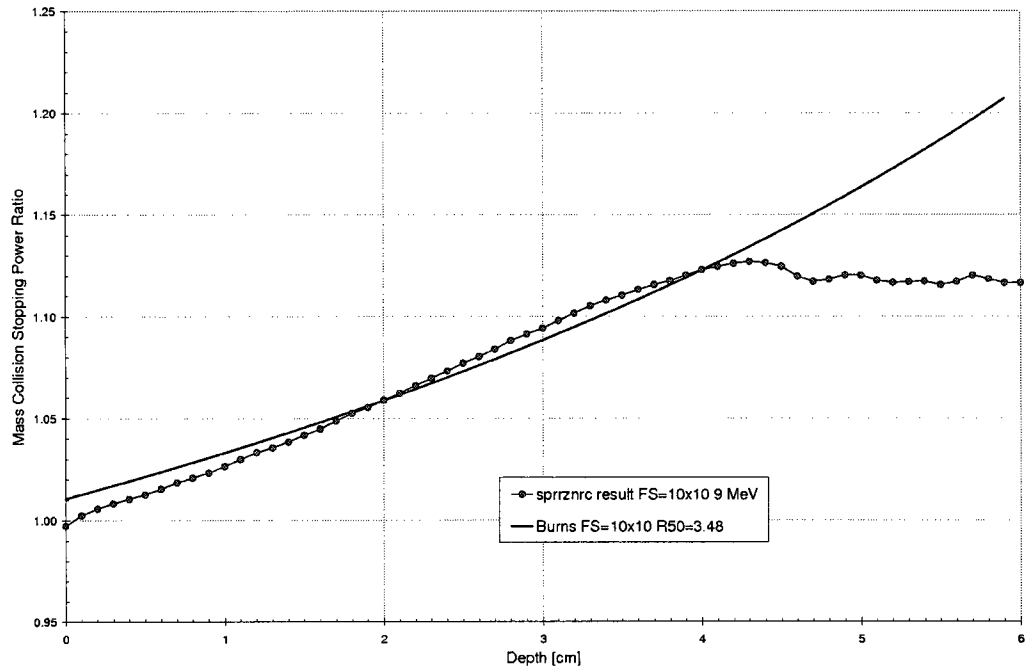

Figure 15: Stopping power ratios from Burns et al. and *sprrznrc*. (9 MeV, 10×10)

The results support the claim of Burns et al. that over z/R_{50} ranging between 0.2 and 1.1 the maximum deviation is limited to 1% (see Figure 16). Around the dose maximum R_{100}, which occurs at approximately 2 cm for a 9 MeV beam, the deviation is only fractions of a percent.

Around and beyond the practical range R_P, the particle fluence contribution from the electron primary beam vanishes. All that is left are bremsstrahlung photons. *sprrznrc* calculations correctly predict a constant stopping power ratio from this point on, because the differential secondary charged particle fluence spectrum is almost constant. We confirmed, that the WP700 system correctly limits the stopping power ratio correction beyond the practical range R_P to the value at R_P.

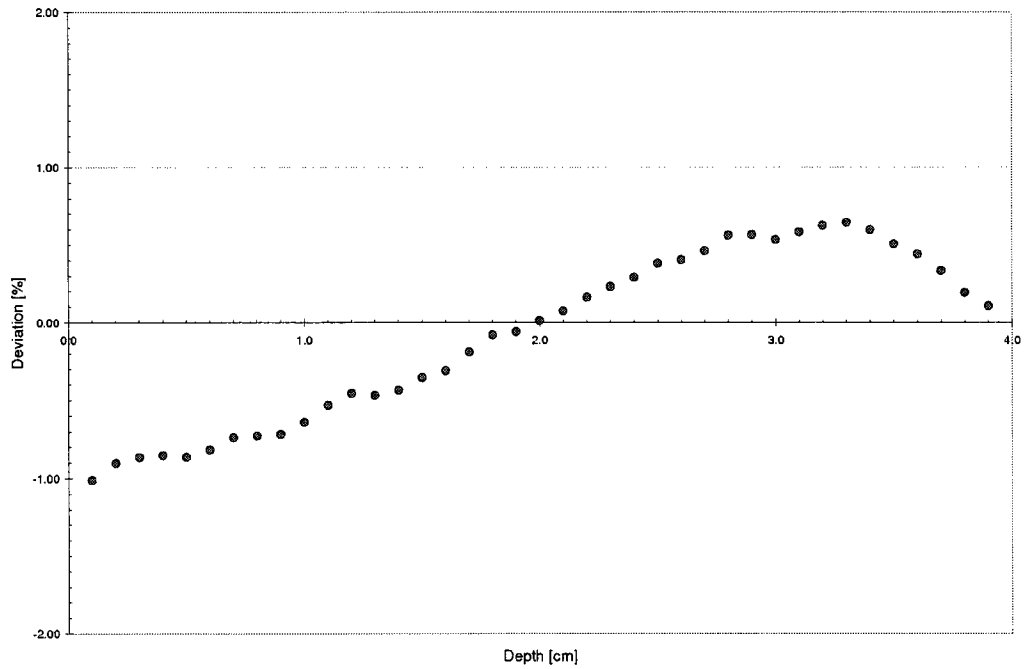

Figure 16: Deviation of SP ratios of *sprrznrc* from Burns et al. (9 MeV, 10×10)

The Wellhöfer WP700 applies the same stopping power ratio correction method (based on Burns' formula for 10×10 fields with R_{50} as parameter) to all measured depth ionization curves regardless of the cutout shape. This prompts the question if the correction is still appropriate for small circular cutouts where the dose maximum is known to shift to significantly smaller depths.

Using *BEAMnrc*, a phase space file was created that reflects the particle fluence just below a 2 cm diameter cutout for a CL21EX linac at 9 MeV. This phase space file served as input to *sprrznrz*. Figure 17 shows the deviation of the *sprrznrz* result from the Burns formula. Over the whole depth range, *sprrznrz*

produces numbers that are approximately 1% smaller than Burns' values. But since the deviation is essentially constant up to about 2.5 cm, no effect on the position of R_{100} is expected.

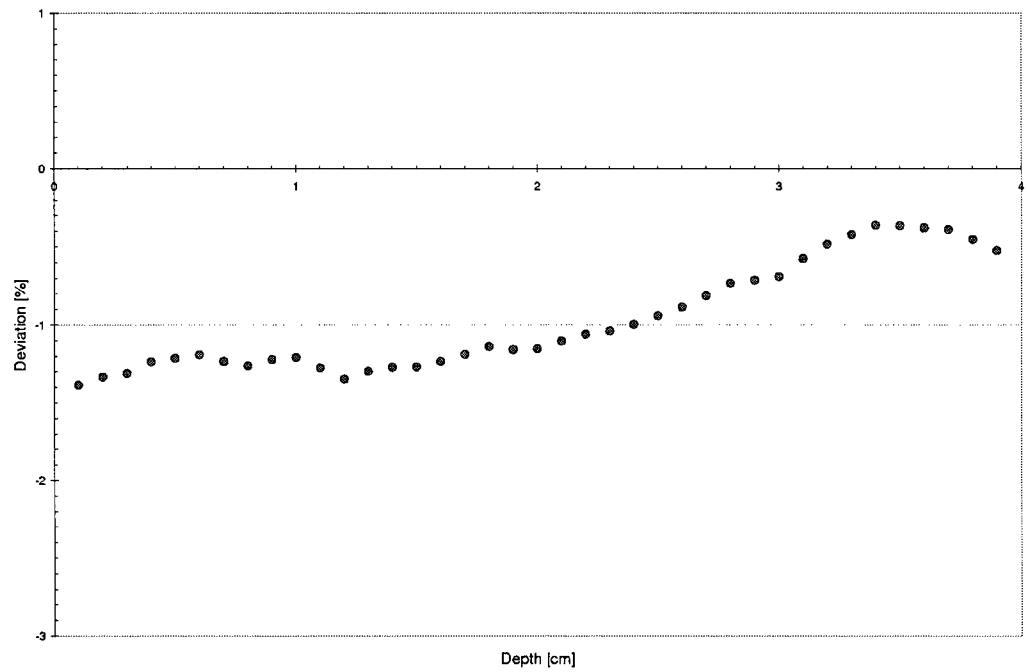

Figure 17: Deviation of SP ratios of *sprrznrc* from Burns et al. 9 MeV, FS=2 cm diam.

Results of PDD measurements

The present set of measurements was made in November 2007 hence we refer to it as "Nov 2007" on figures and tables. Figure 18 shows the PDD curves for a 10×10 cm^2 field at all available linac energies.

PDD curves morph into distributions that peak at shallower depths as the field size becomes smaller. There is little difference between an open 10×10 cm^2 field and a 6 cm diameter cutout over the whole range of energies (some distortion is noticeable at 20 MeV). However, the PDDs of small cutouts start to deviate from an open 10×10 cm^2 field at the lowest treatment energies. Due to the manifold of radiation sources involved in the dose deposition process, no general rule can be given for the size at which deviation occurs. Figures 19 to 23 document the measured PDD curves for all energies and cutout sizes.

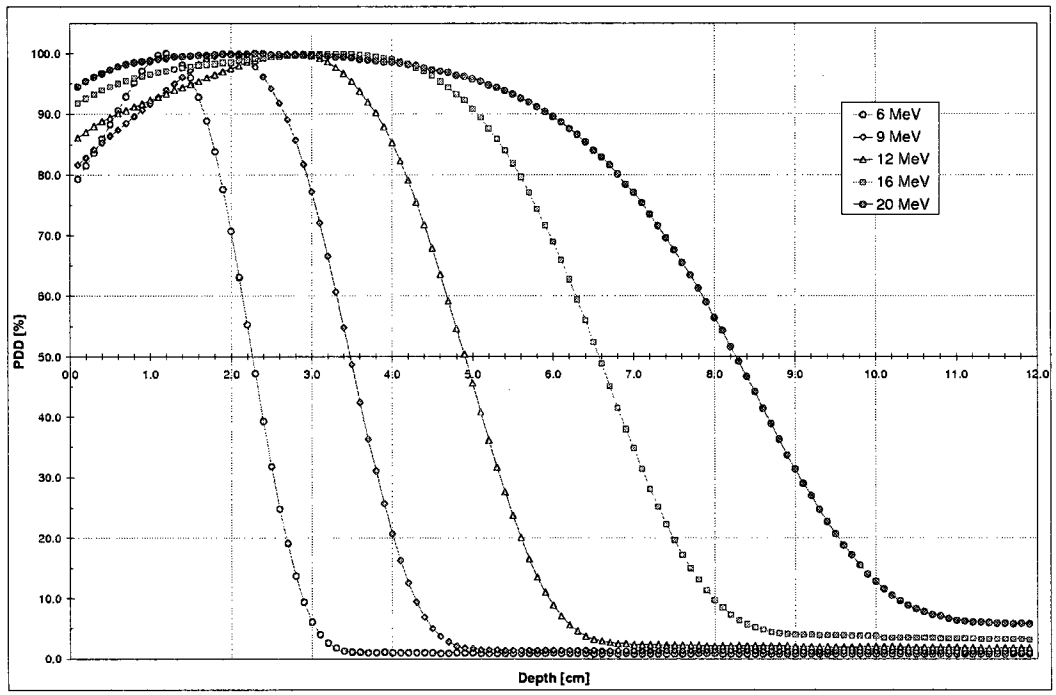

Figure 18: PDDs of a 10x10 reference cutout at nominal energies 6, 9, 12 16 and 20 MeV

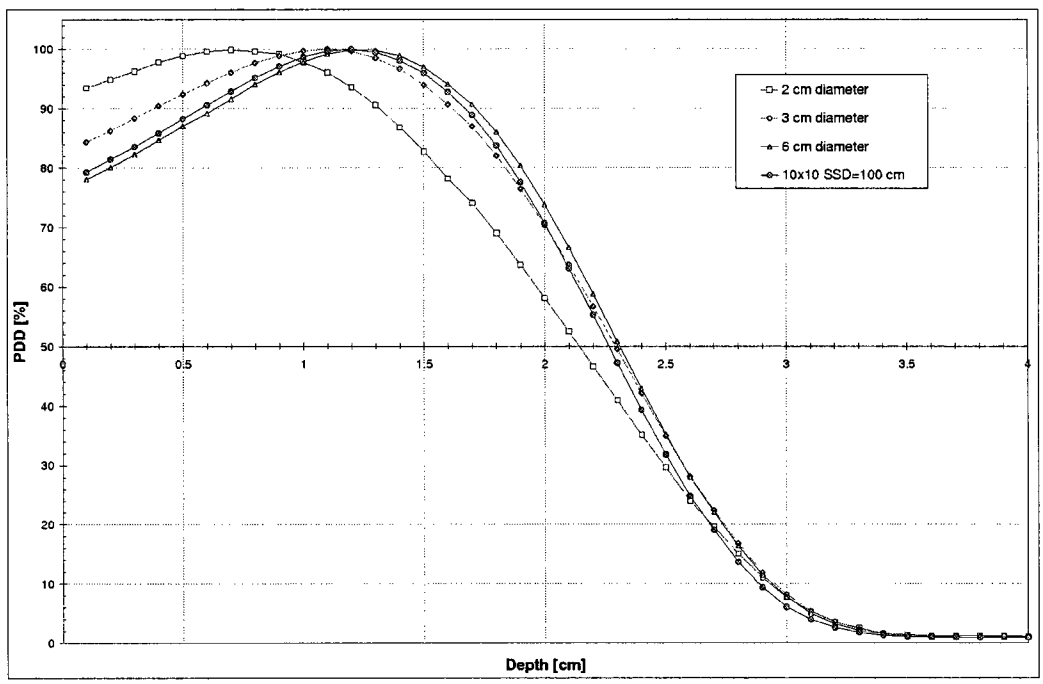

Figure 19: Measured PDD curves at 6 MeV nominal energy

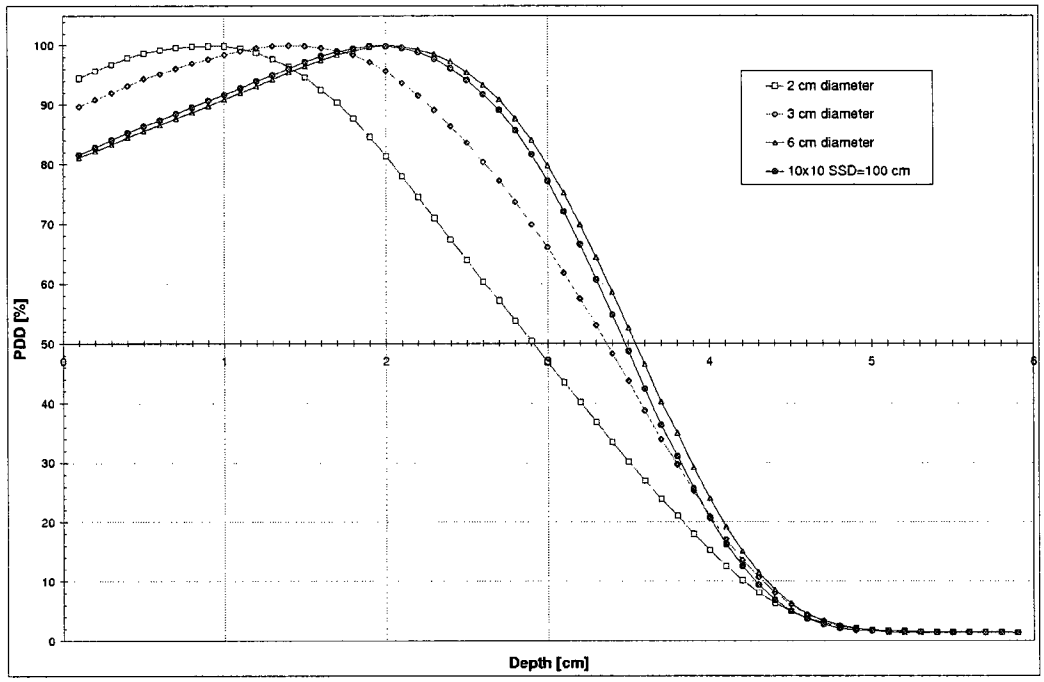

Figure 20: Measured PDD curves at 9 MeV nominal energy

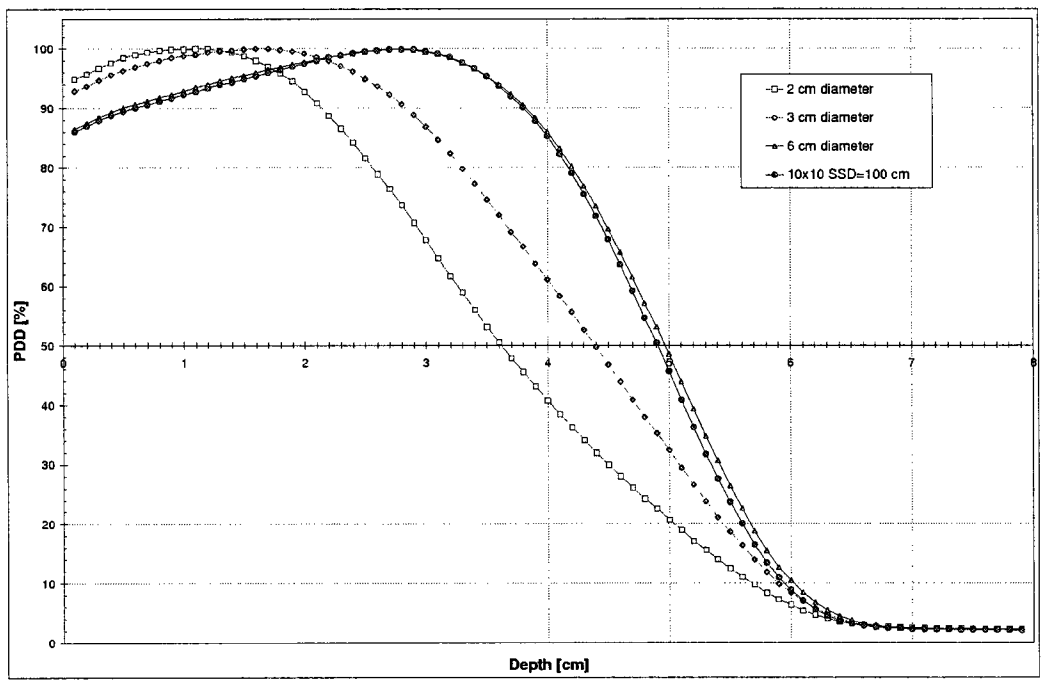

Figure 21: Measured PDD curves at 12 MeV nominal energy

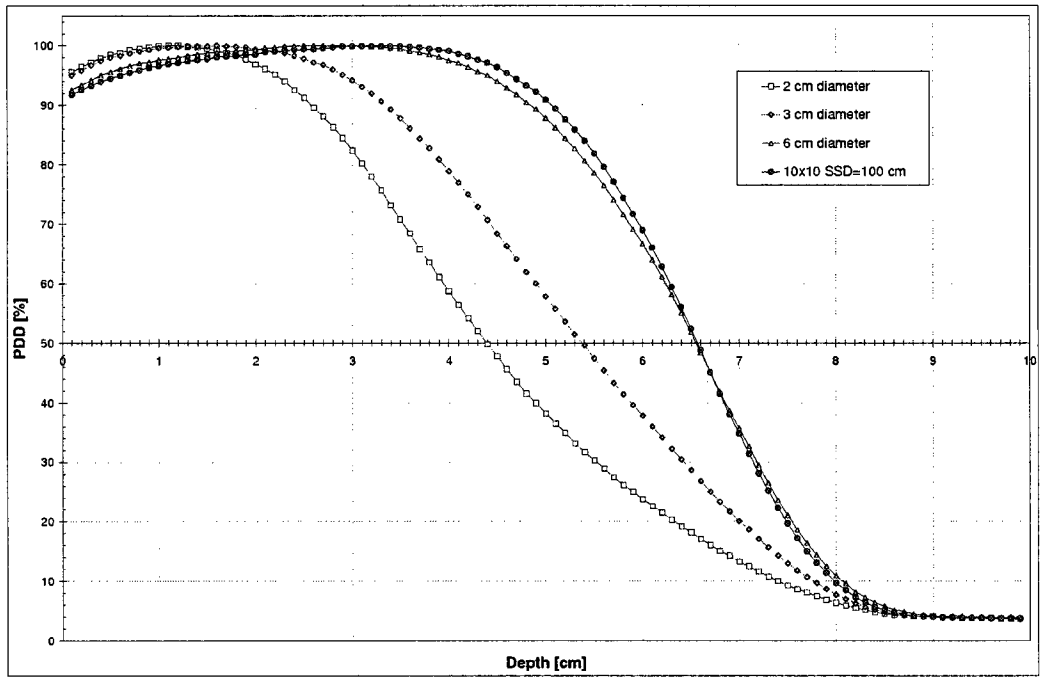

Figure 22: Measured PDD curves at 16 MeV nominal energy

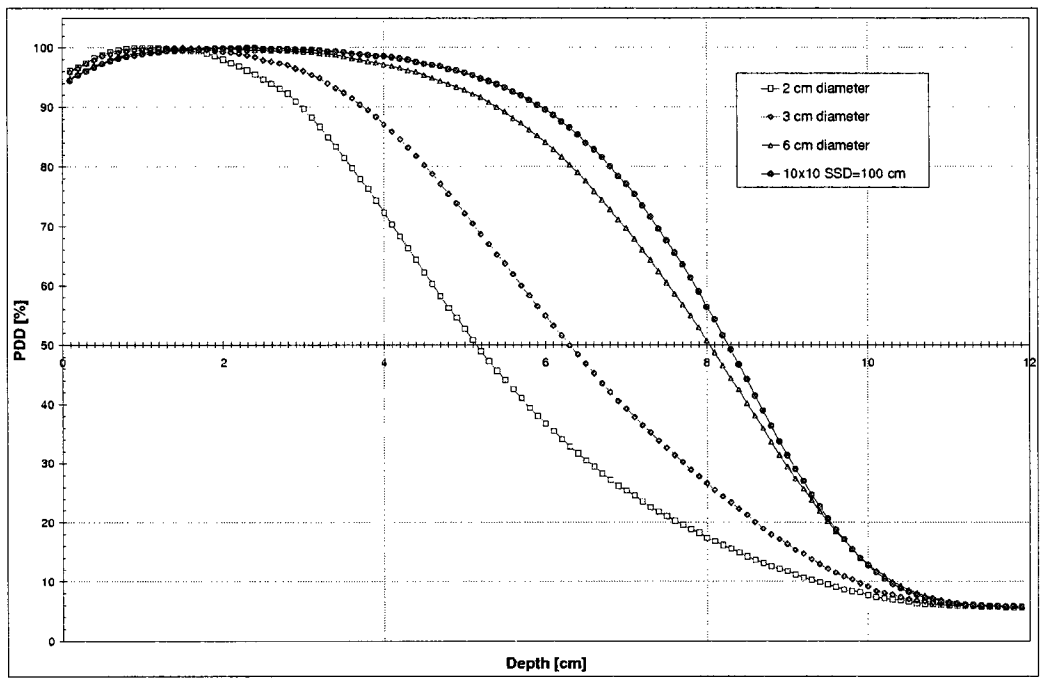

Figure 23: Measured PDD curves at 20 MeV nominal energy

Table 2 lists the values for R_{100} as determined with the software of WP700 system. Where available, the number in brackets indicates a maximum depth that was determined using an independent Microsoft Excel based peak fitting routine. Both results typically agree with each other on a 0.5 mm level.

Energy [MeV]	6 cm diameter	3 cm diameter	2 cm diameter	10x10 SSD=100	10x10 SSD=105	3 cm diam. SSD=105	10x10 SSD=110
6	**1.25** (1.24)	**1.13** (1.09)	**0.72** (0.72)	**1.20** (1.20)	**1.28** (1.27)	**1.09** (1.07)	**1.31** (1.29)
9	**2.04** (2.02)	**1.47** (1.41)	**0.97** (0.88)	**1.97** (1.92)	**2.11** (2.04)	**1.41** (1.36)	**2.08** (2.08)
12	**2.83** (2.74)	**1.70** (1.65)	**1.20** (1.07)	**2.76** (2.76)	**2.90** (2.80)	**1.57** (1.54)	**3.01** (2.90)
16	**3.09** (2.63)	**1.66** (1.48)	**1.19** (1.11)	**3.43** (3.24)	**3.55** (3.46)	**1.72** (1.68)	**3.54** (3.52)
20	**2.0**	**1.7**	**1.1**	**2.5**	**3.0**	**1.7**	**3.4**

Table 2: R_{100} values from PDD measurements calculated with WP700 and Microsoft Excel® (in brackets).

It became soon evident that the PDD curves of open 10×10 cm^2 fields appear to be different from earlier measurements at the Clinac 21EX(B) using the same equipment (See Figure 24 for the PPDs at 6 MeV). According to the available data, the most recent curves appear to have shifted upstream by 0.5 mm in comparison to a measurement in February 2007 and about 1.2 mm if compared to data from April 2004. The cause of this discrepancy is not known. The shift can be explained by an offset in the depth measurement. Taking the March 2004 measurement as the reference, perfect agreement occurs when we shift the February 2007 curve by 0.5 mm and the latest measurement by 1.2 mm upstream. Figure 25 shows the now overlapping PDDs for an open 10×10 cm^2 field at 6 MeV. However, recently repeated PDD measurements reveal the same shift and make a positioning error unlikely.

A small drift of the effective energy is another possible cause. A drop in the effective energy should result in a lower PDD in the buildup region, which is not visible in Figure 25.

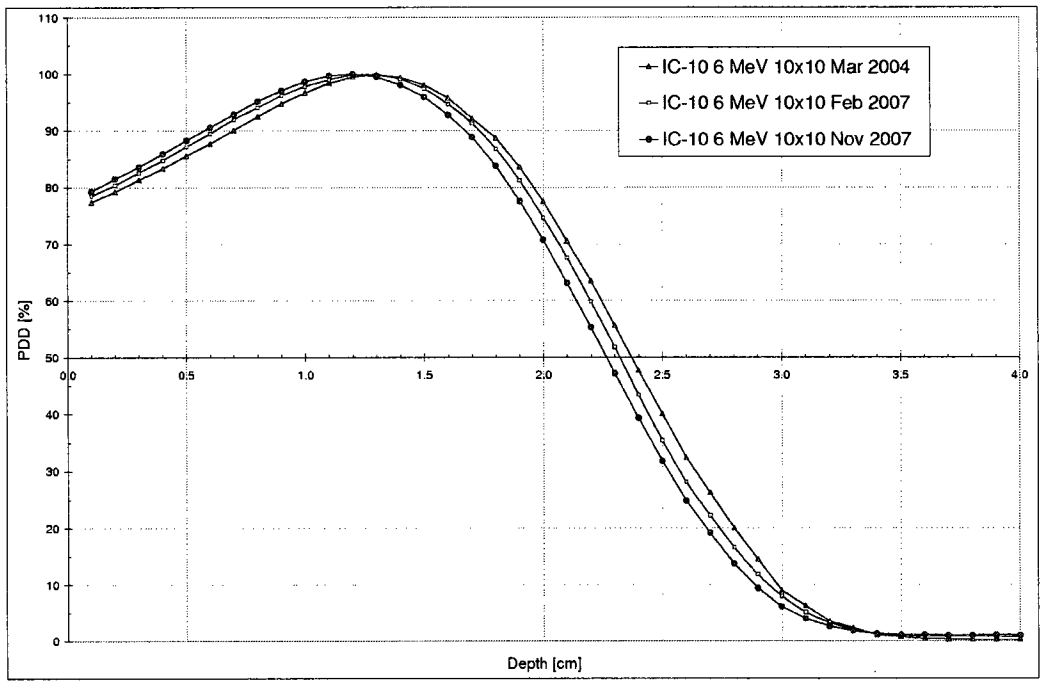

Figure 24: PDD curves from IC-10 measurements at 6 MeV between 2004 and 2007

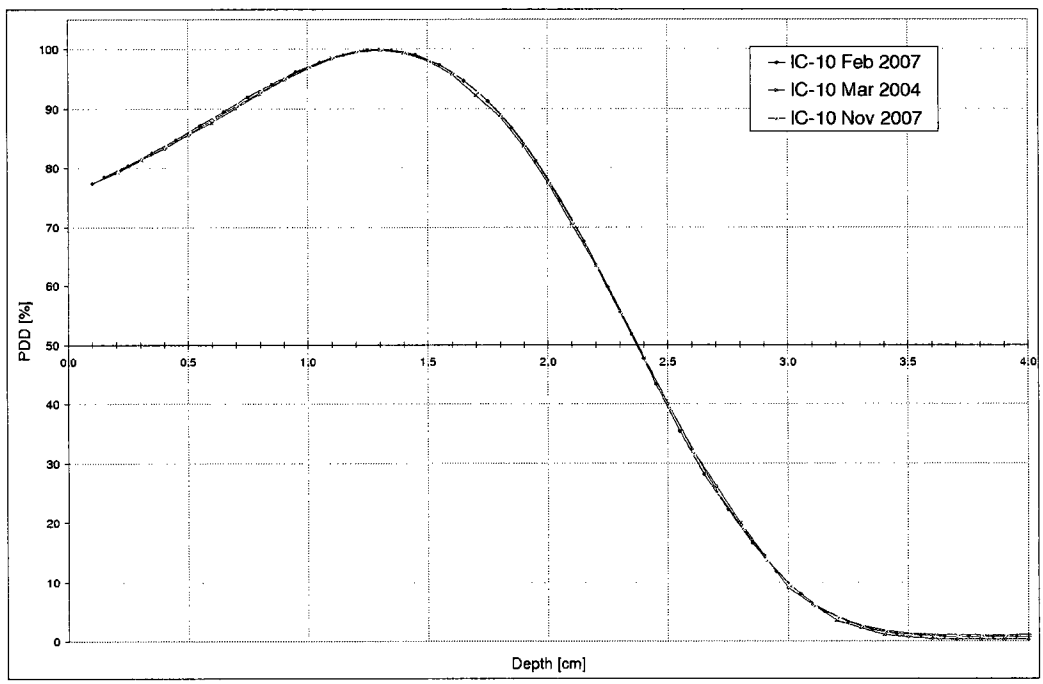

Figure 25: Shifted PDD curves from IC-10 measurements at 6 MeV between 2004 and 2007

Because of their large diameter (6 mm in the case of the IC-10), cylindrical ion chambers integrate the ionization over a rather large range of depths. This is problematic if for PDD measurements 1 mm resolution is aimed for. Some chambers are quite long which makes them prone to loss of charged particle fluence close to field boundaries. A correction for the effective point of measurement always has to be applied.

All this makes a cylindrical ion chamber less than ideal for precision PDD measurements. A better choice are plane-parallel ion chambers or diodes. Plane-parallel (pp) chambers for electron dosimetry do not require a correction for the effective point of measurement, are thinner (about 1 mm) but deliver a smaller signal because of their small active volume. Also, the stopping power ratio correction must still be applied to the measured depth-ionization curves. Diodes have none of these disadvantages. In their dosimetric properties they are water equivalent (no stopping power ratio correction), deliver a large electrical signal and can be made very small. The typical size is smaller than 1 mm.

In the course of this work no diode and plane-parallel ion chamber measurements were not. However, some data is availably from other sources at the MGH. Figure 26 shows three IC-10, one diode and two plane-parallel IC (*Roos*® and *Markus*®, both PTW, Freiburg, Germany) measurements. A depth offset was applied to have all curves match at R_{50}.

Again, the overall shape agreement is obvious for all detector types. Roos and Markus chamber coincide well with IC-10 around the dose maximum. In the buildup region the Roos chamber records a higher dose than the IC-10, the Markus chamber is systematically lower but very close to the IC-10.

All pp ion chambers measure a lower than IC-10 depth-dose around R_P and agree with the diode results in this respect.

The diode stands out in two more features: In the buildup region it registers systematically lower doses than all other detectors and R_{100} lies approximately 2 mm deeper. The differences are large enough to warrant additional measurements with diodes.

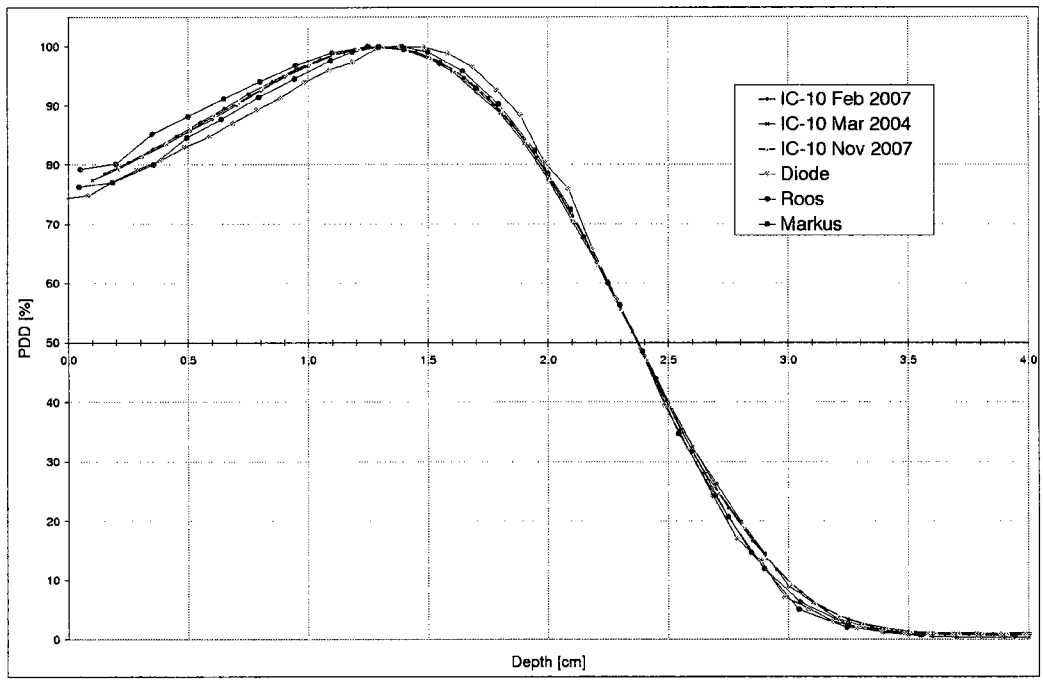

Figure 26: Shifted PDD curves from IC-10, diode and plane-parallel IC measurements

Output factor measurements with an IC-10 ion chamber

Measured output factors are the reference against which the *Cutout Manager* results must be compared. They were measured separately form the PDD curves for the same combinations of cutouts and SSDs as above.

Materials and method

A Standard Imaging *1D Water Scanning System* (Standard Imaging, Inc., Middleton, WI USA) was used with the IC-10 ion chamber from PDD measurements. The scanning system consists of a $42 \times 40 \times 36$ cm^3 water tank, a water control arm with stepping motor and rotary encoder and a remote handheld controller. Positioning accuracy and repeatability are specified as 0.05 mm over the TG-51 range (100 mm). An ion chamber bracket is attached to the control arm. It is made from water equivalent material and fits thimble ion chambers and rigid stem parallel plate chambers. The system is depicted in Figure 27.

In our case, the IC-10 ion chamber was not mounted directly into the ion chamber bracket. Instead, a custom made extension piece made of polymethyl methacrylate

(PMMA) and Teflon® served as an interface between chamber bracket and ion chamber.

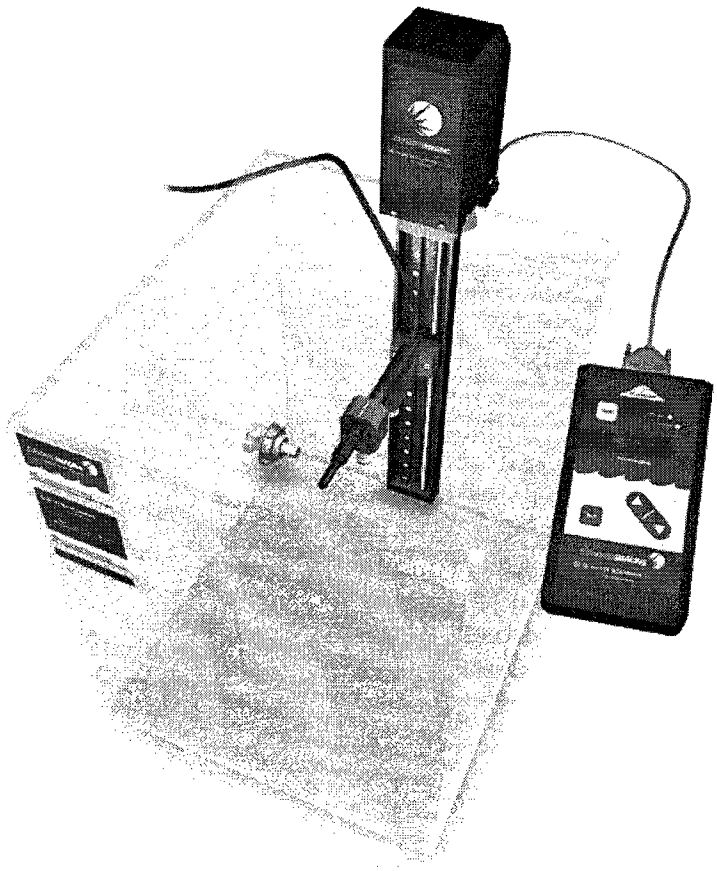

Figure 27: The Standard Imaging *1D Water Scanning System*

The handheld controller is capable of moving the control arm at two speeds, either 1 mm/s or 3.8 mm/s in 0.01 mm increments. After the ion chamber has been moved to a reference position, the relative position, displayed on the controller, can be reset to zero. A battery buffered internal memory allows one to set the chamber depth in the treatment room, then disconnect the controller and re-connect to the serial cable in the control room without losing the set depth point.

The electrometer was a Keithley 6517A set to the 20 nC range. The IC-10 was operated at +300 V.

The *1D Water Scanning System* was placed on the treatment table and the center of the IC-10's sensitive volume was aligned with the beam axis using the crosshair indicator. While this method worked well with the 10×10 cm^2 field and

the 6 cm diameter cutout, a small adjustment was necessary for the smaller circular cutout where the circle's center did not coincide with the beam axis. Figures 28 and 29 show the entire setup at the Varian Clinac 21EX and setup details for the 6 cm circular cutout.

To define the zero depth point, where the central axis of the ionization chamber is at level with the water surface, the IC-10 chamber was first completely immersed in the water. The chamber was then gradually moved upwards until the combined image of the IC-10 and it's total reflection looked like the IC-10. This situation is shown in Figure 30 where the image above the chamber's axis is actually the reflection of mechanical parts in the lower half.

For each combination of nominal energy and cutout shape in Table 3, the IC-10 was moved to specified R_{100} depth + 0.15 cm. The latter shift is necessary since the effective point of measurement lies $0.5 \cdot r_{\text{IC-10}} = 0.15\,cm$ above the ion chamber axis. At 200 monitor units per measurement, several electrometer readings were recorded and averaged. In a last step the average electrometer reading was multiplied with the water-to-air stopping power ratio from Burns et al., calculated for $z = R_{100}$ and R_{50} taken from earlier CL21EX measurements.

Output factors for a cutout/SSD configuration were calculated as the ratio of the averaged and corrected electrometer reading at R_{100} for this configuration divided by the averaged and corrected electrometer reading for a 10×10 cm^2 field at SSD 100. This ratio is further multiplied by 100 to give the effective output in monitor units.

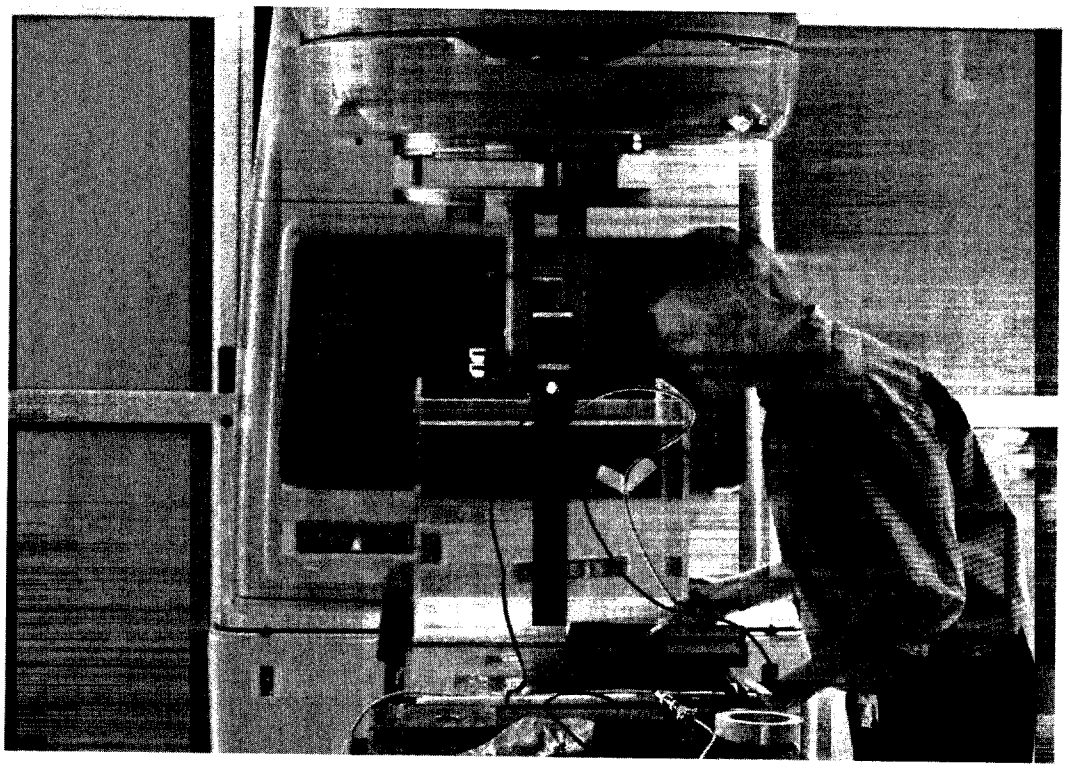

Figure 28: Setup for output factor measurements on the Varian Clinac 21EX

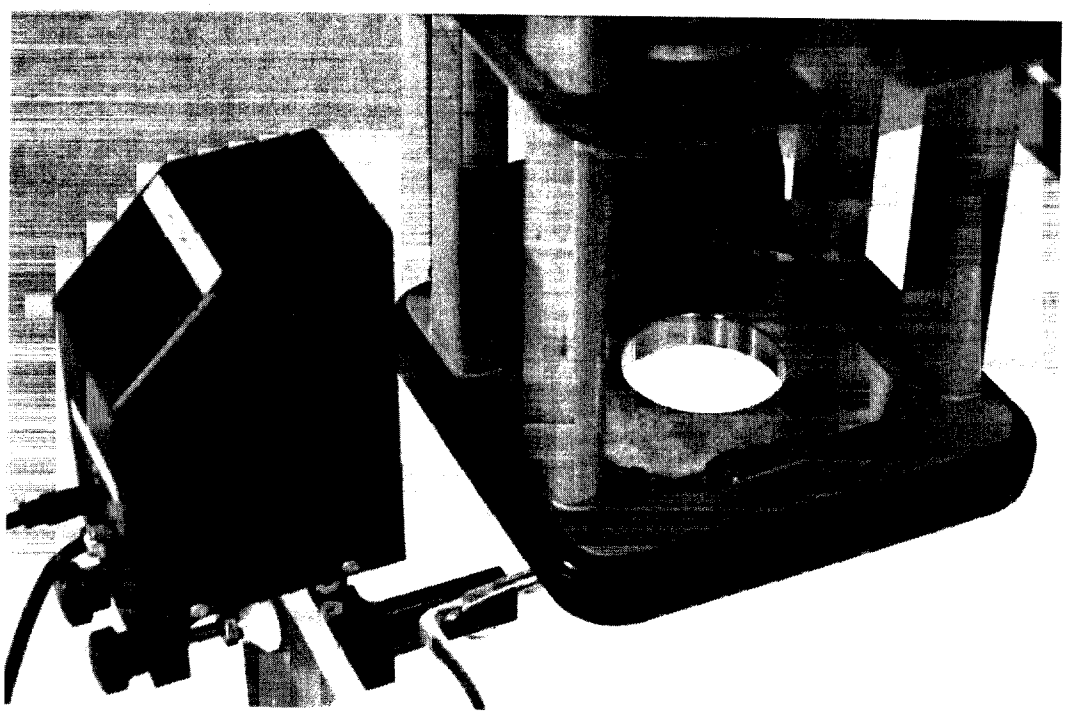

Figure 29: Detail of the setup for measuring the output factor of a 6 cm diameter cutout

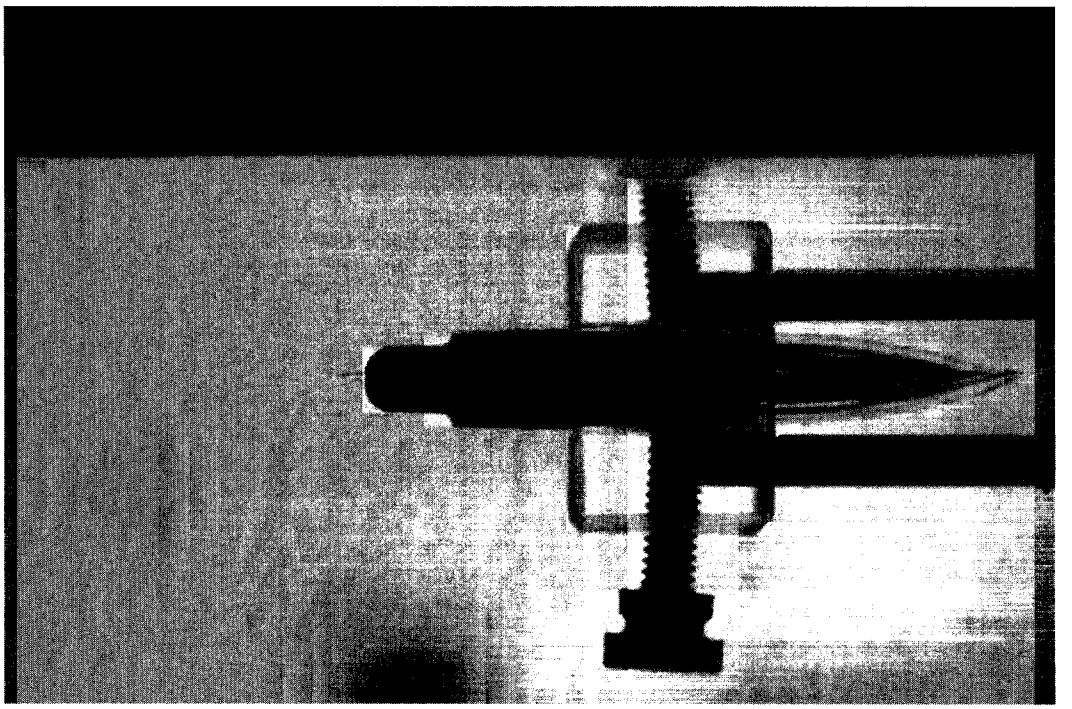

Figure 30: The IC-10 and its total reflection mirror image as seen from below the water level

Results of output factor measurements

The following table lists the final results of our output factor measurements. The average statistical error (precision) is a low 0.05%. It is difficult to estimate the accuracy of these numbers. After the accelerator was tuned to a nominal energy, we measured the drift in the electrometer reading that occurred between the first and the last measurement of each set. The drift was 0.14% in the worst case.

Energy [MeV]	6 cm diameter	3 cm diameter	2 cm diameter	10x10 SSD=100	10x10 SSD=105	3 cm diam. SSD=105	10x10 SSD=110
6	100.9	90.9	76.6	100.0	89.5	73.0	80.6
9	100.4	89.4	81.6	100.0	89.8	76.0	80.9
12	99.3	92.0	87.7	100.0	89.7	80.1	81.0
16	99.5	96.4	93.6	100.0	90.0	84.3	81.4
20	100.8	98.8	96.5	100.0	89.1	86.2	80.5

Table 3: Output factors of test cutouts measured at various SSDs at all nominal energies

Cylindrical ion chambers are not the ideal probes for electron dosimetry, especially in the case of small fields. They integrate over relatively large volumes and underestimate dose in areas close to the field boundaries, where the electron fluence is diminished.

Phase space files

The *Cutout Manager* needs a set of *EGSnrc* phase space files as input for Monte Carlo simulations. There must be a separate phase space file for each usable combination of electron energy and applicator size. The CLINAC 21EX is capable of delivering 6, 9, 12, 16 and 20 MeV electron beams in combination with 6x6, 10x10, 15x15 and 20x20 cm^2 applicators. The rarely used 25x25 cm^2 applicator is omitted. Thus, a total of 20 phase space files are required for a fully modeled linac.

Phase space files are generated using the *BEAMnrcMP* code system that can be installed on top of the *EGSnrcMP* system. This work uses version BEAMnrc07, installed under *Mac OS X*® (with the installation script method for *Linux* and *Unix* systems). For details regarding *BEAMnrcMP* the reader is referred to the *BEAMnrc Users Manual* (Rogers, Walters et al. 2006).

The general workflow for creating a *Cutout Manager* phase space file is as follows:

- In a first step, *BEAMnrcMP* is used to calculate a PDD distribution in a water phantom for a 10x10 reference field. The result is compared to the measured PDD curve and the input parameters to *BEAMnrcMP* are altered until the calculated PDD curve fulfills the matching criteria.
- In a second step, using the final parameter values from the first step, a phase space file is generated for each applicator size at scoring plane with z=93 cm, just above the upper surface of the cutout.

Phase space files require between 160 and 400 million particle histories to be pursued. The higher the nominal electron energy, the higher is the photon contents in the phase space file. Compared to electrons, photons only contribute a small fraction (< 15%) to the dose up and around R_{100} in the PDD curve. Thus, if the number of contributing electrons and with it the statistical uncertainty of the result

is to remain constant, the number of histories used in the *Cutout Manager* must be increased for higher energies. This must be reflected in the size and particle contents of the input phase space files.

BEAMnrc modeling of the CLINAC 21EX

The *BEAMnrc* code system provides a framework for modeling an accelerator by assembling it from *component modules* (CM). Component modules exist for many structures that can usually be found in radiation oncology and diagnostic radiology equipment. This is a non-comprehensive list of CMs for the purpose of modeling the electron mode of a linac:

- SLABS: Multiple slabs of arbitrary thickness. Used for windows, air and air spaces or thin foils.
- CHAMBER: Parallel-plate ion chamber or phantom.
- CONESTAK: Simple stack of truncated cones that can be used for primary collimators.
- CONS3R: Conical structures centered around the z axis that can be used for primary collimators.
- FLATFILT: Stack of truncated cones found in complex flattening filter designs.
- JAWS: Sets of paired bars or jaws.
- APPLICAT: Set of rectangular scrapers to model an electron applicator.
- CIRCAPP: Set of circular scrapers to model an electron applicator.
- PYRAMIDS: Stacked set of truncated pyramids – PYRAMIDS.
- BLOCKS: Treatment blocks or cutouts with arbitrary and/or multiple openings.
- MIRROR: Mirror for field and SSD indicator.

Linac modeling with Varian parameters

Initially, PPD curves were calculated using an accelerator model called CL21E_PDD. Dimensions and materials of the accelerator's mechanical parts were taken from documentation provided by Varian for the purpose of Monte

Carlo simulations. Phase space files were generated using a different model, CL21E, with the tuned energies obtained from the PDD calculations.

CL21E_PDD consists of the following component modules:

1. CONS3R (primary collimator)
2. SLABS (vacuum window)
3. SLABS (upper scattering foil)
4. FLATFILT (lower scattering foil assembly)
5. SLABS (monitor chambers)
6. MIRROR (light indicator mirror)
7. JAWS (jaws),
8. SLABS (reticle)
9. APPLICAT (electron applicator)
10. SLABS (air space)
11. CHAMBER (scoring phantom).

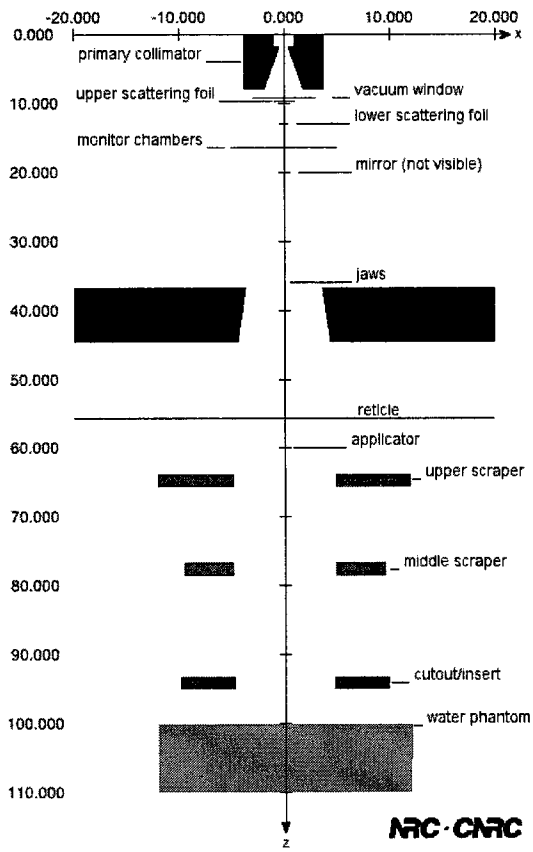

Figure 31: An annotated view of the CL21E_PDD accelerator model generated with *BEAMnrc*

Accelerator model CL21E is mostly identical but does not have the bottom air space and scoring phantom. In CL21E the APPLICAT component module only models the top two scrapers. This is followed by an air space that ends at z=93 cm, where the scoring plane for the phase space file is defined.

CL21E_PDD models the monitor chamber as a stack of 7 Kapton® foil layers and 6 air spaces. While this approach seems to be quite realistic, test do not show any evidence that combining the Kapton layers into just one layer leads to different results.

The material chosen for the applicator scrapers was an alloy of nickel, bismuth and tin with the *EGSnrc* identifier *BISNIC521*. The vertical spacers between scrapers are not modeled. The particle source was a cone shaped, mono energetic electron beam (*BEAMnrcMP* parameter ISOURCE=1) that originated from a point 3.07 cm above the first component module. The radius of the beam at z=0 was set to 0.086 mm.

It was taken into account that for 6 and 9 MeV beams the jaws define a 20×20 cm^2 field at SSD=100 cm, and change to a 14×14 cm^2 field at all other energies.

Results for accelerator models CL21E_PDD/CL21E

Figure 32 shows PDD curves obtained from *BEAMnrcMP* runs with model CL21E_PDD. In high dose areas around R_{100} the statistical dose error is typically 0.5% which is smaller than the radius of the data points. They are displayed together with PDD curves from an IC-10 measurement in February 2007. The energy of the monochromatic electron beam was tuned to match the R_{50} values of both the calculated and measured curve within one tenth of a millimeter (Table 4). Overall, the calculated PDD curves reproduce the measured data quite well. However, at all energies the depth-dose is systematically underestimated in the buildup region, followed by a dose overshoot between R_{100} and R_{50}. Around and beyond R_p, the measured depth-dose is significantly higher than the simulation. At 12 MeV and higher energies the simulation underestimates the bremsstrahlung tail by a large amount. The dose maxima of all calculations are at greater depths for all energies.

From that it can be concluded that not enough dose is deposited in the buildup region above R_{100} and that not enough photons are created to correctly account for the measured bremsstrahlung tail. In principle that situation could be remedied by tuning to higher effective energies. Unfortunately this would shift the calculated dose maximum and R_{50} even to higher depth, in disagreement with the measured values.

Using the tuned energies, phase space files were generated. In all runs ECUT was set to 0.521 MeV and PCUT was 0.01 MeV. Their particle contents is listed in Table 5.

The relatively low total number of particles in these phase space files was deemed sufficient, because a standard precision *Cutout Manager* run would use only 10 million particle histories. At 6 MeV nominal energy even 100 million incident particles result in only 7.4 million particles in the phase space file because most particles are absorbed before making it to the scoring plane. In this case, the CPU time on a 2 GHz AMD Athlon XP platform PC was almost 24 hours!

Phase space files were also generated for all other clinically used applicator sizes and open fields. For this, both collimator field sizes (see Table 1) and applicator dimensions were set to the appropriate values.

Output factor calculations

To setup *Cutout Manager* for output factor calculations, reference doses must first be calculated. For that purpose a cutout shape was created that defines a 10×10 cm^2 field at SSD 100 cm. *Cutout Manager* runs with 80 million histories each, yielded the results listed in Table 6.

After the reference doses had been entered in the preference file, output factors were calculated. The accuracy was set to 40 million particle histories which results in 0.7% to 0.9% statistical error. Tables 7-9 summarize the results for output factors, and absolute and relative deviations from measured values.

To have matching R_{50} values seemed to be a good choice since TG-51 uses R_{50} as a beam quality specifier. However, output factor calculations based on this accelerator model and matching criterion, do not agree well with measured

numbers. They are systematically too low over the whole energy range and cutout shapes. In about 40% of all cases the output factors differ by more than 2% from the measured values, in particular for small and very small cutouts for which a shift in R_{100} and PDD distortion occurs.

This casts doubt on the correctness of the input phase space files and the validity of the "Varian" accelerator model. Monte Carlo simulations based on this model underestimate the dose deposition the buildup region above R_{100} which in turn shifts the calculated R_{100} to greater depths. In summary the "Varian" model does not reproduce the PDDs well at depths from which the dose maximum is taken and the output factor is calculated.

Cone factors

Cone factors are output factors for "open" fields of other than 10×10 cm^2 applicators. Table 10 lists cone factors for the CL21EX(B) as measured in 2004. To calculate cone factors with *Cutout Manager*, cutout shapes were created for 6×6, 15×15, 20×20 and 25×25 cm^2 fields at SSD 100. 40 Million particle histories yield a statistical error of slightly better than 1%.

Calculated cone factors underestimate the measured numbers by a large margin, particularly for larger applicator sizes and, surprisingly, at lower energies. The results of cone factor calculation and their relative deviation from measured values is given in Table 11. Although the PDD curve from *Cutout Manager* calculations agrees well with measured data upon visual inspection (an example for 12 MeV and 15×15 cm^2 field size is given in Figure 33), we suspect that the accelerator model is not refined enough to handle the transition from one applicator size to another correctly.

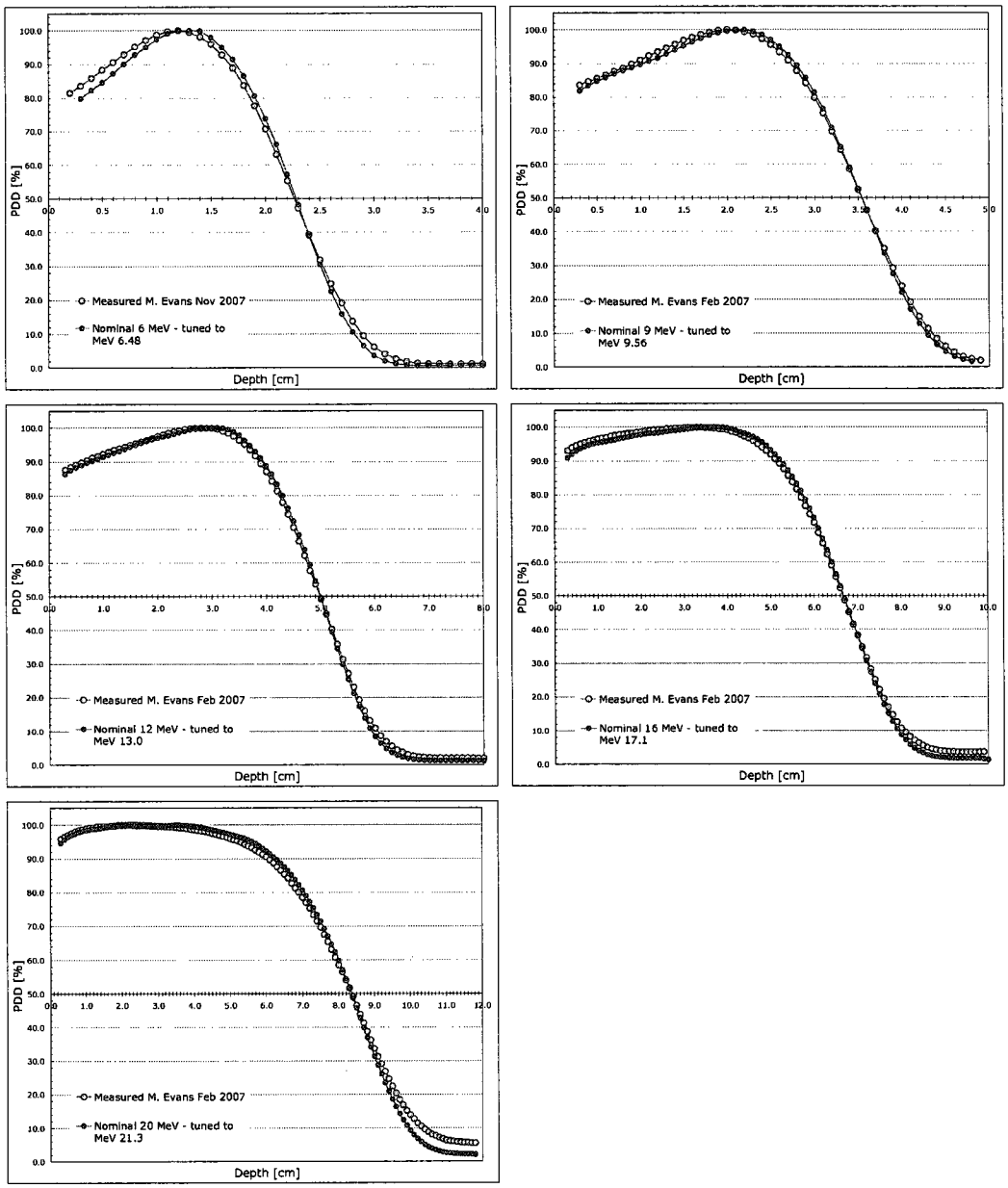

Figure 32: Calculated and measured PDD curves for 6, 9, 12, 16 and 20 MeV electron beams. Accelerator model CL21E_PDD with Varian data

Nominal energy	6 MeV	9 MeV	12 MeV	16 MeV	20 MeV
Tuned energy	6.60 MeV	9.56 MeV	13.0 MeV	17.1 MeV	21.3 MeV

Table 4: Energy tuning for matching R_{50} (model CL21E_PDD with Varian data)

Nominal energy	Incident particles from source	Total particles in file	Total photons in file	Total electrons in file
6 MeV	100,000,000	7,403,785	2,979,113	4,424,672 (59.8%)
9 MeV	100,000,000	16,285,966	8,022,016	8,263,950 (50.7%)
12 MeV	50,000,000	15,960,988	8,929,005	7,031,983 (44.1%)
16 MeV	50,000,000	21,979,482	10,783,975	11,195,507 (50.9%)
20 MeV	50,000,000	33,197,587	17,111,869	16,085,718 (48.4%)

Table 5: Particle contents of phase space files (model CL21E with Varian data)

Energy [MeV]	6	9	12	16	20
Reference Dose [Gy/particle]	1.0790e-13 ±5.0499e-16	1.8407e-13 ±1.2452e-15	2.9573e-13 ±1.8272e-15	4.6800e-13 ±1.8903e-15	6.8624e-13 ±2.8398e-15

Table 6: References doses for accelerator model CL21E with Varian data

Energy [MeV]	6 cm diameter	3 cm diameter	2 cm diameter	10x10 SSD=105	3 cm diam. SSD=105	10x10 SSD=110
6	101.1±0.8 (100.9)	88.2±0.7 (90.9)	72.3±0.6 (76.6)	88.4±0.7 (89.5)	71.0±0.6 (73.0)	79.6±0.7 (80.6)
9	99.5±0.6 (100.4)	86.3±0.8 (89.4)	77.0±0.8 (81.6)	89.0±0.9 (89.8)	72.0±0.7 (76.0)	81.3±0.8 (80.9)
12	98.5±0.9 (99.3)	87.6±0.9 (92.0)	82.8±0.9 (87.7)	90.3±0.9 (89.7)	76.6±0.8 (80.1)	79.4±0.8 (81.0)
16	97.7±1.0 (99.5)	92.5±0.9 (96.4)	89.1±0.9 (93.6)	90.2±0.9 (90.0)	82.5±0.8 (84.3)	82.3±0.8 (81.4)
20	99.1±0.9 (100.8)	98.2± 0.9 (98.8)	96.9±0.9 (96.5)	89.8±0.9 (89.1)	85.4± 0.8 (86.2)	81.2±0.8 (80.5)

Table 7: Output factors from *Cutout Manager* (model CL21E with Varian data. Measured values in brackets)

Energy [MeV]	6 cm diameter	3 cm diameter	2 cm diameter	10x10 SSD=105	3 cm diam. SSD=105	10x10 SSD=110
6	+0.2	–1.7	–4.3	–1.1	–2.0	–1.0
9	–0.9	–3.1	–4.6	–0.8	–4.0	+0.4
12	–0.8	–4.4	–4.9	+0.6	–3.5	–1.6
16	–1.8	–1.9	–4.5	+0.2	–1.8	+0.9
20	–1.7	–0.6	+0.4	+0.7	–0.8	+0.7
	Units: cGy/100 MU					

Table 8: Absolute deviation of calculated OFs from measured values (model CL21E with Varian data)

Energy [MeV]	6 cm diameter	3 cm diameter	2 cm diameter	10x10 SSD=105	3 cm diam. SSD=105	10x10 SSD=110
6	+0.2%	–1.9%	–5.6%	–1.2%	–2.7%	–1.2%
9	–0.9%	–3.5%	–5.6%	–0.9%	+5.3%	+0.5%
12	–0.8%	–4.8%	–5.2%	+0.7%	–4.4%	–2.0%
16	–1.8%	–2.0%	–4.8%	+2.2%	–2.1%	+1.1%
20	–1.7%	–0.6%	+0.4%	+0.8%	+0.9%	+0.9%

Table 9: Relative deviation of calculated OFs from measured values (model CL21E with Varian data)

Field size	6 MeV	9 MeV	12 MeV	16 MeV	20 MeV
6×6	95.9	97.3	96.6	98.7	99.9
15×15	102.2	100.2	99.9	99.7	100.0
20×20	106.7	101.3	98.6	97.1	95.8
25×25	108.6	100.7	96.4	93.8	92.6

Table 10: Measured cone factors for linac CL21EX(B)

Field size	6 MeV	9 MeV	12 MeV	16 MeV	20 MeV
6×6	95.5 (–0.4%)	97.4 (+0.1%)	99.1 (+2.6%)	100.5 (+1.8%)	101.7 (+1,8%)
15×15	99.8 (–2.3%)	99.3 (–0.9%)	98.2 (–1.7%)	96.0 (–3.7%)	95.7 (–4.3%)
20×20	94.1 (–11.8%)	95.0 (–6.2%)	92.7 (–6.0%)	92.3 (–4.9%)	91.3 (–4.7%)
25×25	99.2 (–8.7%)	90.4 (–10.2%)	88.7 (–8.0%)	88.5 (–5.7%)	90.4 (–2.4%)

Table 11: Cone factors from *Cutout Manager*. (model CL21E with Varian data. Deviation from measured values in brackets)

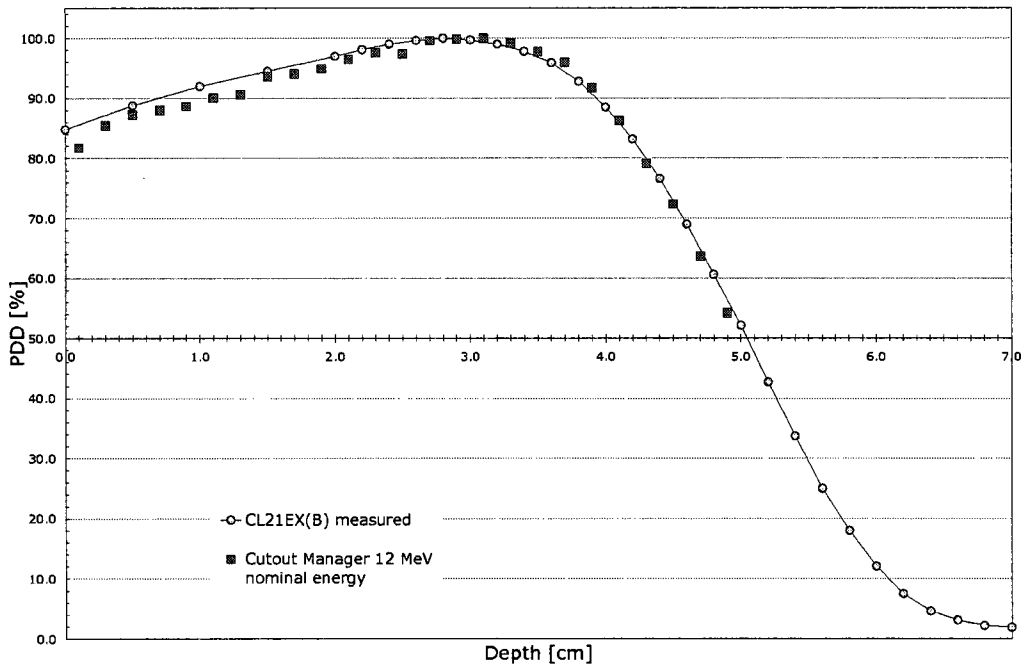

Figure 33: Calculated and measured PDDs for an open 15×15 cm^2 applicator at 12 MeV

Linac modeling with modified scattering foil

As the cutouts become smaller the depth-dose maximum shifts upstream to shallower depths. PDD curves based on Varian parameters and accelerator model CL21EX_PDD systematically underestimate the dose in the buildup region.

When phase space files based on this model are used as input to *Cutout Manager* calculations, this could lead to an underestimate of the maximum dose.

To test this hypothesis, the thicknesses of the foils in the lower scattering foil assembly were tripled. This also has the effect of slightly increasing the bremsstrahlung tail, which had been very low when the standard foil parameters were used.

A new accelerator model, CL21E_APPLIBARS_PDD, was created that included a component module (APPLICAT) to simulate the aluminum spacers between the applicator scrapers. There were also some changes in the modeling of the scrapers and the insert/cutout:

1. CONS3R (primary collimator)
2. SLABS (vacuum window)
3. SLABS (upper scattering foil)
4. FLATFILT (lower scattering foil assembly)
5. SLABS (monitor chambers)
6. MIRROR (light indicator mirror)
7. JAWS (jaws),
8. SLABS (reticle)
9. PYRAMIDS (top scraper)
10. APPLICAT (upper spacers)
11. PYRAMIDS (middle scraper)
12. APPLICAT (lower spacers)
13. BLOCKS (insert)
14. SLABS (air space)
15. CHAMBER (scoring phantom).

Accelerator model CL21E_APPLIBARS_PDD was used to calculate PDD curves and to tune the effective energy. The tuning criterion was matching R_{100} values. Another model, CL21E_APPLIBARS, has the lowest air slab and phantom removed and serves to create the phase space files.

BEAMnrc generated PDDs and their deviation from the measured data are documented in Figures 34 to 38. It is evident that tripling the lower scattering foil results in a much better agreement above and around R_{100}. The effect on R_{50} is inconclusive. A smaller R_{50} – an effect of increased energy loss in the scattering foil – should be offset by higher effective energies (Table 12).

Output factor calculations

Cutout Manager calculations of output factors based on the "thick" scattering foil assembly are in very good agreement with measured values. The RMS deviation is better than 1% for all cutout shapes at standard and extended SSDs. The worst case is –2.4% at 20 MeV at SSD 110 cm (Tables 13-15).

Tripling the thickness of the scattering foils is a drastic step but the results point to the important realization that it is crucial to have an accelerator model that correctly reproduces depth-doses in the buildup region and around R_{100}. This is perfectly understandable, since the dose maximum moves to shallower depths when the cutout becomes smaller.

Cone factors

Similarly, cone factor calculations improve to clinically usable error margins. The RMS error is 1.4% with tendency to overestimate the dose. The worst case is registered for a 6×6 cm^2 field at 9 MeV where the deviation was 3.5% . It would be desirable to conduct a detailed study of output factors for a variety of cutout shapes using other than a 10×10 applicator. Such data is currently not available. Instead a clinically used cutout was digitized and the output factor calculated for a 15×15 cm^2 applicator and 16 MeV. The result, evaluated on the central axis, was 97.3±0.6 or 2.4% below the measured value. Moving the point of interest around leads to better agreement. See Table 19 for more evaluations of clinical cutouts.

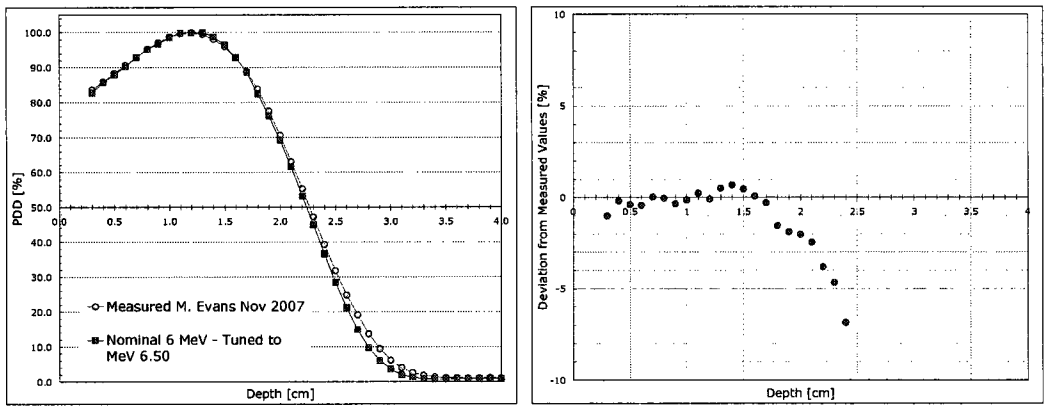

Figure 34: Calculated PDD curve and deviation from measurement (6 MeV, thick scattering foil)

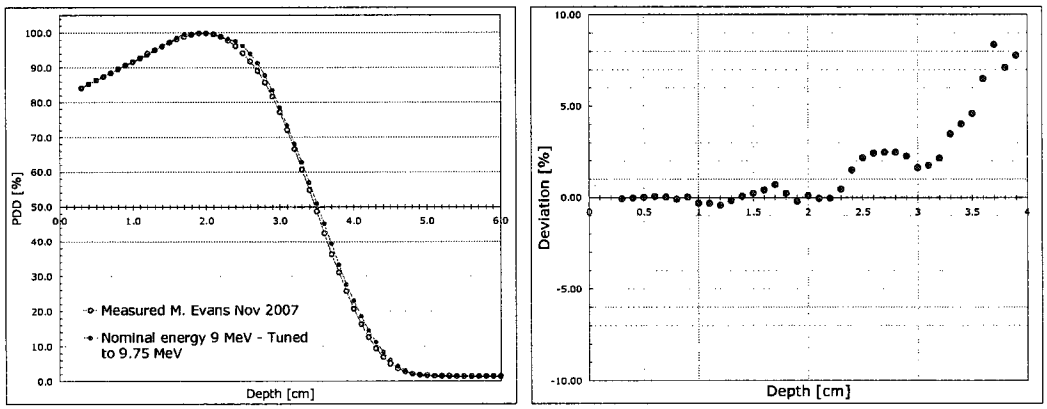

Figure 35: Calculated PDD curve and deviation from measurement (9 MeV, thick scattering foil)

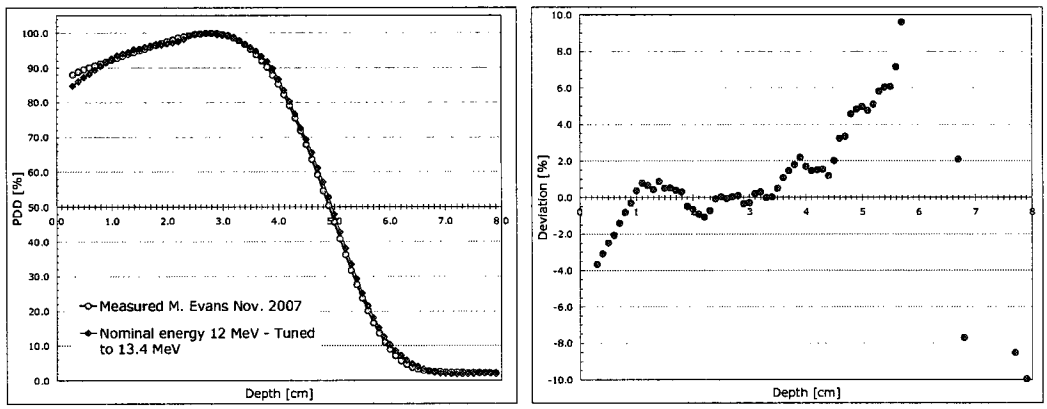

Figure 36: Calculated PDD curve and deviation from measurement (12 MeV, thick scattering foil)

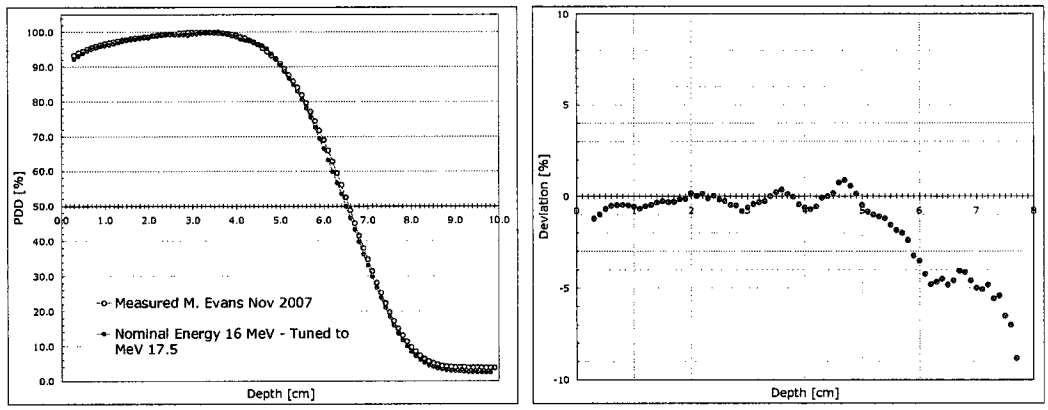

Figure 37: Calculated PDD curve and deviation from measurement (16 MeV, thick scattering foil)

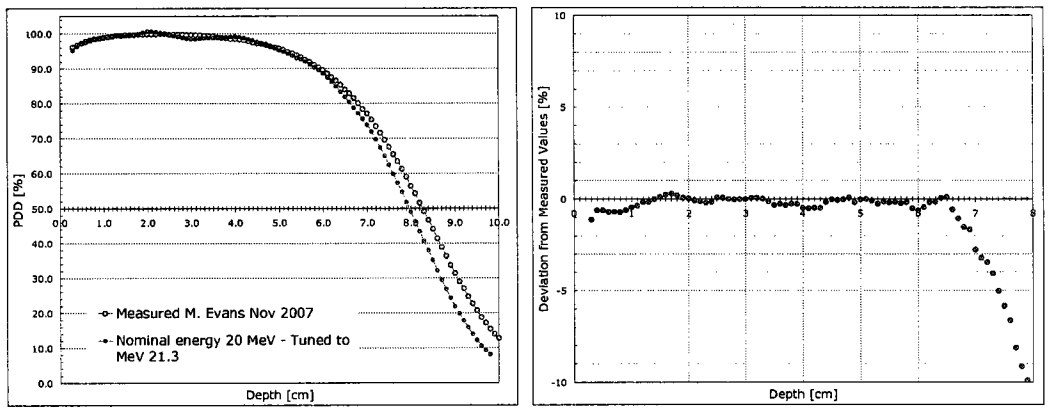

Figure 38: Calculated PDD curve and deviation from measurement (20 MeV, thick scattering foil)

Nominal energy	6 MeV	9 MeV	12 MeV	16 MeV	20 MeV
Tuned energy	6.60 MeV	9.56 MeV	13.0 MeV	17.1 MeV	21.3 MeV

Table 12: Energy tuning for matching R_{100} (thick scattering foil)

Energy [MeV]	6 cm diameter	3 cm diameter	2 cm diameter	10x10 SSD=105	3 cm diam. SSD=105	10x10 SSD=110
6	99.6±0.9 (100.9)	89.5±08 (90.9)	76.3±0.7 (76.6)	89.2±0.5 (89.5)	72.4±0.7 (73.0)	79.8±0.5 (80.6)
9	99.8±1.0 (100.4)	89.1±0.9 (89.4)	81.4±0.8 (81.6)	88.9±0.7 (89.8)	76.3±0.8 (76.0)	80.9±0.6 (80.9)
12	99.5±1.0 (99.3)	91.9±0.9 (92.0)	88.4±0.9 (87.7)	89.7±0.7 (89.7)	81.2±0.7 (80.1)	80.8±0.6 (81.0)
16	99.2±0.8 (99.5)	95.9±0.8 (96.4)	92.1±0.8 (93.6)	91.7±0.8 (90.0)	84.6±0.7 (84.3)	81.9±0.7 (81.4)
20	100.5±0.8 (100.8)	98.5± 0.8 (98.8)	97.1±0.8 (96.5)	90.3±0.7 (89.1)	87.1± 0.8 (86.2)	82.4±0.7 (80.5)

Table 13: Output factors from *Cutout Manager* runs (thick scattering foil. Measured values in brackets)

Energy [MeV]	6 cm diameter	3 cm diameter	2 cm diameter	10x10 SSD=105	3 cm diam. SSD=105	10x10 SSD=110
6	–1.3	–1.4	–0.4	–0.3	–0.6	–0.2
9	–0.6	–0.3	–0.2	–0.9	+0.3	±0
12	+0.2	–0.1	+0.7	0	+1.1	–0.2
16	–0.3	–0.5	–1.6	+1.7	+0.3	+0.5
20	–0.3	–0.3	+0.6	+1.2	+0.9	+1.9
	Units: cGy/100 MU					

Table 14: Absolute deviation of calculated OFs from measured values (thick scattering foil)

Energy [MeV]	6 cm diameter	3 cm diameter	2 cm diameter	10x10 SSD=105	3 cm diam. SSD=105	10x10 SSD=110
6	–1.3%	–1.5%	–0.4%	–0.3%	–0.8%	–0.3%
9	–0.6%	–0.3%	–0.3%	–1.0%	+0.4%	±0.0%
12	+0.2%	–0.1%	+0.8%	±0.0%	+1.2%	–0.3%
16	–0.3%	–0.5%	–1.6%	+1.9%	+0.4%	+0.6%
20	–0.3%	–0.3%	–0.1%	+1.3%	+1%	+2.4%

Table 15: Relative deviation of calculated output factors from measured values (thick scattering foil)

Energy [MeV]	6 cm diameter	3 cm diameter	2 cm diameter	10x10 SSD=100	10x10 SSD=105	3 cm diam. SSD=105	10x10 SSD=110
6	1.3 (1.24)	1.3 (1.1)	0.9 (0.72)	1.3 (1.20)	1.3 (1.27)	1.3 (1.7)	1.3 (1.29)
9	1.9 (2.02)	1.7 (1.41)	1.1 (0.88)	2.1 (1.92)	2.1 (2.04)	1.5 (1.36)	2.1 (2.08)
12	2.5 (2.74)	2.1 (1.65)	0.9 (1.07)	2.7 (2.76)	2.7 (2.80)	1.7 (1.54)	2.9 (2.90)
16	3.1 (2.63)	1.7 (1.48)	1.1 (1.11)	2.9 (3.24)	3.7 (3.46)	1.3 (1.68)	3.9 (3.52)
20	1.9 (2.0)	2.1 (1.7)	1.7 (1.1)	3.3 (2.5)	2.3 (3.0)	1.7 (1.7)	4.3 (3.4)

Table 16: R_{100} values calculated with *Cutout Manager* (thick scattering foil. Measured values in brackets)

Field size	6 MeV	9 MeV	12 MeV	16 MeV	20 MeV
6×6	97.8	100.7	98.7	98.4	101.9
15×15	102.1	99.2	100.6	98.4	98.5
20×20	106.4	104.0	100.8	98.5	06.5

Table 17: Cone factors calculated with *Cutout Manager* (thick scattering foil)

Field size	6 MeV	9 MeV	12 MeV	16 MeV	20 MeV
6×6	+2.0%	+3.5%	+2.1%	–0.3%	+2.0%
15×15	–0.1%	–1.0%	+0.7%	–1.3%	–1.5%
20×20	–0.3%	+2.7%	+2.2%	+1.5%	+0.7%

Table 18: Relative deviation of calculated cone factors from measured values (thick scattering foil)

Cutout Manager results for clinical cutouts

The following table lists measured and calculated output factors for clinically used cutouts. When the deviation was a large, output factors were calculated for other points of interest. The SSD was 100 cm if not otherwise noted.

Cutout Shape	Energy	Applicator	Measured OF	Calculated OF	Deviation	Comment
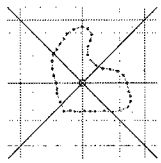	6 MeV	10×10	96.3	99.6±0.7	**+3.4%**	
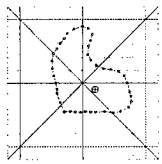	6 MeV	15×15	96.3	99.9±0.8 POI at (1, –0.5)	**+3.7%**	Same as above at a different POI
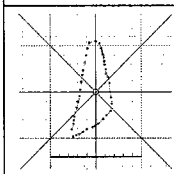	6 MeV	15×15	93.3 location uncertain, Farmer chamber	100.3±1.1	**+7.5%**	Critical shape. Measurement probably incorrect
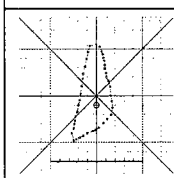	6 MeV	15×15	93.3	98.6±1.1 POI at (0, –1.5)	**+5.6%**	Same as above at a different POI.
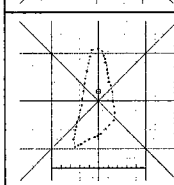	6 MeV	15×15	93.3	96.0±1.0 POI at (0, 1)	**+2.9%**	Same as above at a different POI.
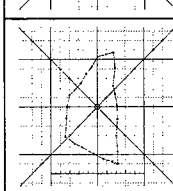	6 MeV	15×15	101.3 location uncertain	102.2±1.0 POI at (0, 0)	**+0.8%**	
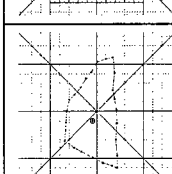	6 MeV	15×15	101.3 location uncertain	102.4±1.0 POI at (–0.5, –1)	**+1.1%**	Same as above at a different POI

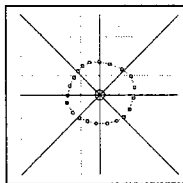	9 MeV	6×6	92.4	92.7±0.8	**+0.3%**	
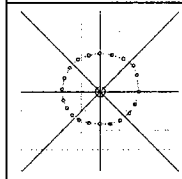	9 MeV	6×6	95.0	94.8±0.7	**–0.2%**	
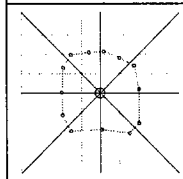	9 MeV	6×6	90.3 Farmer chamber	97.2±0.6	**+7.6%**	Measured value probably too low
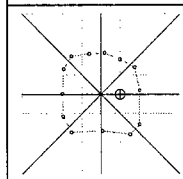	9 MeV	6×6	90.3 POI at (1, 0)	93.0±0.6	**+2.6%**	Same as above at a different POI
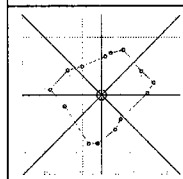	9 MeV	6×6	89.6 Farmer chamber	97.0±0.6	**+8.3%**	Farmer chamber too close to field limits?
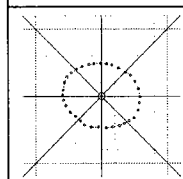	9 MeV	10×10	99.8	99.2±0.9	**–0.6%**	
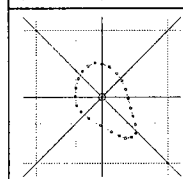	9 MeV	10×10	97.3	97.4±1.0	**+0.1%**	
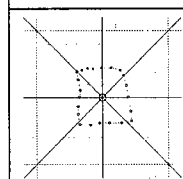	9 MeV	10×10	96.5	96.4±0.9	**–0.1%**	
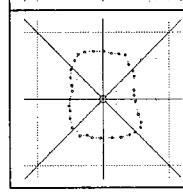	9 MeV	10×10	100.0	99.7±0.9	**–0.3%**	

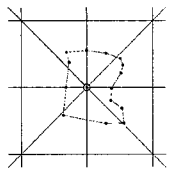	9 MeV	10×10	95.6	97.4±0.8	**+1.9%**	
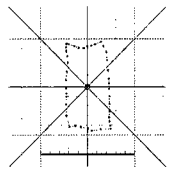	9 MeV	15×15	92.3	93.5±1.1	**+1.3%**	
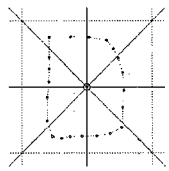	12 MeV	10×10	101.0	100.1±1.0	**–0.9%**	
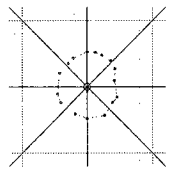	12 MeV	10×10	98.5	96.9±0.8	**–1.6%**	
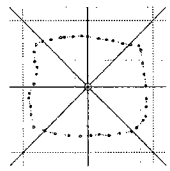	12 MeV	10×10	No data	99.9±1.1		
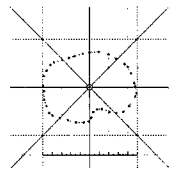	16 MeV	15×15	99.7	97.3±0.6	**–2.4%**	
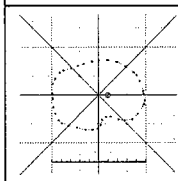	16 MeV	15×15	99.7	98.1±0.6 POI at (1, 0)	**–1.6%**	Same as above at a different POI
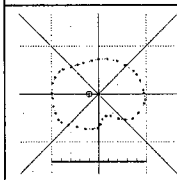	16 MeV	15×15	99.7	99.6±0.9 POI at (–1, 0)	**–0.1%**	Same as above at a different POI
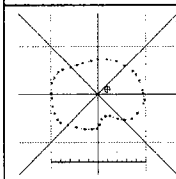	16 MeV	15×15	99.7	98.7±0.7 POI at (1, 0.5)	**–1.0%**	Same as above at a different POI

Table 19: Comparison of measured and calculated output factors for clinically used cutouts

Dose normalization

There is a fundamental difference between dose normalization in Monte Carlo simulations of output factors and clinical measurements. Particularly in the case of cone factors, which are essentially output factors for open square fields other that 10×10 cm^2, this difference may cause simulation results to disagree with measurement.

Output factors are ratios of two numbers, which are either doses or proportional to doses. They quantify how much the maximum absorbed dose on the central axis changes from a reference 10×10 cm^2 field when an arbitrarily shaped cutout is used.

In *EGSnrc* calculations scored doses are normalized to the number of particle histories simulated in a run. One could say that *EGSnrc* normalizes dose to the primary particle current. Dose results are easily comparable, regardless of whether a simulation was performed for 1 million or 100 million incident particles. This is true for all source types including phase space files. Thus, when output factors are calculated with the Monte Carlo technique, they are based on two simulations, each yielding a particle current-normalized dose value.

When output factors are determined clinically, two measurements are necessary: one with a 10×10 cm^2 insert under reference conditions and one with the patient's cutout under treatment conditions. The same amount of monitor units is used for both measurements, effectively normalizing the measured doses to 1 MU. When the output factor is multiplied by 100, the result is the effective output in cGy/100 MU. This procedure insures that the patient receives the correct dose.

Clinically measured doses are NOT normalized to the primary particle (beam) current, but to the accumulated ionization in the monitor chamber, a complex quantity that is affected by the interactions of primary and secondary particles and the (mechanical) treatment setup.

For example, if under otherwise identical conditions, the jaw settings were altered, and reduced backscattering from the jaw would decrease the monitor chamber signal by 10%, the planned number of monitor units would accumulate

in 111.1% of the time before. Even if the new jaw setting had no effect on the dose deposition in the phantom, the measured dose would appear to be 11.1% larger.

The described mechanism potentially affects all output factor measurements for configurations that do NOT uses the jaw settings of the 10×10 cm^2 reference field. Thus, linac manufacturers carefully shield the monitor chamber from the effects of downstream components and the effect is more significant for photon mode than for electrons.

Using the accelerator model CL21E_PDD, we studied the effect of different jaw settings and applicator sizes on a monitor chamber at 12 MeV nominal energy. The monitor chamber has 6 air chambers separated by Kapton® foils. The jaw setting for a 10×10 cm^2 applicator is 14×14 cm^2. The jaws open to 17×17 cm^2 for the 15×15 cm^2 applicator.

Figure 39 shows 6 pairs of data points. Each pair corresponds to a monitor chamber. Monitor chambers with lower dose region numbers are above those with higher numbers.

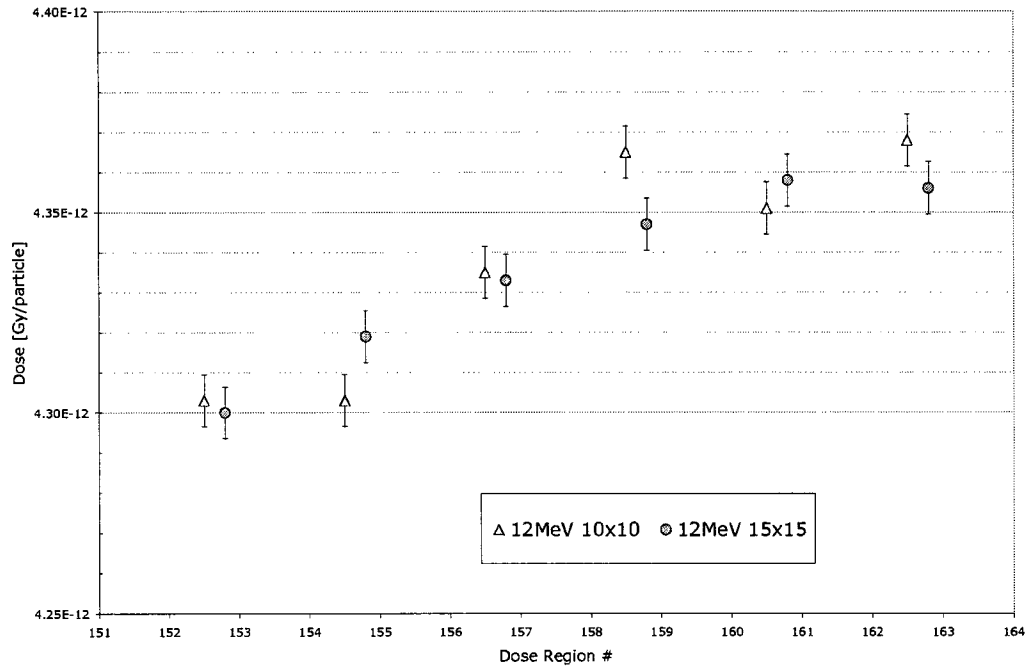

Figure 39: Monte Carlo simulations of absorbed dose to air in monitor chambers for different jaw settings

The statistical error of the calculated absorbed dose is 0.15% which is slightly smaller than the distance of the vertical axis' grid lines. There is no evidence for a dose difference within this error margin.

The Monte Carlo simulation results are encouraging, but it can not be ruled out that changes in the accelerator geometry affect the monitor chamber. Our linac model does not fully describe the intricate details of the treatment head. In particular, the modeling of scattering foils, shielding and jaws may not be detailed enough. It is, however, reassuring that clinical measurements of output factors correctly account for the effect.

Differences between steel and *Cerrobend*® inserts

Varian-supplied inserts for "open" fields are made from steel. We studied the effects of insert materials on PPD curves for 10×10 cm^2 fields at 6 MeV nominal energy. The accelerator model was CL21EX_PDD. Default ECUT was 0.521 MeV. The dose maximum was found to be $1.096(9) \cdot 10^{-13}$ Gy/particle for steel and $1.088(10) \cdot 10^{-13}$ Gy/particle for *Cerrobend*®. Both values agree with each other within the statistical error. Slight differences were noticeable in the shape of the PDD curves (Figure 40). For a *Cerrobend*® insert, the dose maximum appears to be shifted downstream by about 1 mm. At the same time the depth dose is systematically smaller in the buildup region. This behaviour can not be explained by the presence of more energetic electrons since a downstream shift of the dose maximum would be accompanied with a buildup dose increase.

Instead, the effect could be due to increased bremsstrahlung production in steel. Figure 41 shows the percentage difference between steel and *Cerrobend*® PDDs. Above R_p, at about 3 cm, the bremsstrahlung component is several percent higher for the steel insert. If that increase is extrapolated back to the buildup region, where bremsstrahlung contributes typically 8-15% to the depth dose, a net increase in depth dose appears to be possible. More detailed studies of the radiation sources that contribute to the PDD curves are necessary to fully understand the situation.

The *Cutout Manager* is not affected by these results. The maximum depth-doses are identical within their statistical errors and the software uses the correct materials for the reference field calculation and clinical cutout dose calculations.

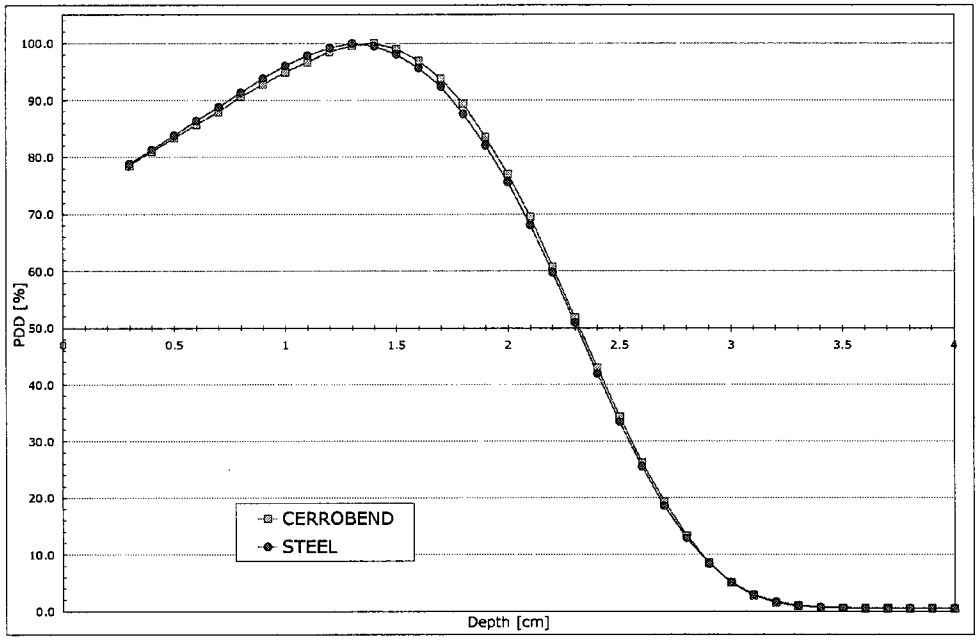

Figure 40: Monte Carlo simulated PDDs for a steel and *Cerrobend*® cutout.

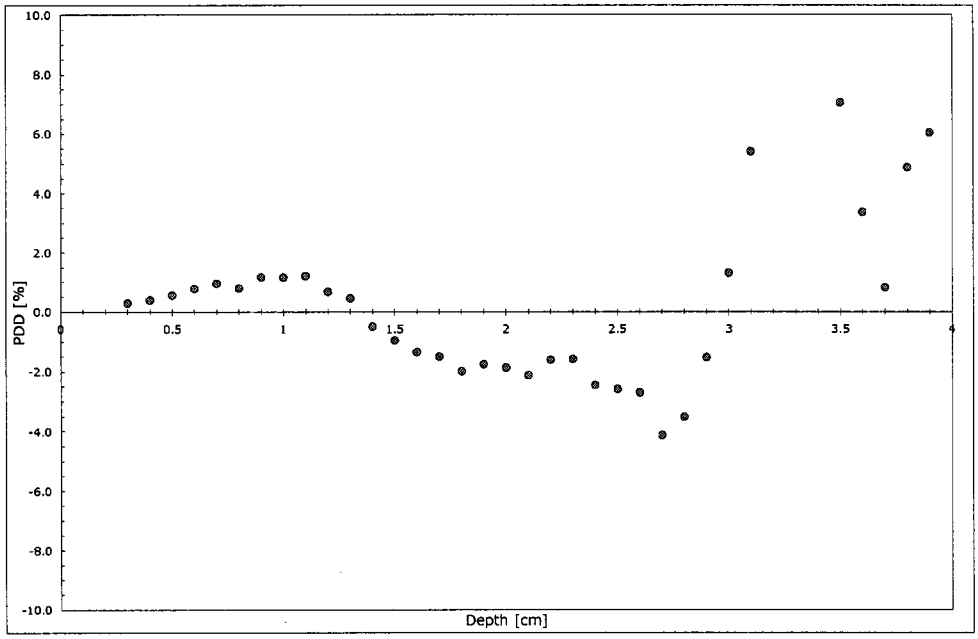

Figure 41: Deviation of Monte Carlo simulated PDDs for a steel and *Cerrobend*® cutout

Radiochromic film measurements

Radiochromic film dosimetry uses the effects of ionizing radiation on a photosensitive emulsion to measure doses, dose profiles and depth doses. Radiochromic films offer the advantage of very high spatial resolution, relatively low sensitivity variation with energy and are insensitive to light. They are self-developing and the change in net optical density is a direct measure of the absorbed dose.

The goal was to study the feasibility of a simple method to measure 2D dose distributions with a letter-size sheet of *GAFCHROMIC® EBT* film, suspended vertically in a water phantom. This should enable us to measure the depth-dose curves and lateral dose profiles at all depths simultaneously. The method described in this section is experimental and the resulting PDD curves, profiles and output factors require further confirmation.

Materials and methods

GAFCHROMIC® EBT film is a registered trademark of *International Specialty Products*. The film is specified to have an energy-independent dose response from keV to MeV, be near-tissue equivalent and water resistant. *GAFCHROMIC® EBT* film reacts to ionizing radiation by a color change that increases absorption of visible light particularly in the red with absorption maxima centered around 583 nm and 635 nm. Figure 42 shows how the net absorption spectra vary with dose. It has been reproduced from (Devic, Tomic et al. 2007) with the author's permission.

Before exposing the film sheets to radiation they are labeled with a permanent marker and scanned with an *Epson Expression® 1680* document scanner in transmission mode (Seiko Epson Corporation, Nagano, Japan). One sheet is kept with the other films but not irradiated. It serves as a monitor for background radiation that may effect the films during the 24h waiting period.

We used a water tank suitable for TG-51 measurements with the inner dimensions $40 \times 35 \times 36$ cm^3 (W×D×H). A *Styrofoam®* block, 7 cm thick, was cut to fit into the water tank's opening, but to slide freely. The center of the Styrofoam® block had a square 20×20 cm^2 wide opening. Vertical grooves were cut in the middle

of the central opening's sides. A letter-size *GAFCHROMIC® EBT* film sheet would later be inserted into these grooves and held in place by friction.

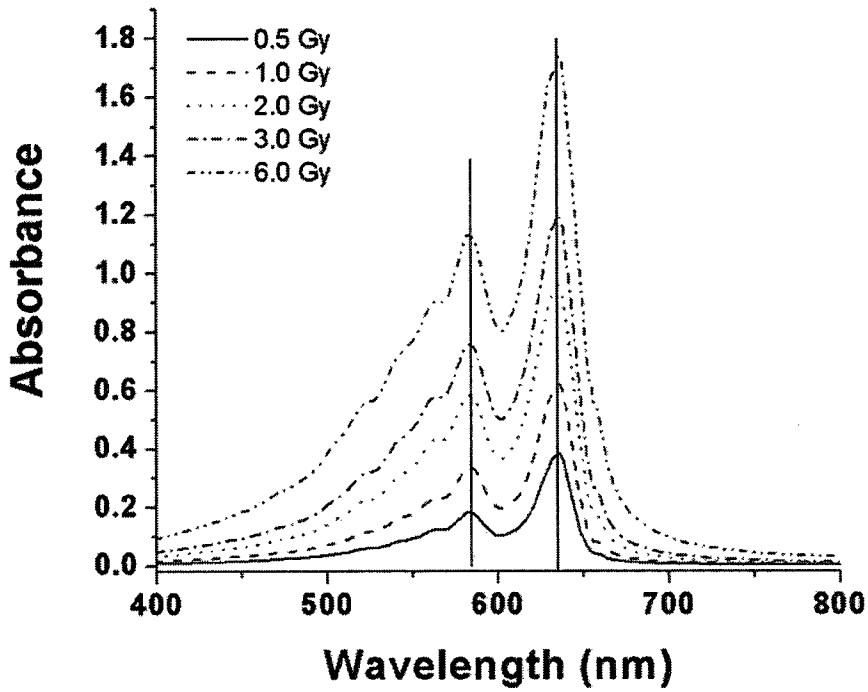

Figure 42: Net absorption spectra of *GAFCHROMIC® EBT* film vs. dose

The setup procedure is as follows: The water tank is put on the couch, centered and filled to about 75% with water. Then the *Styrofoam®* frame is inserted and allowed to float on the water. In this position the frame is secured into place with a couple aluminum bars and metal clamps. Finally the water tank is filled with water until the water surface is level with the *Styrofoam®* frame's upper surface. For the measurement, a film sheet is inserted into the grooves of the Styrofoam® frame. It is moved upwards against a plastic block that is placed above the grooves, flush with the frame's upper surface. This ensures that the film is horizontal and flush with the water surface. In a last step we slide a finger over the top edge of the films to close the water surface. The couch is moved up to bring the water surface to SSD 100 cm, the cutout is installed and the film is irradiated with 400 MU. 400 MU correspond to 4 Gy absorbed dose to water in the dose maximum. We used linac CL21EX(A) with a nominal beam energy of 6 MeV. Figure 43 shows all components in a dummy setup without water.

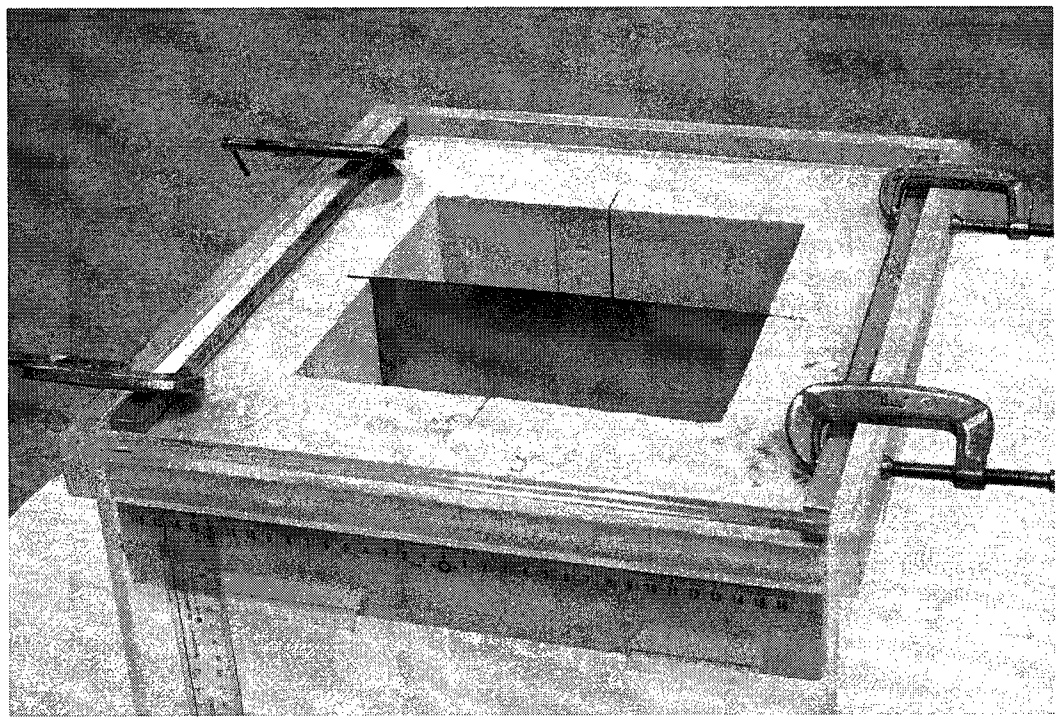

Figure 43: *GAFCHROMIC® EBT* film sheet held by a *Styrofoam®* frame in a water tank

After exposure, the film is quickly removed from the water tank, dried with a towel and stored for 24h before read-out. Data processing with MATLAB® involves isolation of the red component of scanned film images before and after exposure, smoothing with the built-in *Wiener2* filter, co-registration and re-binning of the pixels. The net optical density *netOD* is then calculated on a pixel by pixel basis as the decadic (base-10) logarithm of the ratio of transmission scanner readings before and after exposure:

$$netOD = \log_{10}\left(\frac{I_{unexposed}}{I_{exposed}}\right)$$

The calibration curve that relates dose and net optical density has the analytical form

$$Dose = b \cdot netOD + c \cdot netOD^{n}$$

Our batch of *GAFCHROMIC® EBT* film had been previously calibrated following a process that uses a flat-bed document scanner in radiochromic film dosimetry (Devic, Seuntjens et al. 2005). It yielded the following parameter values: n=2.5, b= 4.902 and c=21.28. In their paper, Devic et al. estimate the dose uncertainty to

be 2% or better at 4 Gy. It should be noted that we did not correct for background exposure and that a different scanner model was used.

Results

As an example, Figure 44 shows a *GAFCHROMIC® EBT* film sheet irradiated with 6 MeV electrons using a 10×10 cm^2 reference cutout at SSD 100 cm. After scanning and digital processing we obtained two-dimensional dose distributions for field sizes of 10×10 cm^2, 2 cm diameter and 3 cm diameter at SSD 100 cm. Their color coded images can be seen in Figures 45 and 46. The scale on the color bar runs from 0 Gy (black) to 4 Gy (white).

The original scan resolution of 150 dpi (or 59.1 dots per cm) is unnecessarily high and introduces statistical noise. The data was re-binned to yield an effective resolution of 1×1 cm^2. For dose measurements the image data was further averaged over a 6×5 mm^2 area, roughly equivalent to the volume of an IC-10 ionization chamber.

Figures 47 to 49 show film-measured central axis PDDs for all field sizes. For reasons of machine availability the film measurements were performed at linac CL21EX(A) whereas the IC-10 measurements were done using the CL21E(B) machine. This should not pose a problem because the beam parameters are matched. Overall, the PPD curves agree well with IC-10 results. There are, however, differences in the buildup region, beyond R_{100} and around R_P. Some of the issues could be attributed to poor alignment of the film and possible errors in measuring the absolute depth. A more precise holding mechanism which also stretches and flattens the submerged film would be a solution. It was also suggested that the film's orientation towards the incoming radiation might effects the results, especially when irradiated from the edge.

The dose maximum on the central axis for the 10×10 cm^2 open field was found to be 4.02 ± 0.08 Gy in very good agreement with the expected value of 4 Gy. Dose maxima on the central axis were also measured for the 2 and 3 cm diameter cutouts. They are listed with derived output factors in Table 20. Film-measured output factors tend to be slightly higher than the IC-10 values, a behavior that is expected because the IC-10 integrates over a larger volume.

Lateral profiles can be easily extracted from our 2D dose data. Figures 50 to 52 show profiles at various depths for all cutout sizes. Based on our data the ICRU criteria for profile flatness and symmetry for a 10×10 cm^2 field at R_{100} are both met. In case of small circular cutouts the dose drops quickly from its maximum value just a few mm off the beam axis. Large-volume ionization chambers, cylindrical or plane-parallel, thus have the tendency to underestimate the central axis dose and produce output factors that are systematically too low.

The present work with radiochromic film is only a first feasibility test. The strength of the method lies in its high spatial resolution and ability to deliver calibrated 2D dose maps from which PDDs, profiles and output factors can be extracted. More measurements using a more precise and reliable positioning mechanism are necessary to clarify the differences in the PDD curves. The output factors, however, might prove to be better than those from ionization chamber measurements.

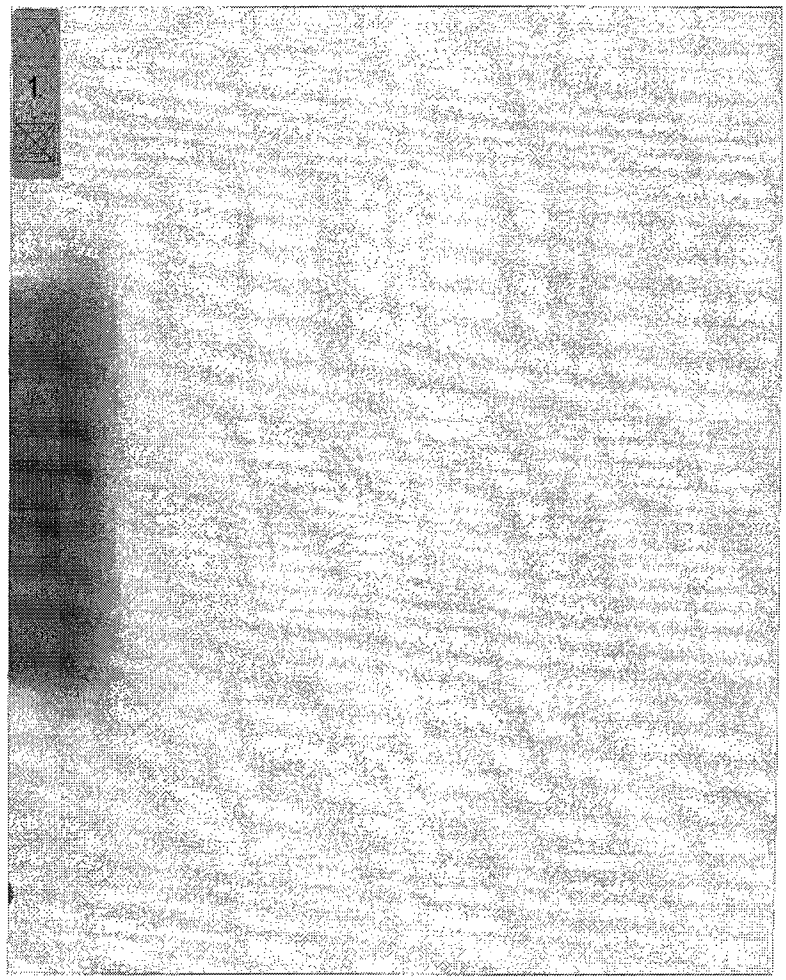

Figure 44: *GAFCHROMIC® EBT* film after irradiation with 6 MeV electrons using a 10×10 cm^2 reference cutout at SSD 100 cm

	10×10 SSD 100	2 cm diameter	3 cm diameter
Maximum dose [Gy]	**4.02±0.08 Gy**	**3.21±0.07 Gy**	**3.76±0.08 Gy**
Output factor	100	**79.9±2.4** (76.6)	**93.5±2.7** (90.9)

Table 20: Dose maxima and output factors measured with *GAFCHROMIC® EBT* film. Measured values in brackets

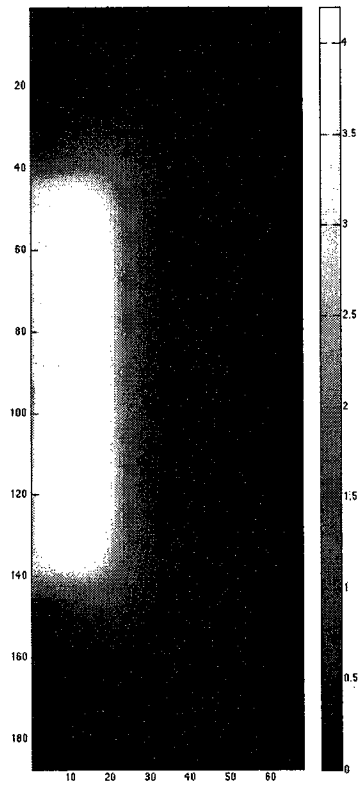

Figure 45: Color coded dose distribution for a 10×10 cm^2 reference cutout at 6 MeV

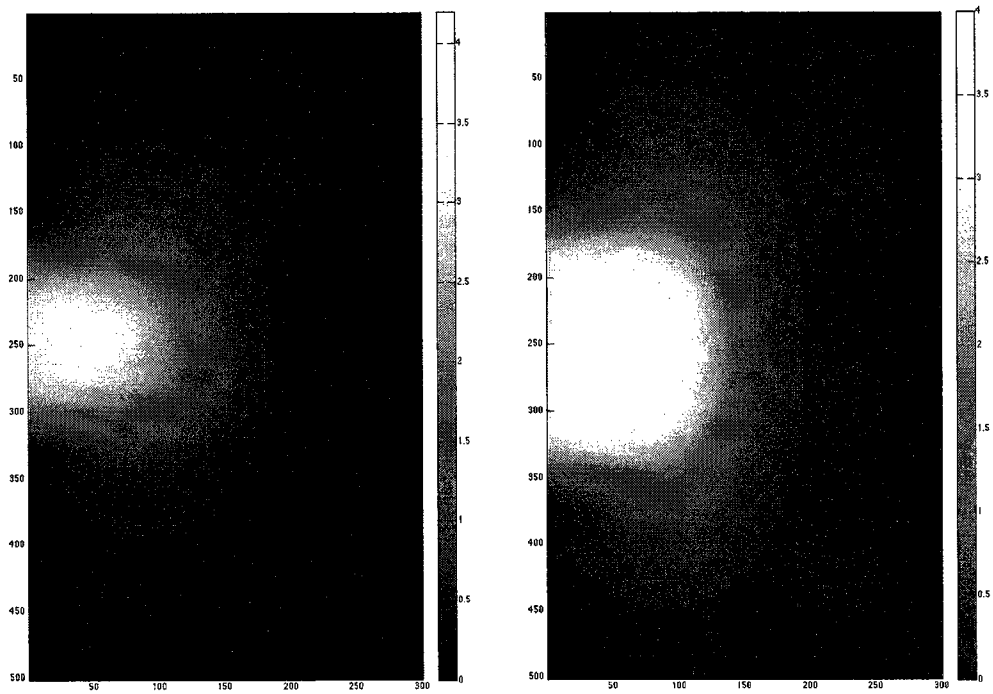

Figure 46: Color coded dose distribution for a 2 and 3 cm diameter cutout at 6 MeV

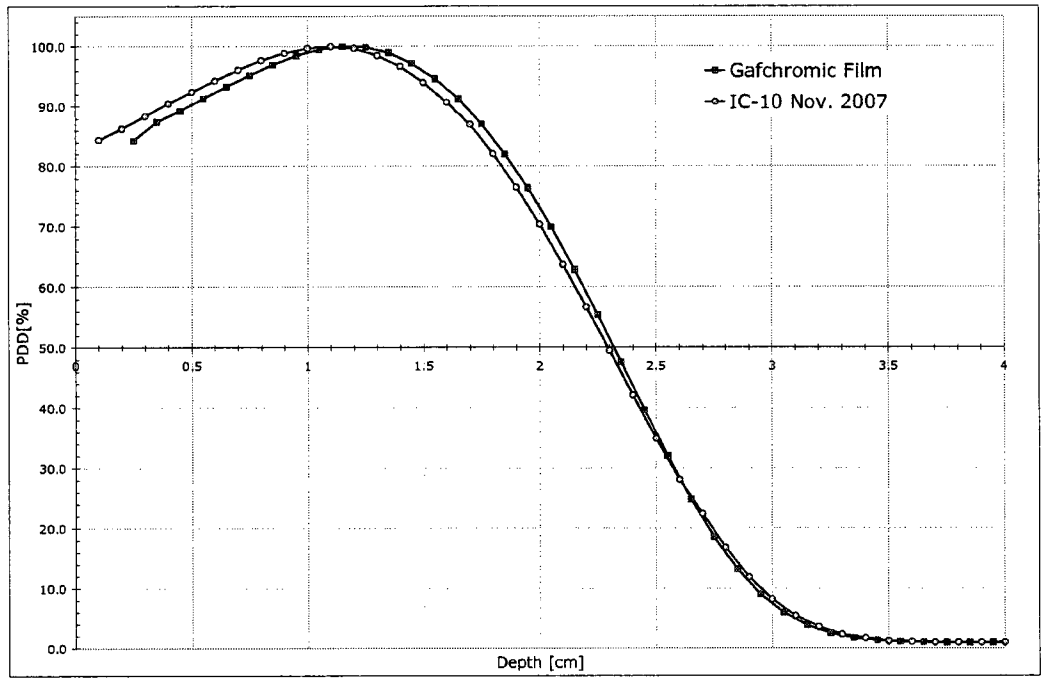

Figure 47: Comparison of PDD curves measured with film and IC-10, 6 MeV, FS=10×10 cm^2

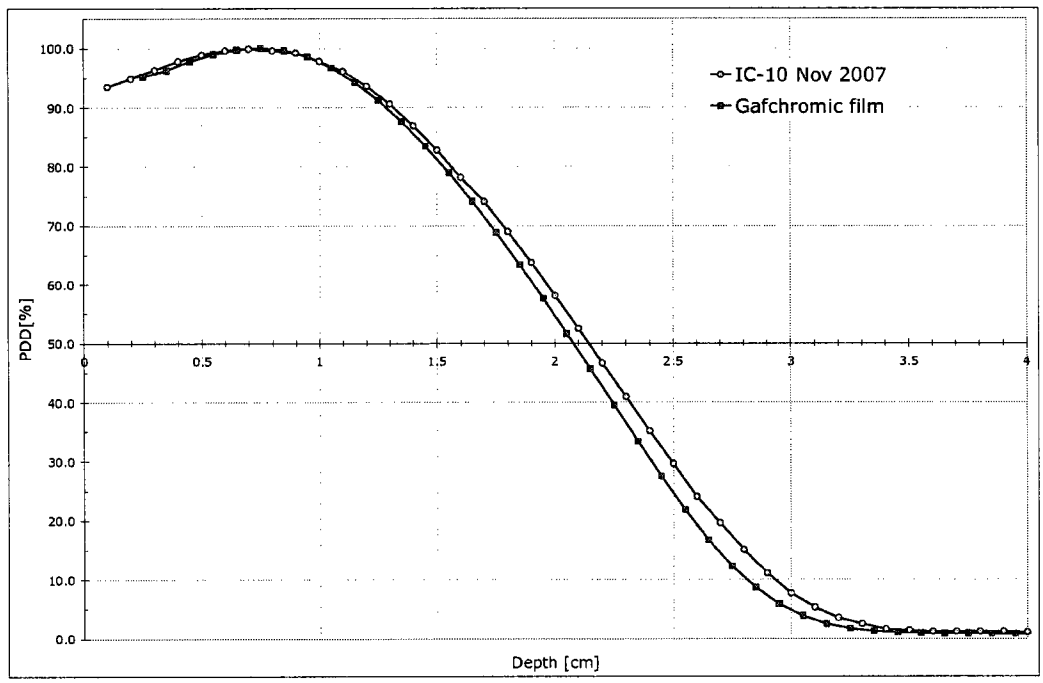

Figure 48: Comparison of PDD curves measured with film and IC-10, 6 MeV, FS=2 cm diam.

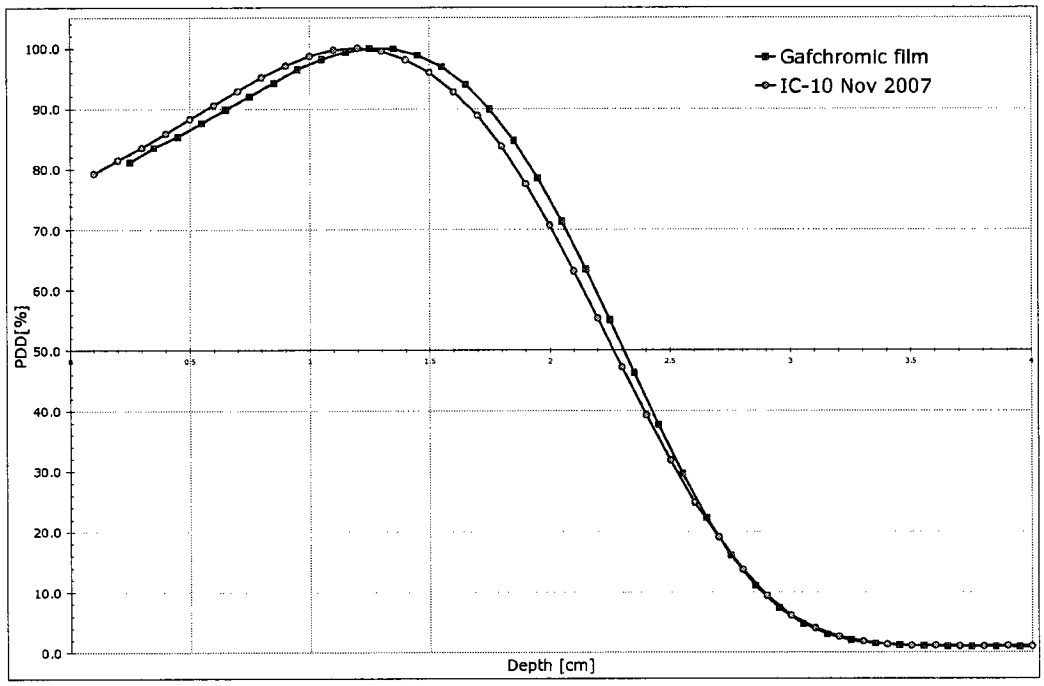

Figure 49: Comparison of PDD curves measured with film and IC-10, 6 MeV, FS=3 cm diam.

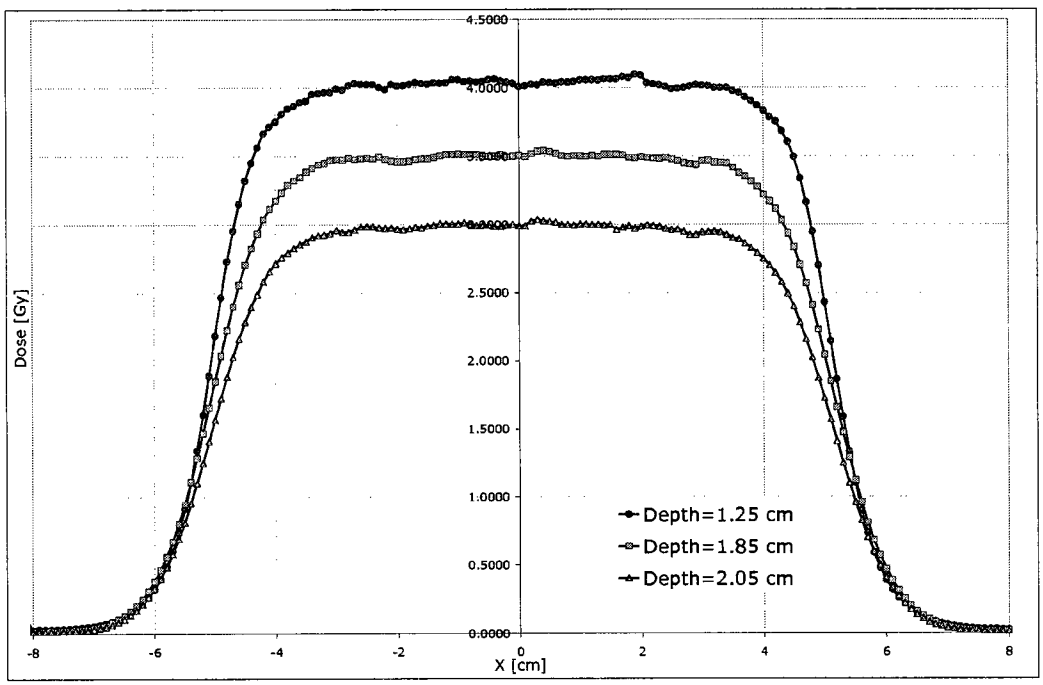

Figure 50: Dose Profile, FS=10×10, 6 MeV. *GAFCHROMIC® EBT* film

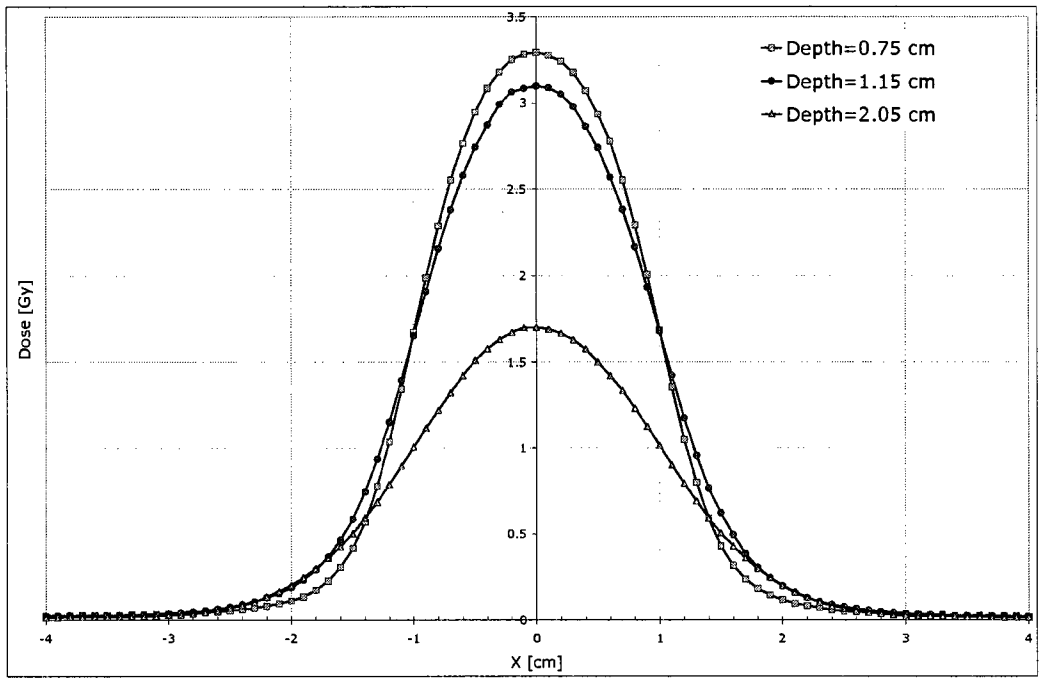

Figure 51: Dose profile, 2 cm diameter cutout, 6 MeV, *GAFCHROMIC® EBT* film

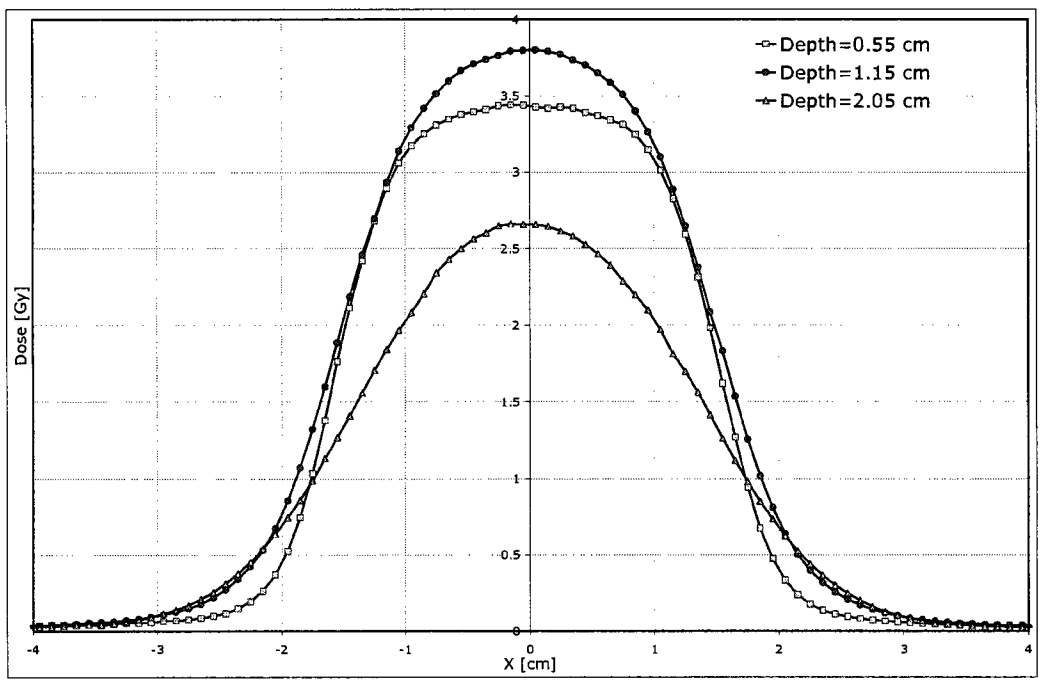

Figure 52: Dose profile, 3 cm diameter cutout, 6 MeV, *GAFCHROMIC® EBT* film

Conclusions and outlook

The objective of this thesis was to develop a software system for Monte Carlo simulation based output factor calculations and to implement it on *Mac Pro*® hardware under *Mac OS X*. An earlier Linux program served as the code base of the present *Cutout Manager*. The *EGSnrc* user code now conforms to the newest multi-platform version *EGSnrcMP* with improved parameter input and progress reporting. It also saw one crucial subroutine replaced with an implementation of an alternative algorithm for the *Inside or Outside Problem* for a point in a polygon.

The graphical user interface of the *Cutout Manager* still offers the same basic capabilities as its predecessor as a subset of its functions. Window layout was completely overhauled to be more logical and user friendly. The most apparent change is the cutout job listing which now avoids cryptic unified cutout job names, followed by extended filtering options including regular expressions. In expert mode the desired accuracy can now be selected by a mouse click. There are also subtle changes to the digitizer and PDD display.

Many improvements to the program's inner workings and object model have been made that are not readily visible: Multiple job splitting and merging of results, support of the `atrun` batch system and random number generator seeding options.

While in its present form the *Cutout Manager* is a perfectly usable, convivial software tool, several improvements could make it even more so. At the heart of problem is the fact that cutout jobs are organized and maintained in the file system. While it will still be necessary to create files as input to batch jobs, all program parameters including cutout jobs should be organized in a relational database.

During the implementation and use of *EGSnrcMP* we encountered a grey zone that warrants further investigation. On the *Mac OS X* platform, user code compiled with the popular *g77* Fortran compiler could yield different results than a Linux version, in particular at high (–O3) optimizations levels. On a Mac, optimization levels should be restricted to –O1 or –O2 to avoid the –ffast-math switch to be applied. According to the *g77* documentation, –ffast-math "Might

allow some programs designed to not be too dependent on IEEE behavior for floating-point to run faster, or die trying".

On some occasions, *EGSnrcMP* user code would loop indefinitely while hatching cross-section data. On the Mac this occurred for global ECUT=0.7 MeV and ICRU700 type PEGS4 files at NOOPT and OPT optimization level, while the code ran correctly for levels DEBUG and –O1. It was also reported that some NRC-provided user code, like *dosxyznrc*, would not compile on the Mac with default options.

Lastly, some unexplained wavy modulation occurred on the PDD curves at high electron energies. This was particularly visible during simulations of the triple thickness scattering foil with ECUT=0.7 MeV and Fortran optimization level FOPT=–O2 (Figures 36 to 38).

While numerical results obtained on a Mac generally agree with other operating system platforms, the issues described above cast a shade of doubt on the *EGSnrcMP* implementation under *OS X*. Since the *EGSnrcMP* code base is the same on all Unix platforms, the problem may lie within the Fortran compiler. *g77* needs to be extensively tested, benchmarked and version controlled for use with *EGSnrc* or eventually be replaced by another product.

When compared to measured values, the results of output calculations clearly show the importance of matching the PDDs from linac simulations with measured data, particularly in the buildup region and around the depth-dose maximum. If the accelerator model is not capable of reproducing the PDDs over the whole range of depths, it is preferable to tweak it for matching R_{100} (instead of R_{50}), regardless of what happens further downstream.

Measured PDD data is obtained under reference conditions, i.e. field size $10\times10\ \text{cm}^2$ at SSD 100 cm. The resulting effective energies of the primary electron beam are then used to create the phase space input files for the *Cutout Manager* system for all applicator sizes. While this procedure yields excellent results for the $10\times10\ \text{cm}^2$ applicator, it seems to break down when other applicator sizes are used. At this point the only explanation is that the accelerator model does not correctly describe the applicator. As a matter of fact, the

applicator geometry is far more complex as described in simple APPLICAT or PYRAMIDS component modules and the modeling of the vertical spacer bars is probably not very realistic. It is also uncertain what materials are used in the real applicators. A possible way out of this is to base output factor calculations for other than reference size fields on the dose ratio between the clinical cutout $D_{cutout,FS}$ and the open field $D_{open,FS}$, multiplied by the measured cone factor CF_{FS}:

$$OF(cutout,FS) = \frac{D_{cutout,FS}}{D_{ref,10x10}} = \frac{D_{cutout,FS}}{D_{open,FS}} \cdot CF_{FS}$$

First results seem to support this course of action, although it would be preferable to have an accelerator model that correctly describes the transition from reference conditions to the clinically used applicator size.

AAPM Task Group 25 clearly defines output factor as "the ratio of dose per monitor unit U at d_{max}, for a given field size F to that for the reference field size F_0 at its own $d_{max,0}$". In the real world precision dose measurements are ionization measurements with extended ionization chambers, corrected for effective points of measurements and stopping power ratios. Ionization is collected over large volumes, sometimes longer than 2 cm. Since the measurement is performed at the supposed dose maximum, parts of the chamber will be located in the buildup region. Particularly in the case of electron beams the charged particle fluence is significantly perturbed by the presence of the ion chamber. There is also the issue of dose bleeding when the point of interest comes close to the cutout borders. As a result of this, the output factor is rather what was measured in a particular setup than what the AAPM defines. Monte Carlo simulations offer the best way out of this situation, where a statistical error of 1% is achievable with the additional benefit of PDD curves and 2D output factor maps.

To summarize, *Cutout Manager* is a Monte Carlo simulation based software system capable of calculating output factors with typically 1% statistical error. When the accelerator model reproduces measured PDDs in the buildup region and

around R_{100}, calculated and measured output factors are in good agreement with precision measurements of circular cutouts at SSD 100 cm and extended SSD. Compared to measurements of clinical cutouts with an assumed error margin of 2%, *Cutout Manager* delivers consistent numbers while avoiding the typical shortcomings of the measuring process. The agreement is particularly good in cases that use a 10×10 cm^2 applicator, where the same phase space file is used for both the evaluation of cutout doses and the reference dose. The transition to other applicator sizes is more challenging since jaw positions and applicator dimensions change. While calculated output factors of such clinical cutouts are perfectly acceptable, it would be desirable to have a more refined linac model that is tested against precision measurements of test cutouts using other than reference applicator sizes. An other alternative is to calculate reference doses for open fields at all applicator sizes instead of the 10×10 cm^2 reference dose and correct with measured cone factors.

Appendix A – IMPLEMENTATION

This section describes selected topics of the *Cutout Manager's* technical implementation. The software components are discussed and some particularities of the implementation platform, *Mac OS X*®, are highlighted. To allow for a smooth installation, a sample installation procedure is presented.

It is outside the scope of this work to explain programming techniques, operating systems and program packages like REALbasic®, g77, *EGSnrc* or *BEAMnrc* in detail. For that the reader is referred to existing documentation, available for download from Internet sites.

Program components

The user-visible part of the *Cutout Manager* system is the graphical user interface. Under its hood works the *EGSnrc* particle transport code and execution layer. The *Mac OS X*® operating system provides file system services, command shells, shell scripting and a batch system.

The *Cutout Manager* graphical user interface (CMGUI)

The central task of the CMGUI is to manage cutout jobs and display results. A complete account of its user functions can be found in the USER'S GUIDE chapter. In this section we focus on implementation details.

The REALbasic® integrated development environment

CMGUI is a *Mac OS X*® application, developed and compiled for the Mac Intel platform with REALbasic® 2007 Release 3. REALbasic® is an integrated development environment that creates native applications for Macintosh, Windows and Linux operating systems. It is a registered trademark of REAL Software Inc., Austin, Texas. Compared to its main rival product, Microsoft Visual Basic, REALbasic® has the advantage of a much smaller footprint, cross-compilation capabilities and lower cost.

Cutout job administration on the file system level

Technically, a cutout job is a set of parameters, input data and result data. All information related to a cutout job is stored in the computer's file system. Depending on the processing status, two or more data files are associated with

each job. The CMGUI creates, alters and deletes these files or passes them to a command shell for execution.

Unique cutout job identifier (UCJI)

When a cutout job is initially created, it is given a unique name. It is under this unique name that all job related information is stored in files with different extensions. The unique cutout job identifier is constructed from pull-down menu selections and text entered in the *Cutout Workbench.*

It has the following form:

<linac ID>_<Energy>_<Applicator size>_<Patient ID>_<Field name>

On the *Mac OS X*® platform, the UCJI must not contain any blank characters or special characters like forward slash / , backslash \ or a hyphen – . Since the UCJI is automatically generated from other data, relevant entries in the preferences file and user specified data should only use numbers [0-9] letters [a-z, A-Z] and the underscore character to fill blank spaces.

Cutout job directories and files

All information pertaining to cutout jobs is stored in the *control file directory*. The absolute path to this directory is a parameter in the preferences file. One can use the CMGUI to temporarily point the control file directory to a different location. When a cutout job is saved from the *cutout workbench* tab, two text files are created in the control file directory:

- *<UCJI>***.egsinp** – The first part of this file contains input data for the *cutoutmp* EGS user code followed by cutout job parameters, that are used by the CMGUI.
- *<UCJI>***.egscutoutdata** – Contains data describing the cutout shape.

When the CMGUI is active, it constantly monitors the progress of running cutout jobs. During execution and after successful completion of such jobs, two additional text files can be found in the control file directory:

- *<UCJI>***.egslog** – After successful completion, this file contains the concatenated logs of all scheduled batch (sub-)jobs.

- *<UCJI>*.**egsbatchdata** – Contains the depth-dose profile in Gy/particle and derived information during job execution and after completion.

Cutout job execution

The *Cutout Manager* allows a cutout job to be split into several (sub-)jobs that can execute concurrently. This feature is particularly beneficial for multi-core and/or multi-processor hardware platforms. When a job is released for execution, the CMGUI creates as many .egsinp and .egscutoutdata files in the control file directory as the job splitting level indicates. For example, if the number of multiple jobs is 3, the following files are created:

- *<UCJI>*_**JOB1.egsinp**, *<UCJI>*_**JOB2.egsinp**, *<UCJI>*_**JOB3.egsinp**,
- *<UCJI>*_**JOB1.egscutoutdata**, *<UCJI>*_**JOB2. egscutoutdata**, *<UCJI>*_**JOB3. egscutoutdata**

The contents of the .egscutoutdata files is identical. The number of histories in each of the sub-jobs' .egsinp file is only a fraction, in our case one third, of the original number of histories in the *<UCJI>*.**egsinp** file.

To ensure that the sub-jobs' calculation results are independent, each .egsinp file receives a different random number generator seed, either randomly selected or manually predetermined.

In the next step, each sub-job is submitted to the batch queue using an EGSnrcMP shell script. This shell script also creates directories in the control file directory:

egsrun_*<batch job #>*_*<UCJI>*_**JOB***<sub-job #>*_*<computer name>*

During execution, these directories contain .egslog and .egsbatchdata files with the following naming convention:

- *<UCJI>*_ **JOB***<sub-job #>*.**egsbatchdata**
- *<UCJI>*_ **JOB***<sub-job #>*.**egslog**

Once a batch sub-job is finished, the above .egsbatchdata and .egslog files are moved up into the control file directory and the containing folder is deleted.

A running CMGUI monitors the progress of sub-jobs, and when it detects the successful completion of all sub-jobs, it combines their individual results into the above mentioned *<UCJI>*.egsbatchdata and *<UCJI>*.egslog text files. The sub-job input files and data files are subsequently deleted.

CMGUI preferences

When the *Cutout Manager* starts, initial settings are loaded from a text file that is located in the same directory as the executable program. The file is called *CutoutManager.pref* . Below is a typical example. The 3 digit line numbers are not part of the data:

```
000 CL21EX,CL23
001 6,9,12,16,20
002 6x6,10x10,15x15,20x20,25x25
003 ./phsp/CL21E
004 8.1697e-14±3.7761e-16
005 1.2720e-13±5.4160e-16
006 1.8323e-13±1.1332e-15
007 2.6457e-13±1.7143e-15
008 3.5827e-13±1.9353e-15
009 6,9,12,15,18,22
010 6x6,10x10,15x15,20x20,25x25
011 ./phsp/CL23
012 1.0407e-13±5.0907e-16
013 0.1691E-12±0.1334E-14
014 0.2001E-12±0.3220E-14
015 0.2084E-12±0.1734E-14
016 0.2207E-12±0.2280E-14
017 0.2626E-12±0.2461E-14
018 CERROBEND521,STEEL521ICRU,PB521ICRU,AL521ICRU,CERROBEND700[…]
019 AIR521ICRU,AIR700ICRU
020 H2O521ICRU,H2O700ICRU,SW521ICRU,SW700ICRU,ICRPBONE700ICRU[…]
021 34
022 /Users/cutout/egsnrcmp/user_codes/cutoutmp
023 /Users/cutout/egsnrcmp/user_codes/
024 /Users/cutout/egsnrcmp/specs/i386-apple-darwin8.10.1-g77.conf
025 $HEN_HOUSE/scripts/run_user_code_batch
026 cutoutmp
027 4
028 password
```

The first line contains a comma-separated list of treatment unit names available to the *Cutout Manager* (line 000). In the example two linacs, CL21EX and CL23, are defined. For each treatment unit follows a block of lines that lists available energies, applicator sizes, path to phase space files and reference doses for all available energies (lines 002-007). The lines for the energies and applicator sizes are comma separated lists of values. It is important that the applicator specification follows the pattern <*number*>x<*number*>, for example 12x12. Only

square applicator sizes are permitted. Likewise it is important that the separator between the reference dose per particle and its error is the "±" character.

The rest of the lines contain the following information:

- Comma-separated list of PEGS codes for the cutout material (line `016`).
- Comma-separated list of PEGS codes for air gap materials (line `017`).
- Comma-separated list of PEGS codes for the phantom material (line `018`).
- Screen resolution in pixels per cm for the digitizer window (line `019`).
- Absolute path to the control file directory (line `020`).
- Absolute path to the *EGSnrc* user code directory (line `022`)
- Absolute path to the *EGSnrc* configuration file (line `023`).
- Absolute path to the *EGSnrc* batch script (line `024`).
- Name of the PEGS cross-section file without .pegs4dat extension (line `025`).
- Number of multiple jobs for distributed computing (line `026`).
- Password to enter expert mode (line `027`).

Random number seeding in distributed computing

When a cutout job is split into sub-jobs, each sub-job must receive a different initial seed for the RANLUX random generator. Otherwise the results would not be statistically independent and could not be merged to form a combined final result. *Cutout Manager* allows the advanced user to fine tune the execution environment. It is possible to force single job execution and to feed the jobs with fixed seeds.

The hard coded default setting for distributed computing is to run a cutout job as 2 multiple jobs with random seeds. The number of sub-jobs can be overridden in the preferences file. The resulting default settings are visible in the *Distributed Computing Defaults* box on the Preferences tab. In expert mode it is possible to disable job-splitting ("Run as a single job"), change the number of sub-jobs ("Run as n multiple jobs with seeds...") and to force the system to use fixed seeds from a comma-separated list. The default list of fixed seeds is initially hardcoded into the application (19, 34, 79, 41, 7, 49, 88, 12) but can be altered.

The same box has a read-only field that displays a sequence of random numbers between 0 and 100. There are as many numbers as there are multiple jobs. They are updated every 3 seconds. When a cutout job using random seeding is saved from the *Cutout Workbench* tab, the seeds are taken from this (changing) sequence of numbers.

In expert mode, a similar *Distributed Computing* box is available on the *Cutout Workbench* tab. The settings here apply to the currently loaded cutout job and are retained upon saving. When the *Reset* button is pressed, all fields on the *Cutout Workbench* tab are cleared and the box's values revert to the defaults on the *Preferences* tab.

The *cutoutmp* user code

cutoutmp is an executable *EGSnrc* program that calculates depth-dose profiles for arbitrary cutout shapes. Its source code has two components: a MORTRAN source called *cutoutmp.mortran* and a small C source called *phsp_rw.c* .

The predecessor of *cutoutmp.mortran*, called *cutout.mortran*, was based on *EGSnrc* V3 and is incompatible with *EGSnrcMP*. *cutoutmp.mortran* now contains calls to *EGSnrcMP* subroutines to properly initialize and close the I/O environment. The data input from .egsinp files was standardized and extended. *cutoutmp* now uses RANLUX luxurity level 2 for random number generation, a compromise between quality and speed.

Central *EGSnrc* subroutines like *HOWFAR, HOWNEAR* and *AUSGAB* remained untouched. For a detailed description of these routines the reader is referred to C. Albaret's M.Sc. thesis (Albaret 2004). However, the geometry subroutine *inside_cutout* had to be completely rewritten since the old code in *cutout.mortran* would result in asymmetric lateral dose profiles in the water phantom. This behavior is shown in Figure 53 for a 10×10 field at 9 MeV. The effect only occurs with the *g77* compiler on the *Mac OS X*® platform. The source of the problem is not known but it may be related to accumulated rounding errors in trigonometric functions.

A new algorithm (http://en.wikipedia.org/wiki/Point_in_polygon) for the *inside_cutout* subroutine completely avoids the use of trigonometric functions and

corrects the problem (Figure 54). The new Mortran code counts how often a horizontal ray originating at a given coordinate (px, py) crosses the shape boundaries. If the number of crossings is even, the point lies outside the cutout hole and the boolean variable `inside` is set to the value "`.false.`". If the number is odd, `inside` is returned as "`.true.`" :

```
subroutine inside_cutout(px,py,inside);
real*8 px,py;
logical inside;
;COMIN/GEOM/;
integer counter;
integer i;
real*8 xinters;
real*8 p1x, p1y;
real*8 p2x, p2y;

p1x=x_cutout(1); "Load first cutout point"
p1y=y_cutout(1);
counter=0;

"Note that n_cutout_points is already incremented by 1"
DO i=2,n_cutout_points [
   p2x=x_cutout(i);
   p2y=y_cutout(i);
   IF py.gt.dmin1(p1y, p2y) [
      IF py.le.dmax1(p1y, p2y) [
         IF px.le.dmax1(p1x, p2x) [
            IF (p1y.ne.p2y) [
               xinters=(py-p1y)*(p2x-p1x)/(p2y-p1y)+p1x;
               IF (p1x.eq.p2x).or.(px.le.xinters) [
                  counter=counter+1;
               ]
            ]
         ]
      ]
   ]
   p1x=p2x;
   p1y=p2y;
]

IF ( mod(counter,2)=0 ) [ inside=.false.; ]
ELSE [ inside=.true.; ]

return;
end;
```

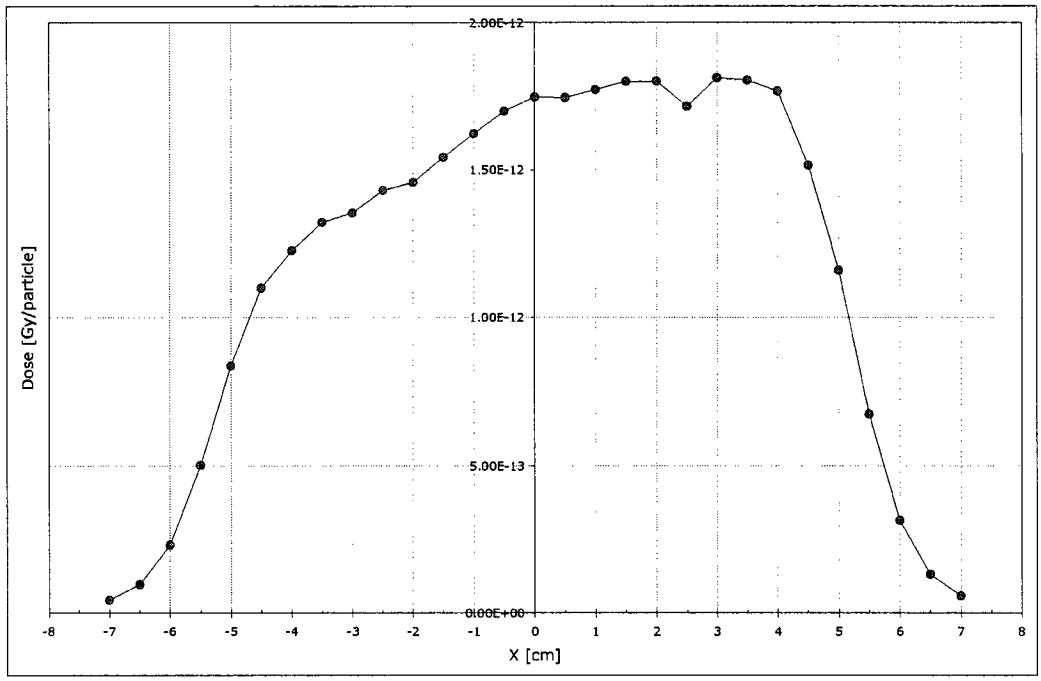

Figure 53: Asymmetric lateral beam profile caused by the original *inside_cutout* subroutine

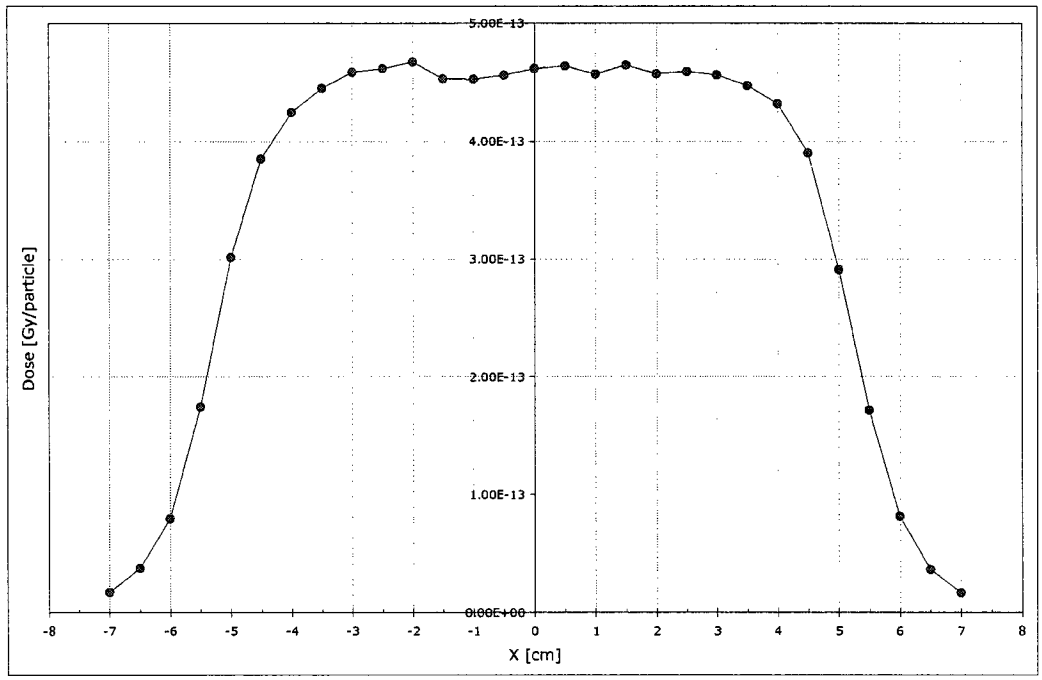

Figure 54: Symmetric lateral dose profiles with the new *inside_cutout* subroutine

To verify that *cutoutmp* transports electrons and photons correctly, *Cutout Manager* was set up to write an output phase space file during output factor calculations for a u-shaped cutout at 12 MeV and a 10×10 cm^2 field. The phase

space file records all particles that cross the lower cutout plane at approximately z=95 cm. The file was analyzed using the *beamdp* tool which is part of *EGSnrc* (invoked via *beamdp_gui*).

Figure 55 shows the contour of the u-shaped cutout as it appears in the *Cutout Digitizer* window. The shape was defined using 35 waypoints and the evaluation point (point-of-interest) is at (0,0).

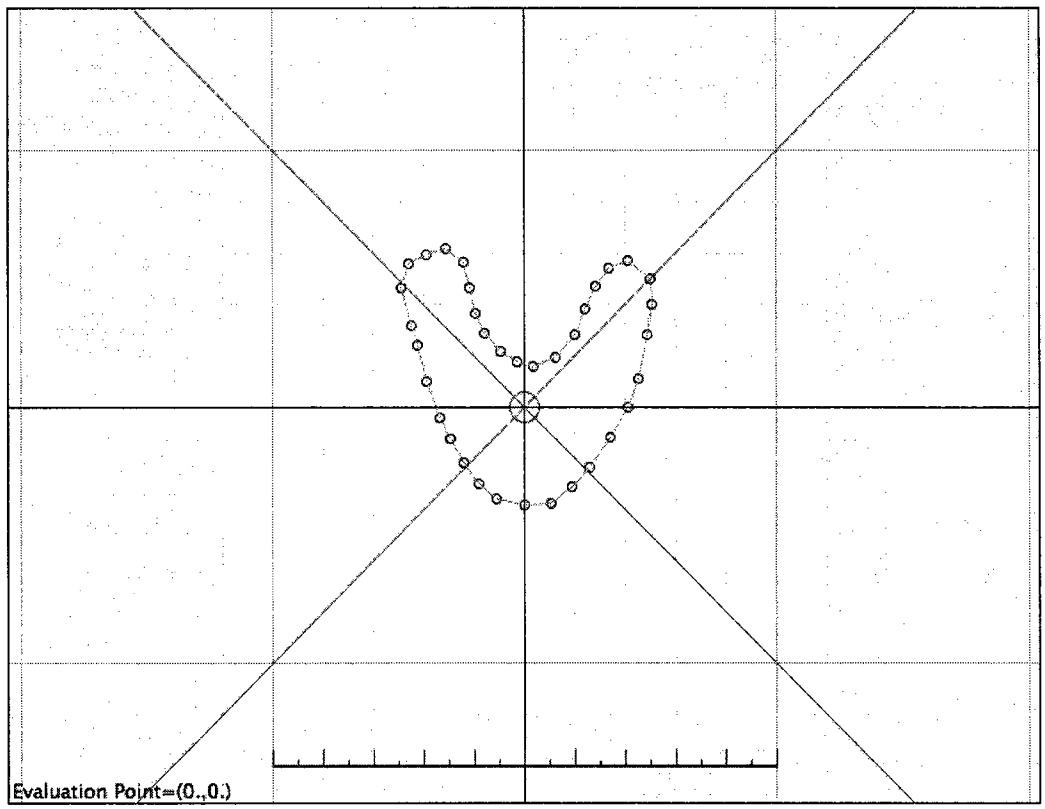

Figure 55: Contours of a u-shaped in the *Cutout Digitizer*

Figure 56 is a 2D scatter plot of electrons at z=95 cm for all energies. Only the first 3000 electrons in the phase space file were plotted. As expected, the vast majority of the electrons can be found in a region within the cutout contour. The stray electrons make up for about 3% of the total electron number.

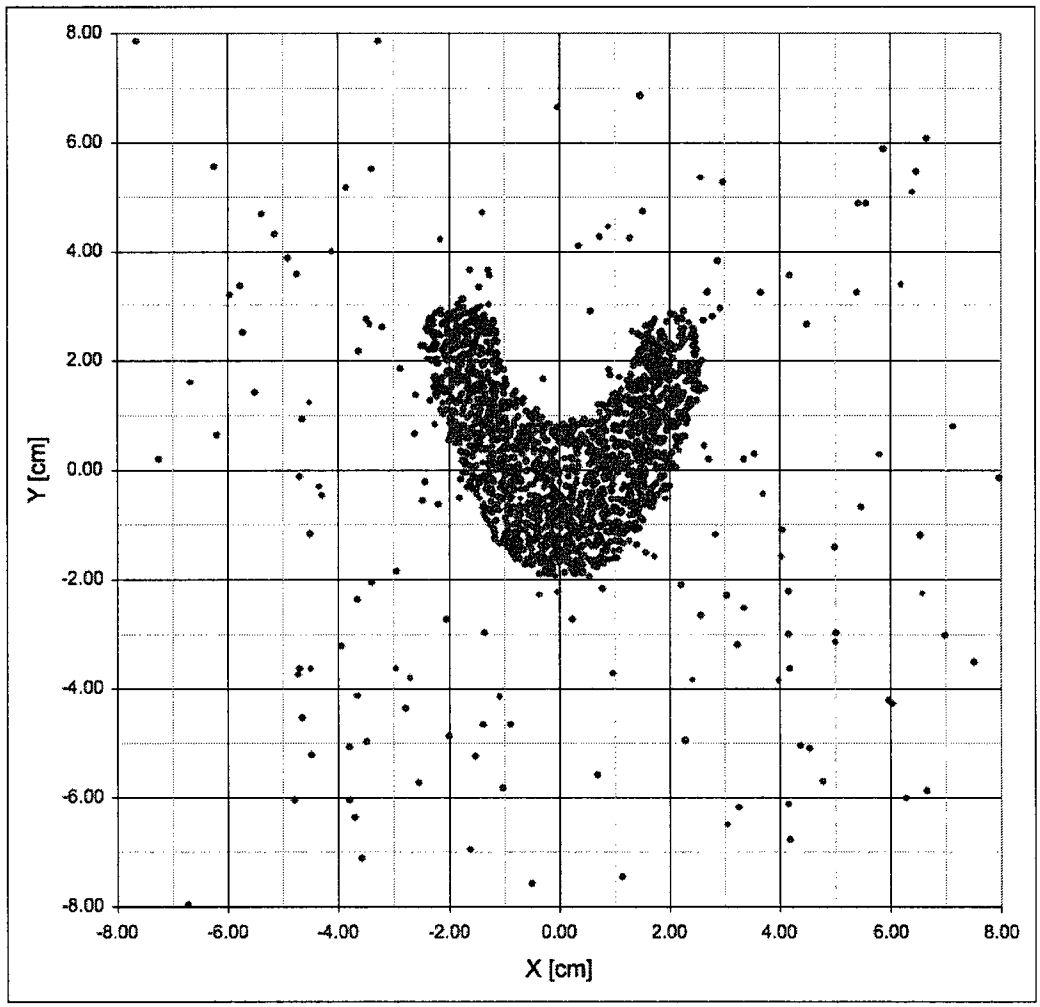

Figure 56: Electrons of all energies in PHSP file for a u-shaped cutout

Photon distributions are plotted in Figures 57 and 58. It is interesting that for high energy photons (1 MeV and up) no clear pattern resembling the cutout contour emerges. A possible explanation is that energetic photons are primarily created in bremsstrahlung events by electrons in the cutout. When the forward-directed electrons initially hit the cutout material they have MeV energies. The resulting bremsstrahlung is predominantly forward directed, the characteristic angle $\theta_{max} \leq 10°$ for electron energies equal or larger than 1 MeV. As the electrons lose energy in subsequent collisions they are scattered into many directions and the maximum angle for bremsstrahlung emission approaches $90°$. This produces a more isotropic radiation pattern. At the same time low energy photons are suppressed due to absorption in the cutout material.

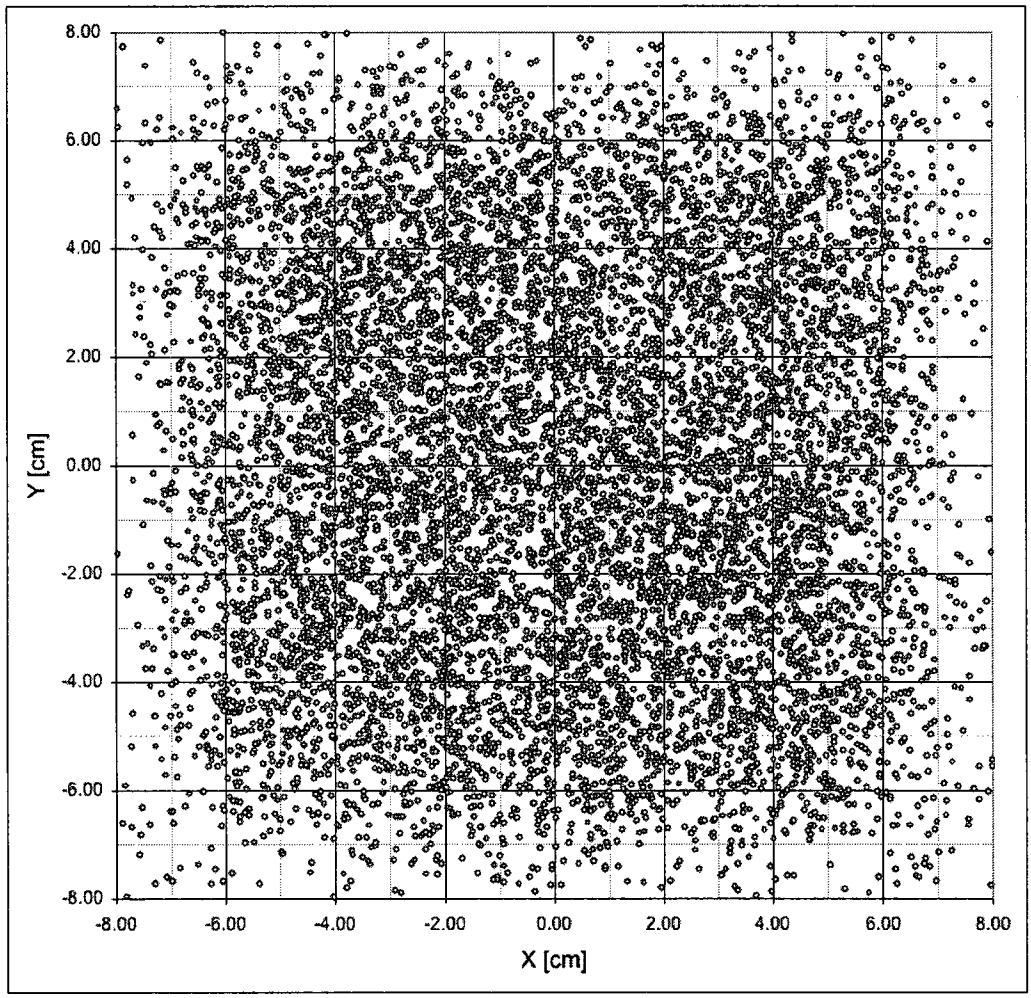

Figure 57: High energy photons (>1 MeV) in PHSP file for a u-shaped cutout

Low energy photons are clearly concentrated in an area below the cutout hole (Figure 58). They are created, together with some high energy photons, in the upstream linac components, predominantly in the scattering foils. The thin foils do not absorb them and they proceed through the cutout hole.

From the presented phase space data it can be concluded that the transport algorithm in *cutoutmp* works correctly.

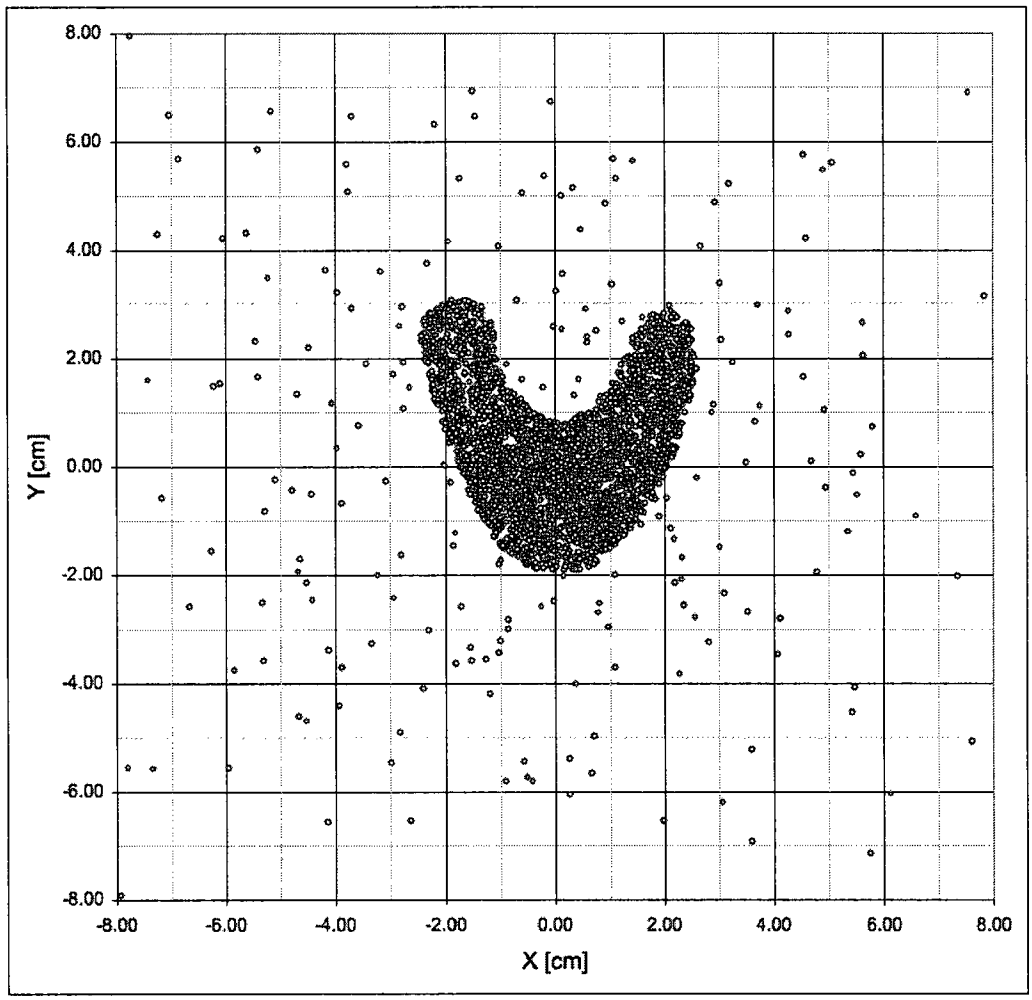

Figure 58: Low energy photons (0.01–0.1 MeV) in a PHSP file for a u-shaped cutout

Installation notes

Installation of the *Cutout Manager* system should commence with the creation of a dedicated user with administrator rights, for example "cutout". Log on to this user to proceed.

EGSnrc installation

This work uses the terms *EGSnrc* and *EGSnrcMP*. *EGSnrc* is the name of the system and family of codes for Monte Carlo simulation of coupled electron-photon transport. *EGSnrcMP* (or *EGSnrc V4*) is the recent multi-platform release of the *EGSnrc* system. We used *EGSnrcMP* patch level V4-r2-2-5 and followed installation method 3 which is suitable for *Mac OS X*®.

BEAMnrc is a Monte Carlo simulation system for modeling radiotherapy sources based on *EGSnrc*. *BEAMnrcMP* is the latest multi-platform version of *BEAMnrc* and requires *EGSnrcMP*. We use *BEAMnrcMP* version *2007* to model the linear accelerator and create phase space files. *BEAMnrc* is NOT required to run the *Cutout Manager*. For installation instructions regarding *BEAMnrc* the reader is referred to the *BEAM* home page.

For a standard *EGSnrcMP* environment, the following files are required:

- *g77-intel-bin.tar.gz* – The *g77* version 3.4 compiler.
- *V4_EGSnrc.tar* – The main system.
- *V4_EGSgui.tar* – The source code for the GUIs.
- *V4_manuals.tar* – The documentation.
- *V4_spinms.tar* – The spin data base.
- *V4_user_codes.tar* – The NRC user codes.
- *install_egs* – The installation script. Sometimes called *install_egs.sh*.
- *qt-mac-free-3.3.7.tar.gz* or higher (optional).
- *pirs877.pdf* – contains detailed installation instructions.

Download the *g77* distribution from http://hpc.sourceforge.net and the EGSnrc archives and files from http://www.irs.inms.nrc.ca/EGSnrc/EGSnrc.html . *qt-mac-free-3.3.7.tar.gz* is needed for building the *EGSnrc* GUIs and available for download from ftp://ftp.trolltech.com/qt/source. *Cutout Manager* does NOT require any *EGSnrc* GUIs.

The installation starts with the *g77* compiler. Uncompress and unpack *g77-intel-bin.tar.gz* into a temporary directory and copy or move the newly created *usr* folder to document root of the system device where a */usr* directory should already exist. No further action is required for *g77*. Note that copying the *g77* files into */usr* requires administrator rights.

For *EGSnrcMP*, download all files into a temporary directory. In a bash shell, `cd` to this directory, make *install_egs* executable with `chmod u+x ./install_egs` and run it with the command `./install_egs`. Accept the default options, and choose a folder like */Users/cutout/egsnrcmp* as the directory where you want to install EGSnrc. Compile the user codes but do NOT build the GUIs. On *Mac Pro*

computers with Intel processors *qt-mac-free-3.3.7.tar.gz* may not install correctly and thus making the GUIs will fail.

Enter the following lines to */Users/cutout/.bash_profile*:

```
PATH=/usr/local/bin:$PATH"
export PATH
export EGS_HOME=/Users/cutout/egsnrcmp/user_codes
export EGS_CONFIG=/Users/cutout/egsnrcmp/specs/_
      i386-apple-darwin8.11.1-g77.conf
. Users/cutout/egsnrcmp/scripts/egsnrc_bash_additions
```

Doing so will ensure that whenever the bash shell is started, it will gain access to the *g77* compiler in */usr/local/bin* and that the *EGSnrcMP* environment of user "cutout" is correctly defined. The name of the configuration file may be different from *i386-apple-darwin8.11.1-g77.conf* because it depends on the *Mac OS X* version and the type of FORTRAN compiler.

User code *cutoutmp* installation

In the *user_code* folder create a directory called *cutoutmp*. The newly created directory will also be home of the *Cutout Manager* control files. Copy the following files from the distribution medium to the *cutoutmp* directory:

- *cutoutmp.mortran* – The MORTRAN source code for transporting particles through the cutout and dose scoring.
- *phsp_rw.c* – The C source code for reading and writing phase space files.
- *Makefile* – The main makefile read my the make utility
- *cutoutmp.make* – A cutoutmp specific include to the *Makefile*.
- *cutoutmp.io* – This file defines the mapping of files to FORTRAN unit numbers and is read by *EGSnrc* routines during the execution of *cutoutmp*.

Open a *bash* shell and change the default directory to the *cutoutmp* directory. You may first use the command `make clean` to remove all files of a former built. Build the *cutoutmp* executable with the command `make FOPT="-O2"` . It is recommended to use either optimization level O2 or O1, since the default level, O3, may lead to run-time errors.

Enabling the *atrun* batch system

The *EGSnrcMP* batch script uses the `at` command to submit jobs to the batch queue. *Mac OS X*® is derived from the BSD implementation of Unix and has a built-in batch system that is disabled by default. As a consequence the bash shell commands `at`, `batch`, `atq` and `atrm` are initially not available. To use these commands one must first (as root) enable atrun by running:

```
launchctl load -w _
/System/Library/LaunchDeamons/com.apple.atrun.plist
```

in a command shell window. Alternatively this can be done using the `sudo` command. See the Unix `man` pages for help on `at`.

CMGUI installation

Although the CMGUI can reside anywhere on the hard drive, it is recommended to install it in the *cutoutmp* directory, where the user code and *EGSnrc* input files are located. Only two files are necessary:

- CutoutManagerOSX.app – The main application.
- CutoutManager.pref – The preferences file.

At the same location create two directories named *phsp* and *outphsp*. They are home to EGSnrc phase space files created during the commissioning of the software (*phsp*) or as output of the *Cutout Manager* system (*outphsp*).

Edit the preferences file to reflect your clinical and software environment. As a minimum one should enter the desired treatment units and applicable energies and applicator sizes. Create sufficient lines for the reference doses, for example `2.000e-13±1.000e-15` . During commissioning these doses will be set to the correct values. Adjust the digitizer screen resolution, paths to directories and EGSnrc run script. Enter the correct number of available CPU cores and set a password for expert mode access.

Appendix B – BEAMnrc INPUT FOR JAW SETTINGS

When an applicator is installed into the accessory mount and a nominal energy is selected, the linac jaws automatically close to a manufacturer-defined field size. For a Clinac 21EX these field sizes are listed in Table 1. This appendix provides listings of BEAMnrc input for the JAWS component module. All data is for field sizes at SSD 100 cm. Note also that ECUT is explicitly set to 0.7 MeV. Set ECUT to the desired value or to "0" if the system wide default value is to be used.

FS=11×11 cm^2

```
********** start of CM JAWS with identifier jaws  **********
22, RMAX
JAWS set to 11x11 at 100cm SSD
2, # PAIRED BARS OR JAWS
Y
27.861, 35.622, 1.53235, 1.95921, -1.53235, -1.95921,
X
36.7, 44.461, 2.01850, 2.44535, -2.01850, -2.44535,
0.7, 0.01, 0, 0,
0.7, 0.01, 0, 10,
W521ICRU
0.7, 0.01, 0, 11,
W521ICRU
```

FS=14×14 cm^2

```
********** start of CM JAWS with identifier jaws  **********
22, RMAX
JAWS set to 14x14 at 100cm SSD
2, # PAIRED BARS OR JAWS
Y
27.861, 35.622, 1.95027, 2.49354, -1.95027, -2.49354,
X
36.7, 44.461, 2.56900, 3.11227, -2.56900, -3.11227,
0.7, 0.01, 0, 0,
0.7, 0.01, 0, 0,
W521ICRU
0.7, 0.01, 0, 0,
W521ICRU
```

FS=17×17 cm^2

```
********** start of CM JAWS with identifier jaws  **********
22, RMAX
JAWS set to 17x17 at 100cm SSD
2, # PAIRED BARS OR JAWS
Y
27.861, 35.622, 2.36819, 3.02787, -2.36819, -3.02787,
X
36.7, 44.461, 3.11950, 3.77919, -3.11950, -3.77919,
0.7, 0.01, 0, 0,
0.7, 0.01, 0, 0,
W521ICRU
0.7, 0.01, 0, 0,
W521ICRU
```

FS=20×20 cm^2

```
********** start of CM JAWS with identifier jaws  **********
22, RMAX
JAWS set to 20x20 at 100cm SSD
2, # PAIRED BARS OR JAWS
Y
27.861, 35.622, 2.786, 3.562, -2.786, -3.562,
X
36.7, 44.461, 3.67, 4.446, -3.67, -4.446,
0.7, 0.01, 0, 0,
0.7, 0.01, 0, 10,
W521ICRU
0.7, 0.01, 0, 11,
W521ICRU
```

FS=22×22 cm^2

```
********** start of CM JAWS with identifier jaws  **********
22, RMAX
JAWS set to 22x22 at 100cm SSD
2, # PAIRED BARS OR JAWS
Y
27.861, 35.622, 3.06471, 3.91842, -3.06471, -3.91842,
X
36.7, 44.461, 4.03700, 4.89071, -4.03700, -4.89071,
0.7, 0.01, 0, 0,
0.7, 0.01, 0, 10,
W521ICRU
0.7, 0.01, 0, 11,
W521ICRU
```

FS=25×25 cm^2

```
********** start of CM JAWS with identifier jaws  **********
22, RMAX
JAWS set to 25x25 at 100cm SSD
2, # PAIRED BARS OR JAWS
Y
27.861, 35.622, 3.48263, 4.45275, -3.48263, -4.45275,
X
36.7, 44.461, 4.58750, 5.55762, -4.58750, -5.55762,
0.7, 0.01, 0, 0,
0.7, 0.01, 0, 0,
W521ICRU
0.7, 0.01, 0, 0,
W521ICRU
```

FS=27×27 cm^2

```
********** start of CM JAWS with identifier jaws  **********
22, RMAX
JAWS set to 27x27 at 100cm SSD
2, # PAIRED BARS OR JAWS
Y
27.861, 35.622, 3.76124, 4.80897, -3.76124, -4.80897,
X
36.7, 44.461, 4.95450, 6.00223, -4.95450, -6.00223,
0.7, 0.01, 0, 0,
0.7, 0.01, 0, 10,
W521ICRU
0.7, 0.01, 0, 11,
W521ICRU
```

FS=28×28 cm^2

```
********** start of CM JAWS with identifier jaws  **********
22, RMAX
JAWS set to 28x28 at 100cm SSD
2, # PAIRED BARS OR JAWS
Y
27.861, 35.622, 3.90054, 4.98708, -3.90054, -4.98708,
X
36.7, 44.461, 5.13800, 6.22454, -5.13800, -6.22454,
0.7, 0.01, 0, 0,
0.7, 0.01, 0, 10,
W521ICRU
0.7, 0.01, 0, 11,
W521ICRU
```

FS=30×30 cm^2

```
********** start of CM JAWS with identifier jaws  **********
22, RMAX
JAWS set to 30x30 at 100cm SSD
2, # PAIRED BARS OR JAWS
Y
27.861, 35.622, 4.17915, 5.34330, -4.17915, -5.34330,
X
36.7, 44.461, 5.50500, 6.66915, -5.50500, -6.66915,
0.7, 0.01, 0, 0,
0.7, 0.01, 0, 10,
W521ICRU
0.7, 0.01, 0, 11,
W521ICRU
```

Appendix C – BEAMnrc INPUT FOR APPLICATOR MODELING

BEAMnrc component module APPLICAT was used to model the upper two applicator scrapers in accelerator model CL21E and all three scrapers for $10\times10cm^2$ field size in model CL21E_PDD. The scraper material has the PEGS4 identifier BISNICRU521. It is an alloy of 58% bismuth and 42% tin (mass) with a combined density of 8.72 g/cm^3.

6×6 cm^2 applicator

```
********** start of CM APPLICAT with identifier applicat  **********
27, RMAX
6x6 applicator
78.54, ZBACK
2, 0, #SCRAPERS, SQUARE
63.75, 1.65, 3.58, 4.42, 0, 0
76.5, 2.025, 3.305, 4.695, 0, 0
0.7, 0.01, 0, 0,
BISNICRU521
BISNICRU521
```

10×10 cm^2 applicator

```
********** start of CM APPLICAT with identifier applicat  **********
27, RMAX
10x10 applicator
95.0, ZBACK
3, 0, #SCRAPERS, SQUARE
63.75, 1.75, 4.84, 7.137, 0, 0
76.5, 2.025, 4.83, 4.76, 0, 0
93.02, 1.8, 4.75, 5.1, 0, 0
0.7, 0.01, 0, 0,
BISNICRU521
BISNICRU521
STEEL521ICRU
```

15×15 cm^2 applicator

```
********** start of CM APPLICAT with identifier applicat  **********
27, RMAX
15x15 applicator
78.54, ZBACK
2, 0, #SCRAPERS, SQUARE
63.75, 1.75, 6.375, 6.5, 0, 0
76.5, 2.025, 6.7, 6.85, 0, 0
0.7, 0.01, 0, 0,
BISNICRU521
BISNICRU521
```

20×20 cm^2 applicator

```
********** start of CM APPLICAT with identifier applicat  **********
27, RMAX
20x20 applicator
78.54, ZBACK
2, 0, #SCRAPERS, SQUARE
63.75, 1.65, 12.55, 6.82, 0, 0
76.5, 2.025, 13.075, 4.94, 0, 0
0.7, 0.01, 0, 0,
BISNICRU521
BISNICRU521
```

25×25 cm^2 applicator

```
********** start of CM APPLICAT with identifier applicat  **********
27, RMAX
25x25 applicator
78.54, ZBACK
2, 0, #SCRAPERS, SQUARE
64.2, 1.6, 19.5, 5.0, 0, 0
76.5, 2.0, 21.3, 5.0, 0, 0
0.7, 0.01, 0, 0,
BISNICRU521
BISNICRU521
```

LIST OF REFERENCES

Albaret, C. (2004). Automated System for Monte Carlo determination of cutout factors of arbitrarily shaped electron beams. Medical Physics Unit. Montreal, McGill University. **M.Sc.**

Almond, P. R., P. J. Biggs, et al. (1999). "AAPM's TG-51 protocol for clinical reference dosimetry of high-energy photon and electron beams." Med Phys **26**(9): 1847-70.

Bruinvis, I. A., A. Van Amstel, et al. (1983). "Calculation of electron beam dose distributions for arbitrarily shaped fields." Phys Med Biol **28**(6): 667-83.

Bruinvis, I. A., A. van Amstel, et al. (1983). "Dose calculations for arbitrarily shaped electron beams." Acta Radiol Suppl **364**: 73-9.

Burns, D. T., G. X. Ding, et al. (1996). "R50 as a beam quality specifier for selecting stopping-power ratios and reference depths for electron dosimetry." Med Phys **23**(3): 383-8.

Chen, F. S. (1988). "An empirical formula for calculating the output factors of electron beams from a therac 20 linear accelerator." Med Phys **15**(3): 348-50.

Devic, S., J. Seuntjens, et al. (2005). "Precise radiochromic film dosimetry using a flat-bed document scanner." Med Phys **32**(7): 2245-53.

Devic, S., N. Tomic, et al. (2007). "Absorption spectroscopy of EBT model GAFCHROMIC film." Med Phys **34**(1): 112-8.

Hogstrom, K. R., M. D. Mills, et al. (1981). "Electron beam dose calculations." Phys Med Biol **26**(3): 445-59.

Hu, K. S., W. E. Enker, et al. (2002). "High-dose-rate intraoperative irradiation: current status and future directions." Semin Radiat Oncol **12**(1): 62-80.

International Commission on Radiation Units and Measurements. (2004). Prescribing, recording, and reporting electron beam therapy. ICRU report 71. Oxford, Eng., Oxford University Press.

Jones, D., P. Andre, et al. (1990). "A method for the assessment of the output of irregularly shaped electron fields." Br J Radiol **63**(745): 59-64.

Jursinic, P. A. and R. Mueller (1997). "A sector-integration method for calculating the output factors of irregularly shaped electron fields." Med Phys **24**(11): 1765-9.

Kapur, A., C. M. Ma, et al. (1998). "Monte Carlo calculations of electron beam output factors for a medical linear accelerator." Phys Med Biol **43**(12): 3479-94.

Kawrakow, I. and D. W. O. Rogers (2006). The EGSnrc Code System. Ionizing Radiation Standards. Ottawa, National Research Council of Canada.

Khan, F. M., K. P. Doppke, et al. (1991). "Clinical electron-beam dosimetry: report of AAPM Radiation Therapy Committee Task Group No. 25." Med Phys **18**(1): 73-109.

Kurup, R. G., G. P. Glasgow, et al. (1995). "Output factors for irregularly shaped electron fields." Med Dosim **20**(3): 155-9.

Kutcher, G. J., L. Coia, et al. (1994). "Comprehensive QA for radiation oncology: report of AAPM Radiation Therapy Committee Task Group 40." Med Phys **21**(4): 581-618.

Kuten, A., M. Stein, et al. (1991). "Total-skin electron irradiation for cutaneous T-cell lymphoma: the Northern Israel Oncology Center experience." Strahlenther Onkol **167**(7): 392-6.

Le Bourgeois, J. P., E. Haddad, et al. (1987). "The indications for total cutaneous electron beam radiation therapy of mycosis fungoides." Int J Radiat Oncol Biol Phys **13**(2): 189-93.

Mayles, P., A. E. Nahum, et al. (2007). Handbook of radiotherapy physics : theory and practice. New York, Taylor & Francis.

McParland, B. J. (1989). "A method of calculating the output factors of arbitrarily shaped electron fields." Med Phys **16**(1): 88-93.

McParland, B. J. (1989). "Methods of calculating the output factors of rectangular electron fields." Med Dosim **14**(1): 17-21.

McParland, B. J. (1992). "An analysis of equivalent fields for electron beam central-axis dose calculations." Med Phys **19**(4): 901-6.

Mills, M. D., K. R. Hogstrom, et al. (1982). "Prediction of electron beam output factors." Med Phys **9**(1): 60-8.

Mills, M. D., K. R. Hogstrom, et al. (1985). "Determination of electron beam output factors for a 20-MeV linear accelerator." Med Phys **12**(4): 473-6.

Muller-Runkel, R. (1992). "Dosimetry of shaped electron fields using a radial integration method." Med Dosim **17**(4): 207-11.

Rogers, D. W., B. A. Faddegon, et al. (1995). "BEAM: a Monte Carlo code to simulate radiotherapy treatment units." Med Phys **22**(5): 503-24.

Rogers, D. W. O. (2002). "Monte Carlo Techniques in Radiotherapy." Physics in Canada **58**(2): 63-70.

Rogers, D. W. O., B. Walters, et al. (2006). BEAMnrc Users Manual. Ionizing Radiation Standards. Ottawa, National Research Council of Canada.

Tenhunen, M. and T. Lahtinen (1994). "Relative output factors of asymmetric megavoltage beams." Radiother Oncol **32**(3): 226-31.

Turian, J. V., B. D. Smith, et al. (2004). "Monte Carlo calculations of output factors for clinically shaped electron fields." J Appl Clin Med Phys **5**(2): 42-63.

Verhaegen, F., C. Mubata, et al. (2001). "Monte Carlo calculation of output factors for circular, rectangular, and square fields of electron accelerators (6-20 MeV)." Med Phys **28**(6): 938-49.